

**ANTIMICROBIAL nHA COATING FOR TRAUMATIC  
BONE INJURIES**

**Zineb BENZAIT**

**Master Thesis  
Nanoscience and Nanoengineering Department  
Nanomaterials Program**

**Prof. Dr. Mehmet ERTUĞRUL  
2015**

**All rights reserved**

**ATATÜRK UNIVERSITY  
GRADUATE SCHOOL OF NATURAL AND APPLIED SCIENCES**

**MASTER THESIS**

**ANTIMICROBIAL nHA COATING FOR TRAUMATIC BONE  
INJURIES**

**Zineb BENZAIT**

**DEPARTMENT OF NANOSCIENCE AND NANOENGINEERING  
Nanomaterials Program**

**ERZURUM  
2015**

**All rights reserved**



TURKISH REPUBLIC  
ATATURK UNIVERSITY  
GRADUTE SCHOOL of NATURAL and  
APPLIED SCIENCES



THESIS APPROVAL FORM



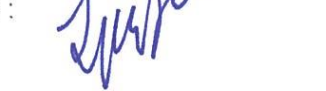
ANTIMICROBIAL nHA COATING FOR TRAUMATIC BONE INJURIES

This study, prepared by Zineb BENZAIT, under supervision of Prof. Dr. Mehmet ERTUĞRUL, has been approved on the date of 15 / 01/ 2015 as Master Thesis, in the Department of Nanoscience and Nanoengineering – Graduate School of Natural and Applied Sciences, by the below-named thesis committee with **majority/unanimously** (✓/.....).

President : Prof. Dr. Akgun ALSARAN

Member : Prof. Dr. Mehmet ERTUĞRUL

Member : Assoc. Prof. Emre GÜR

Signature :   
Signature :   
Signature : 

The above-mentioned result;

Has been approved in accordance with Institute Administrative Committee on the date of 29. / 01. / 2015 and resolution number 09 / ... 122.

  
Prof. Dr. İhsan EFEOĞLU  
Institute Director

**Note:** Reproduction of authentic or quoted notifications, charts, figures and images of this thesis is subject to provisions of Law on Intellectual and Artistic Works law number 5846.

## **ABSTRACT**

Mater Thesis

### **ANTIMICROBIAL nHA COATING FOR TRAUMATIC BONE INJURIES**

Zineb BENZAIT

Atatürk University  
Graduate School of Natural and Applied Sciences  
Department of Nanoscience and Nanoengineering

Supervisor: Prof. Dr. Mehmet ERTUĞRUL.

Nanostructured hydroxyapatite coatings with titanium oxide buffer layers were deposited on stainless steel substrates by two methods: Radio Frequency Magnetron Sputtering (RF-MS) and Ultrasonic Spray Pyrolysis Technique (USPT). Honey as a promising antimicrobial agent was subsequently loaded to the coatings through its adsorption by hydroxyapatite. These prepared antimicrobial coatings are expected to have excellent properties and great trauma bone wounds treatment with the prevention from Multidrug-Drug Resistant (MDR) bacterial infections.

**2015, 109 pages**

**Keywords :** nano-hydroxyapatite (nHA), antimicrobial coatings, Radio Frequency Magnetron Sputtering (RF-MS), Spray Pyrolysis Technique (SPT), titanium oxide buffer layer.

## ÖZET

Yüksek Lisans Tezi

### TRAVMATİK KEMİK YARALANMALARI İÇİN ANTİMİKROBİYAL nHA KAPLAMA

Zineb BENZAIT

Atatürk Üniversitesi  
Fen Bilimleri Enstitüsü  
Nanobilim ve Nanoteknoloji Anabilim Dalı

Danışman: Prof. Dr. Mehmet ERTUĞRUL.

Titanyum oksit ara tabakalı nanoyapılı hidroksiapatit kaplamalar paslanmaz çelik altlıklar üzerine RF-Saçtırma Yöntemi ve Ultrasonik Spray Pyrolysis tekniği olmak üzere iki metot kullanılarak büyütüldü. Gelecek vaat eden bir antimikrobiyal madde olarak bal daha sonra hidroksiapatit kaplı yüzeyler üzerine kaplanarak bu yüzeyler tarafından adsorbe edilmesi sağlanmıştır. Bu hazırlanan antimikrobiyal kaplamalar mükemmel özelliklere sahip ve MDR bakteriyel enfeksiyonlardan koruması ile büyük travmalı kemik yaralarının tedavisi için oldukça umut vericidir.

**2015, 109 sayfa**

**Anahtar Kelimeler:** Nano-hidroksiapatit, antimikrobiyal kaplamalar, RF Magnetron Saçılma, Spray Pyrolysis Teknik, titanyum oksit ara tabaka

## ACKNOWLEDGEMENTS

Having arrived to Turkey, to Ataturk University at the start of October 2012, I was privileged to have the guidance and support of my dear supervisor Professor Mehmet ERTUĞRUL, not only concerning my studies and my thesis, but also in any obstacles or challenges I have faced during these two years. So, first of all, I would like to express my most sincere appreciation to him. It was my fortune to have this precious opportunity to study and work with this greatest supervisor. Indeed, only Allah knows how much I admire him and I am thankful for his time, consideration, patience, kindness and modesty.

I would like to thank Professor Mehmet ERTUĞRUL again and also to thank RA.Demet TATAR for their continued help and expertise throughout this thesis. Sincerely, RA.Demet TATAR was very helpful, guider and friendly. Many thanks to Professor Hasan EFFOĞLU who showed me and allowed me to use XRD. Further thanks should go to all my master teachers, my classmates and the lab staff and especially Sadna IŞIK and Somayeh JAFARPOUR. The work of Asst. Sibel MARKOÇ, Asst. Fatmanur TUZLUCA and RA. Özkan YEŞİLBAĞ is greatly acknowledged with regard to the analysis of the synthesized coatings by FE-SEM, I was really overwhelmed by their gentleness and hospitality when I went to Erzcincan.

My special acknowledgement is for the organizers of Turkish Scholarships program which provides me with financial support. Without this program, I could not study abroad and achieve one of my big goals.

I would like to express my great appreciation to my friends who make the life in Turkey so beautiful, especially my wonderful international friends: Sophia, Nassiha, Ghada,

Ayişe, Bochra, Meysa, Dina, Amani, Safia, Lubaba, Ryma, Leyla, Artina, Silvyana, Shukri, Jamila, Mubarek, Raed, Muhammed, Gülbahar, Mehbube, Fadime, Lela and Nigare .. etc (the list will not finish), also to my Turk friends: my dear Nuriye, Halime, Nülfir Hoca, Rümeysa, Suendem and Raziye Abla, Melek, Şeyma, Merve, Üşra, Binnaz, Duygu, Hafize, Ayşe, Neslihan, Mustafa Abi, Nur Abla, Rabia, Habibe and Makbule, Zeki Hoca, Numan Abi, Cemil Hoca, Hatice Abla, Veysel Hoca, Hacer Abla ...all my association friends, my Arabic students, my dear dorm-mates: Aysel Abla, Elif, Ayla, Mervenur and Damlanur. Particular mention is made to Hatice and Nurcan Abla who have continually encouraged me and supported me emotionally and have been real sisters.

I will never forget my Algerian friends even if I am far from them, distance means so little when someone means so much! I will not start mentioning their names otherwise I will write pages and pages, but I cannot accept to not mention Asma, Meriem, Chafia, Yasmin, Yousra, Zahira, Sarah, Aicha, Soumaya, Khansaa, Fouziya, Nadjet, Houda ..etc

Finally, I thank the kindest and greatest parents in the world: my mother Meriem BAHA and my father Abd-Elhafidh BENZAIT, you are physically so far away from me but always close to me in spirit, thank you for your infinite love, for your patience and prayers, for your firm support that has been enlightening my life. Thank you for making me who I am! Thank you also dear brothers: Ibrahim, Mohammed and Mossaab, I am very thankful to Allah for having all you great people around me!

**Zineb BENZAIT**

**January, 2015**

## TABLE OF CONTENTS

ABSTRACT.....	i
ÖZET.....	ii
ACKNOWLEDGEMENTS .....	iii
LISTE OF ABBREVIATIONS .....	vii
LISTE OF FIGURES .....	viii
LISTE OF TABLES.....	x
<b>1.INTRODUCTION.....</b>	<b>1</b>
1.1. Orthopedic Implants .....	2
1.2. Hydroxyapatite Coatings in Orthopedic Implants.....	2
1.3. nHA Coating Techniques .....	4
1.3.1. Different thin film deposition techniques.....	4
1.3.2. Required nHA coating proprieties.....	6
1.3.2. Choice of nHA coating technique .....	7
1.4. Improvement of HA Coatings by TiO <sub>2</sub> Buffer Layer.....	11
1.5. Magnesium-Doped Hydroxyapatite Thin Films.....	14
1.6. Antimicrobial Coatings .....	16
1.6.1. Orthopedic implant infections .....	16
1.6.2. Use of antibiotics .....	17
1.6.3. Multi Drug-Resistant (MDR) bacteria .....	19
1.6.4. Use of Antimicrobial Peptides (AMP) .....	20
1.6.5. Limitation of AMP use in implant coatings .....	20
1.6.6. Honey as a promising antimicrobial agent in antimicrobial coatings .....	22
1.6.7. Stainless steel as implants based-material in trauma surgery case.....	23
<b>2. PREPARATION OF TITANIUM OXIDE BUFFER LAYER BY SPRAY</b>	
<b>    PYROLYSIS TECHNIQUE.....</b>	<b>25</b>
2.1. Introduction to the Second Chapter .....	25
2.2. Materials and Methods .....	25
2.2.1. Spray Pyrolysis Technique (SPT) .....	25
2.2.3. Preparation of TiO <sub>2</sub> thin films .....	36
2.2.4. Coatings characterization methods.....	38
2.3. Results and Discussions .....	39
2.3.1. Effect of post-deposition heat treatment .....	39
2.3.2. Effect of substrate temperature.....	40
2.3.3. Effect of nozzle-to-substrate distance .....	47
2.3.4. Effect of adding oxygen to the deposition atmosphere .....	48
2.3.6. Thickness of the prepared buffer layers .....	58



2.4. Conclusion of the Second Chapter .....	58
<b>3. PREPARATION OF HYDROXYAPATITE COATINGS BY RF-MS TECHNIQUE.....</b>	<b>59</b>
3.1. Introduction to the Third Chapter .....	59
3.2. Materials and Methods .....	59
3.2.1. Fundamentals of sputtering .....	59
3.2.2. Advantages and disadvantages of RF-MS.....	64
3.2.3. RF magnetron sputtering of hydroxyapatite thin films .....	65
3.2.4. Components of RF-MS equipment used .....	68
3.2.5. Preparation of hydroxyapatite target .....	70
3.2.6. Experimental details about HA nano-coatings synthesized by RF-MS .....	72
3.3. Results and Discussions .....	73
3.3.1. Effect of substrate /buffer layer.....	73
3.3.2. Effect of RF-MS sputtering power.....	77
3.3.3. Thickness of the nHA coatings synthesized by RF-MS.....	81
<b>4. PREPARATION OF HYDROXYAPATITE COATINGS BY ULTRASONIC SPRAY PYROLYSIS TECHNIQUE.....</b>	<b>82</b>
4.1. Introduction to the Forth Chapter .....	82
4.2. Materials and Methods .....	82
4.2.1. Ultrasonic Spray Pyrolysis Technique (USPT).....	82
4.2.2. The equipment used.....	83
4.2.3. n-HA precursor solution preparation.....	84
4.3.3. Formation of nHA coatings.....	85
4.3. Results and Discussions .....	86
4.3.1. Effect of substrate temperature.....	86
4.3.2. Effect of post heat-treatment temperature .....	92
4.3.3. Influence of substrate and buffer layer.....	93
4.3.4. Thickness of the nHA coatings synthesized by RF-MS.....	97
4.3.5. Effect of magnesium doping .....	97
4.3.6. Honey incorporation into nHA coatings .....	102
<b>5. CONCLUSION.....</b>	<b>103</b>
BIBLIYOGRAPHY .....	105
CURRICULUM VITAE (CV).....	111

## LISTE OF ABBREVIATIONS

A	Anatase
AMP	Antimicrobial peptides
CVD	Chemical Vapor Deposition
EDAX	Energy dispersive X-ray analysis
FE-SEM	Field Emission Scanning Electron Microscope
MDR	Multi-Drug Resistant bacteria
nHA	Nano-hydroxyapatite
R	Rutile
RF-MS	Radio Frequency Magnetron Sputtering
SPT	Spray Pyrolysis Technique
S.S	Stainless steel
TCP	Tricalcium phosphate
USPT	Ultrasonic Spray Pyrolysis Technique
XRD	X-Ray Diffractometry

## LISTE OF FIGURES

<b>Figure 1.1.</b> Various types of thin film deposition techniques .....	5
<b>Figure 1.2.</b> Crystallographic matching between HA and anatase, and HA and rutile .....	13
<b>Figure 2.1.</b> General schematic of a spray pyrolysis deposition process.....	26
<b>Figure 2.2.</b> Spray pyrolysis droplets modifying during their transport.....	32
<b>Figure 2.3.</b> Summary of SPT processes as a function of temperature .....	33
<b>Figure 2.4.</b> Schematic diagram of the home-made SPT Equipment .....	34
<b>Figure 2.5.</b> Pneumatic atomizing nozzle used.....	35
<b>Figure 2.6.</b> XRD patterns of films before and after heat-treatment (D=35cm, O <sub>2</sub> ) .....	39
<b>Figure 2.7.</b> XRD patterns of TiO <sub>2</sub> thin films deposited at different temperatures .....	41
<b>Figure 2.8.</b> Effect of substrate temperature on SPT processes.....	42
<b>Figure 2.9.</b> Different SPT processes and formed thin films proprieties according to substrate temperature. ....	43
<b>Figure 2.10.</b> Procedure of FWHM values determination.....	45
<b>Figure 2.11.</b> Representative FESEM image of the film deposited at 420°C and annealed at 700°C.....	46
<b>Figure 2.12.</b> Energy dispersive X-ray analysis (EDAX) of the film deposited at 420°C and annealed at 700°C.....	46
<b>Figure 2.13.</b> XRD patterns of TiO <sub>2</sub> thin films deposited at 30 and 35 cm .....	47
<b>Figure 2.14.</b> XRD patterns of TiO <sub>2</sub> films deposited under different atmospheres, after annealing at 700°C .....	48
<b>Figure 2.15.</b> XRD patterns of TiO <sub>2</sub> films as-deposited under different atmospheres....	50
<b>Figure 2.16.</b> Anatase amount determination using Spur–Meyer’s equation.....	54
<b>Figure 2.17.</b> Representative FESEM images of the films deposited at 420°C under different atmospheres, annealed at 700°C.....	55
<b>Figure 2.18.</b> EDAX of the film deposited under high-pressure O <sub>2</sub> -rich atmosphere .....	56
<b>Figure 2.19.</b> EDAX of the film deposited low-pressure O <sub>2</sub> -rich atmosphere .....	57
<b>Figure 2.20.</b> EDAX of the film deposited under normal atmosphere .....	57
<b>Figure 2.21.</b> Cross-section of TiO <sub>2</sub> (R) buffer layer prepared in normal environment ..	58
<b>Figure 3.1.</b> Basic concept of RF-MS.....	63
<b>Figure 3.2.</b> The home-build RF-MS system used .....	69
<b>Figure 3.3.</b> Schematic diagram of RF-MS system used.....	70
<b>Figure 3.4.</b> Schematic representation of the compacting process .....	71
<b>Figure 3.5.</b> XRD patterns of HA deposited onto A or R buffer layer by RF-MS .....	74
<b>Figure 3.6.</b> Representative FESEM images of the HA films deposited onto different substrates at 150W .....	75

<b>Figure 3.7.</b> Representative high magnificated FESEM images and their EDX analysis of HA films deposited onto different substrates at 150W .....	76
<b>Figure 3.8.</b> XRD patterns of HA deposited onto stainless steel substrate by RF-MS....	77
<b>Figure 3.9.</b> XRD patterns of HA/TiO <sub>2</sub> (R)/S.S using different RF powers.....	78
<b>Figure 3.10.</b> Representative FESEM images of the HA/TiO <sub>2</sub> (R)/S.S films deposited using different RF-MS discharge powers.....	79
<b>Figure 3.11.</b> High magnificated FESEM images and their EDX of the HA/TiO <sub>2</sub> (R)/S.S films deposited using different RF-MS discharge powers	80
<b>Figure 3.12.</b> Cross-section of HA/TiO <sub>2</sub> (R)/S.S deposited using 150W power .....	81
<b>Figure 4.1.</b> Ultrasonic SPT system used .....	84
<b>Figure 4.2.</b> XRD patterns of HA/TiO <sub>2</sub> (A)/S.S thin films deposited at different temperatures .....	87
<b>Figure 4.3.</b> Representative FESEM images of the HA/TiO <sub>2</sub> (A)/S.S films deposited at different temperatures and annealed at 700°C .....	90
<b>Figure 4.4.</b> EDX analysis of the HA/TiO <sub>2</sub> (A)/S.S films deposited at 420°, 380° and 350°C respectively. ....	91
<b>Figure 4.5.</b> Representative FESEM images of typical HA/TiO <sub>2</sub> (A)/S.S films.....	91
<b>Figure 4.6.</b> XRD patterns of HA/ TiO <sub>2</sub> (A)/S.S thin films deposited at 420°C and annealed at 600°C and 700°C .....	92
<b>Figure 4.8.</b> XRD patterns of nHA coatings deposited at 420°C on different substrates .....	94
<b>Figure 4.9.</b> Representative FESEM images of the HA films deposited in different substrates. ....	95
<b>Figure 4.10.</b> EDX analysis of the HA films deposited at 420° on rutile, anatase and stainless steel respectively .....	96
<b>Figure 4.11.</b> Cross-section of HA/TiO <sub>2</sub> (R)/S.S deposited at 420°C using USPT .....	97
<b>Figure 4.12.</b> XRD patterns of Mg doped-nHA coatings deposited at 420°C in different substrates. ....	98
<b>Figure 4.13.</b> Representative FESEM images of the Mg doped-HA films deposited on different substrates.....	99
<b>Figure 4.14.</b> High magnificated FESEM images of the Mg doped-HA films deposited on rutile, anatase and S.S respectively .....	100
<b>Figure 4.15.</b> EDX analysis of the Mg-doped HA films deposited at 420° on rutile, anatase and stainless steel respectively .....	101

## LISTE OF TABLES

<b>Table 1.1.</b> Chemical and structural comparison of teeth, bone, and HA.....	3
<b>Table 1.2.</b> Comparison of different methods to deposit hydroxyapatite coating .....	8
<b>Table 2.1.</b> Values of crystallite size (D) and dislocation density ( $\delta$ ) for TiO <sub>2</sub> deposited at different temperatures.....	45
<b>Table 2.2.</b> Values of crystallite size and dislocation density for TiO <sub>2</sub> deposited at 420°C under different atmospheres, annealed at 700°C.....	53

## 1. INTRODUCTION

Hydroxyapatite coated metallic implants are largely used for the treatment of different orthopedic fractures including traumatic bone injuries. Despite the use of these implants within 20 years of clinical experience, researches in this field continue to be carried out in the aim of developing appropriate coating methods that produce nano-hydroxyapatite thin films with highly desired properties, and also to solve several issues such as preventing from orthopedic implant infections which face especially the traumatic cases characterized by high rate of bacterial contamination especially in war zones.

In this work, two advantageous techniques were used to synthesize nano-hydroxyapatite (nHA) coatings: Radio Frequency Magnetron Sputtering (RF-MS) and Ultrasonic Spray Pyrolysis Technique (USPT) were carefully studied and their parameters were investigated in order to prepare nHA films with favorite properties such as crystallinity, surface homogeneity and controlled thickness. Furthermore,  $\text{TiO}_2$  of both anatase and rutile phases were prepared using SPT to enhance nHA formation into their surfaces. Magnesium that has shown in previous studies its biocompatibility and its positive impact on bone fractures healing was additionally doped into nHA coatings synthesized by USPT.

One of this thesis purposes is the development of antimicrobial coatings for traumatic bone injuries. Thus, honey that has shown its high and quick antimicrobial activity even against Multi-Drug Resistant (MDR) bacteria has been loaded into the prepared nHA coatings, in order to provide promising and more cost effectiveness solution compared to traditional antibiotics and antimicrobial peptides (AMP).

This work has several perspectives and should be pursued by carrying out in-vitro and in-vivo tests in the aim of studying bone growth analysis, cell attachment and -most essentially- antimicrobial activity, to confirm the great potential of these antimicrobial coatings and their further use in trauma wound treatment in the future.

### **1.1. Orthopedic Implants**

Orthopedic implants are used worldwide for fixation of long bone fractures and non-unions, for correction and stabilization of spinal fractures and deformities, for replacement of arthritic joints, and for other orthopedic and maxillofacial applications. The primary aim of these devices is to provide mechanical stabilization so that optimal alignment and function of bone can be maintained during physiologic loading of bones and joints. In this way, the implants facilitate the relief of pain and more normal use of the injured limb or body part, and thus faster earlier return to function (Goodman *et al.* 2013).

### **1.2. Hydroxyapatite Coatings in Orthopedic Implants**

Metallic implants like stainless steel, titanium (Ti) and its alloys are widely used for orthopedic and dental applications because they exhibit excellent mechanical properties and biocompatibility (they are not biotoxic). However, although Ti metal and stainless steel are biocompatible, they are not a bioactive materials and hence cannot tightly bond to living bone (Zhang 2013).

Considerable research interest to develop biomedical materials with enhanced bioactivity is ongoing. Nano-hydroxyapatite (nHA)  $\text{Ca}_{10}(\text{PO}_4)_6(\text{OH})_2$  has a great chemical and structural similarity to natural bone and has been found to be bioactive: it encourages bone ingrowth by allowing a direct bond between surrounding tissue and the implanted ceramic. However, its poor mechanical properties (poor tensile strength and resistance to impact as well as their brittle nature) limit its use in direct implantation. To combine the biological performance of HA and the mechanical properties of metallic implants, the most successful approach is to apply a HA coating on the metallic implant surface (Li 2009; Goodman *et al.* 2013; Zhang 2013).

**Table 1.1.** Chemical and structural comparison of teeth, bone, and HA (Dorozhkin 2009)

Composition, wt%	Enamel	Dentin	Bone	HA
Calcium	36.5	35.1	34.8	39.6
Phosphorous	17.1	16.9	15.2	18.5
Ca/P ratio	1.63	1.61	1.71	1.67
Total inorganic (%)	97	70	65	100
Total organic (%)	1.5	20	25	--
Water (%)	1.5	10	10	--
Crystallographic properties: Lattice parameters ( $\pm 0.003 \text{ \AA}$ )				
a-axis (Å)	9.441	9.421	9.41	9.430
c-axis (Å)	6.880	6.887	6.89	6.891
Crystallinity index	70-75	33-37	33-37	100

The previous table illustrates the chemical and structural similarities between HA, enamel, dentin, and bone. The synthesized HA should be in the nanoscale to mimic that of



bone and because nHA exhibits higher bioactivity (increased osteoblast adhesion and differentiation) comparing to micrometer structured HA (Catledge *et al.* 2002). nHA is very important in biomedical field, especially in the current era of nanotechnology and bioapplications (Zhang 2013), it has proven itself to be the most successful implant coating made with 20 years of clinical experience, and nowadays, nHA-based coatings are one of the most frequently used implant coatings in the field of orthopedic surgery and trauma (Jim *et al.* 2013).

### **1.3. nHA Coating Techniques**

#### **1.3.1. Different thin film deposition techniques**

There are several methods for thin film synthesis, these methods summarized in Figure 1.1 are divided into two groups according to the nature of the deposition process (physical or chemical) and phase of the reactants in case of chemical method (gas, liquid).

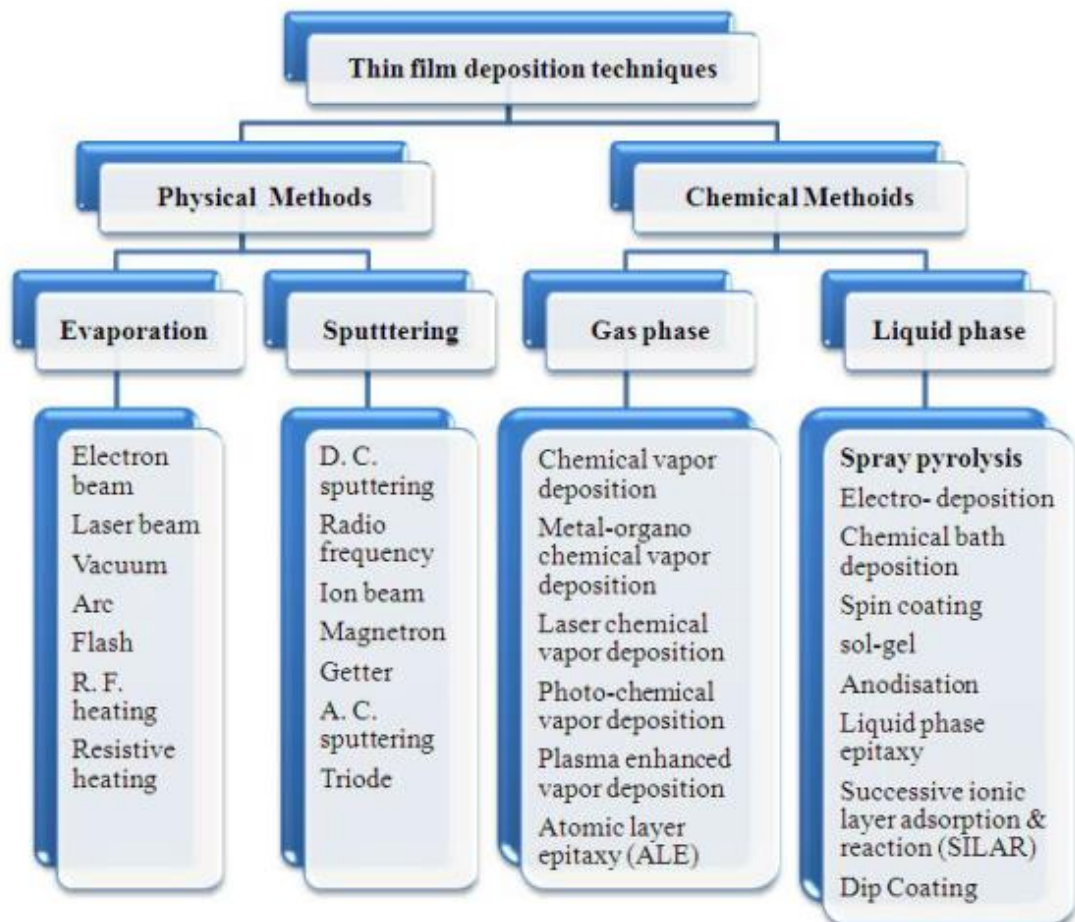


**Figure 1.1.** Various types of thin film deposition techniques (Chourashiya 2013)

The choice of a particular method depends on the next factors:

- 1- Material to be deposited
- 2- Nature of the substrate
- 3- Required film proprieties
- 4- Application of the films.

### **1.3.2. Required nHA coating proprieties**

To choose a suitable method for coating nHA, it is important to know the proprieties required in orthopedic implants application. For example, in United States, HA coatings obtained by a chosen process should verify the guidelines set by the US Food and Drug Administration (FDA): it should be more than 62% in crystallinity, and than 95% in purity, Ca/P molar ratio should be neither less than 1,67 nor more than 1,76, finally tensile strength has to be superior to 55,8 MPa (Sitharaman 2011).

Noting that bone–implant interfacial strength is greatly influenced by HA coating crystallinity. Less crystalline films are more susceptible to quick dissolution. Therefore, films crystallinity is a very important propriety that should be ensured. What is more, the tendency of cracks to appear on the coating and metal interface after implantation of the device leads to the dissociation of the coating, as the dissociation increases, there is an increasing possibility of phagocytosis and inflammation to occur. Hence, CaP coatings must be able to adhere strongly, must not possess defects as this plays a very important role in osteogenesis and bone tissue replacement. Another very important characteristic is nHA film thickness which must be a compromise among a number of limiting conditions: the thinner the coating, the better its mechanical properties, but in the first few months, very thin nHA surfaces may dissolve during the process of acquiring bone union. On the other hand, a thick coating of more than 100 $\mu$ m may suffer from fatigue failure under tensile loading (Zhang 2013).

### **1.3.2. Choice of nHA coating technique**

In fact, there is no standard protocol for producing HA thin films with perfect proprieties. Several of HA coating techniques (Table 1.2) have been used and studied extensively, every technique has its advantages and disadvantages, and differs in the proprieties and the performance -in vitro and in vivo- of films obtained.

Table 1.2 details the advantages and disadvantages of some currently available coating techniques.

**Table 1.2.** Comparison of different methods to deposit hydroxyapatite coating (Zhang 2013)

Technique	Thickness ( $\mu\text{m}$ )	Advantages	Disadvantages
Thermal spraying	30–200	High deposition rate Low cost	Line-of-sight technique High temperature Rapid cooling produces amorphous coating
Sputter coating	0.5–3	Uniform thickness Dense coating	Line-of-sight technique Time consuming Produces amorphous coatings
Electron-beam deposition	$\sim 1$	Uniform thickness Dense coating	Line-of-sight technique Time consuming Produces amorphous coatings
Dip coating	50–500	Inexpensive Can coat complex substrates	High sintering temperatures Thermal expansion mismatch
Electrophoretic deposition	0.1–2.0	Uniform thickness High deposition rates Can coat complex substrates	High sintering temperatures Difficult to produce crack-free coating
Hot isostatic pressing	0.2–2.0	Dense coating	Expensive High temperature Thermal expansion mismatch Cannot coat complex substrates Elastic property differences
Biomimetic coating	<30	Bone-like apatite formation Can coat complex substrates	Time consuming Requires replenishment and constant conditions
Pulsed laser deposition	$\sim 0.05$ –10	Coating with crystalline and amorphous Dense and porous coating Control over phases and Ca/P ratio	Line-of-sight technique Expensive High substrate temperature
Dynamic mixing Sol-gel	0.05–1.3 <1	High adhesive strength Low processing temperatures Can coat complex shapes Low cost as coatings are	Amorphous coatings Some processes require controlled atmosphere processing Expensive raw materials

**Table 1.3.** (continued) Comparison of different methods to deposit hydroxyapatite coating (Zhang 2013)

Technique	Thickness ( $\mu\text{m}$ )	Advantages	Disadvantages
Ion beam-assisted deposition	~0.03–4	Uniform thickness Dense pore-free coating High reproducibility and controllability over microstructure and composition	Line-of-sight technique Expensive Amorphous coatings
Powder plasma spray (PPS)	~30–300	High deposition rates Micro-rough surface and porosity	Line-of-sight technique High temperature Rapid cooling produces crack Poor control of chemical and physical coating parameters Nonuniform thickness Poor control of biodegradation
Liquid plasma spray (LPS) and suspension plasma spray (SPS)	~5–50	High deposition rates Pure (only HA phase) Crystalline Nearly fully dense and highly porous coating can be obtained Excellent control on the coating microstructure	Line-of-sight technique Expensive High temperature Nonuniform thickness
RF magnetron sputtering	~0.04–3.5	Uniform thickness Dense pore-free coating Can coat heat-sensitive substrates High-purity films Control over coating structure (amorphous or crystalline) and Ca/P ratio	Line-of-sight technique Expensive Time consuming Low deposition rate
Electrochemical deposition	<95	Low processing temperature Highly crystalline deposit Can coat complex shapes Control over thickness composition and microstructure	Long deposition time causes uneven thickness and formation of crack and holes

Currently, the commercially used method that produces HA coated implant materials is plasma-spray technique that has different advantages such as its high deposition rate, however it produces thick coatings ( $>50\mu\text{m}$ ) which have weak mechanical strength (Thian *et al.* 2011), and it operates at a very high temperature, which induces thermal decomposition of HA and formation of secondary mineral phases, such as tricalcium phosphate (TCP) (López *et al.* 2013). Surfaces of HA-coated implants that are high in amorphous and TCP phases are susceptible to a faster dissolution which badly affects cellular viability and proliferation. Unfortunately, plasma spraying technique has numerous disadvantages such as nonstoichiometric, and non-uniform coating, poor adhesion between the coating and the substrate, micro-cracks on coating surface, and relatively low crystallinity (Narayanan *et al.* 2008; Zhang 2013).

A very interesting alternative to plasma spraying method would be radio frequency magnetron sputtering (RF-MS). This technique produces thin films that are very well adhered, defect free and homogeneous in composition (Boyd *et al.* 2003; Byd *et al.* 2006; Coe 2008; Thian *et al.* 2011; López *et al.* 2013). The strong bond between the RF-MS coated HA and the substrate is due to mechanical interlocking and chemical bonding (Zhang 2013). Furthermore, RF-MS produces nanostructured coatings that mimic bone apatite mineral (López *et al.* 2013). This technique is chosen to be used in this work to synthesis HA nano-coatings, and it is discussed in detail in the third chapter.

Despite its advantages, RF-MS is relatively complex, time consuming, expensive and line of sight method. Hence, another alternative technique which is Ultrasonic Spray Pyrolysis Technique (USPT) is also used in this work to deposit HA thin films.

Indeed, USPT offers simplicity of the apparatus and operation, cost-effective and high crystallinity coatings, in addition to good control of films thickness (Ye and Troczynski 2008). This method is also detailed in the fourth chapter.

#### **1.4. Improvement of HA Coatings by TiO<sub>2</sub> Buffer Layer**

As cited before, Titanium is the most widely used material for orthopedic implants. Its good biological properties are due to the beneficial properties of the very thin oxide (TiO<sub>2</sub>) formed natively on Ti surface. In addition to being stable in the physiological environment, titanium oxides increase calcium ion interactions, which are important for protein and subsequent osteoblast adhesion (Xia *et al.* 2011).

It is reported in literature that the crystalline phases of titanium dioxide, anatase and rutile, have good ability to induce hydroxyapatite formation on the surface. It is also stated that HA can be formed on TiO<sub>2</sub> crystalline structure better and faster than on its amorphous structure formed naturally on titanium surface (Uchida *et al.* 2003; Xia *et al.* 2011). Therefore, coating metal substrates (titanium, stainless steel) with crystalline TiO<sub>2</sub> buffer layer is an interesting astuteness to enhance HA thin film formation.

The reason of the enhanced HA formation is its lattice match with that of anatase or of rutile (Figure 1.2): the corresponding superlattice nets have  $X_{HA}=9.42 \text{ \AA}$  and  $Y_{HA}=16.31 \text{ \AA}$  in apatite,  $X_A=9.51 \text{ \AA}$  and  $Y_A=16.08 \text{ \AA}$  in anatase, and  $X_R=9.19 \text{ \AA}$  and  $Y_R=16.39 \text{ \AA}$  in rutile. The mismatch between  $X_{HA}$  and  $X_A$  and between  $Y_{HA}$  and  $Y_A$  is 1.0% and 1.4%, respectively, whereas those between  $X_{HA}$  and  $X_R$  and between  $Y_{HA}$  and  $Y_R$  is 2.5% and 0.5%, respectively. Another justification is the fit of the HA (0001) plane to the anatase



(110) plane or to the rutile (101) plane which show a close superposition of hydrogen-bonding groups in these crystals. In addition, the hydroxyl groups of HA marked with an \* are better superposed on the oxygen atoms of anatase, marked \*\*, than on those of rutile, which are marked \*\*\*. This may lead to higher nucleation of the crystallized species of HA and more facilitated orientation in case of anatase than of rutile (Uchida *et al.* 2003).

It was proposed that formation of HA on a Titania gel –in case of wet methods- is induced by the abundant Ti-OH groups on TiO<sub>2</sub> gel surface, this is due to hydrogen bond interaction between Ti-OH groups of TiO<sub>2</sub> gel and OPO<sub>3</sub><sup>-3</sup> or OH<sup>-</sup> of HA. These hydroxyl groups (Ti-OH) of TiO<sub>2</sub> are produced by adsorption and dissociation of water, and their number is known to decrease with increasing heat treatment temperature. These Ti-OH groups are arranged on the anatase (110) surface matching the HA (0001) in a better way than on the rutile (101) due to better superposition as it is explained above. Therefore, in case of using wet methods, anatase is speculated to lead to favorable HA formation comparing to rutile (Xia *et al.* 2011), hence TiO<sub>2</sub> anatase buffer layers may be preferred to be prepared before synthesizing nHA coatings.

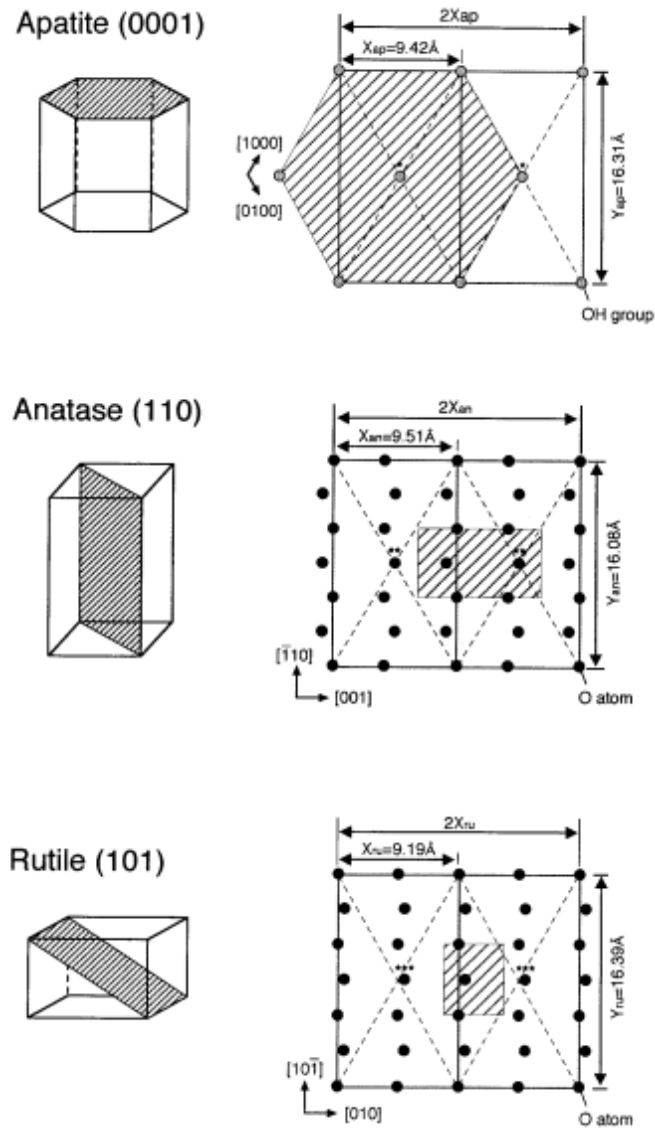


**Figure 1.2.** Crystallographic matching between HA and anatas, and HA and rutile (Uchida *et al.* 2003)

Nevertheless, some researchers have reported contradictory results: Yang *et al.* (2004) reported that for spark-anodized samples, apatite was formed most efficiently on rutile or mixtures of anatase and rutile. Under Bai *et al.* (2011) experimental conditions, a mixed

A/R nanotube structures were more efficient than the plain A structure. Tsuchiya *et al.* (2006) also found that the amount of HA particles is higher for the mixed structure than for only anatase one. All the previous writers said that the reason for this unclear situation might be the influence of surface morphology.

What is more, some researchers preferred to use TiO<sub>2</sub> rutile buffer layer for HA thin film formation, their justification is that rutile phase is more suitable for implant materials thanks to its thermodynamical stability and to its high corrosion resistance comparing to anatase (Kasemanankul *et al.* 2009).

Anyway, both anatase and rutile phases exhibit excellent biocompatibility properties, and shows fast and good nHA formation, enhanced mechanical and chemical stability of HA coating in vitro, and also superior osteoblastic cellular response (Lee *et al.* 2007). Thus, TiO<sub>2</sub> thin films -either anatase or rutile- are prepared in this work and used as buffer layers for nHA coating synthesis. Complete information about their preparation method and the obtained results with discussions are reported in the second chapter of this thesis.

### **1.5. Magnesium-Doped Hydroxyapatite Thin Films**

Synthesized HA does not well mimic the HA of natural bone: its composition is somewhat different than that of bone mineral, bone mineral is typically calcium deficient and contains different substitutions like magnesium (Mg<sup>2+</sup>), sodium (Na<sup>+</sup>), potassium (K<sup>+</sup>), fluoride (F<sup>-</sup>), and chloride (Cl<sup>-</sup>) ions. So a more appropriate chemical formula for biological HA is (Ca, M)<sub>10</sub>(PO<sub>4</sub>, Y)<sub>6</sub>(OH, X)<sub>2</sub> where M represents a substitution cation and X and Y represent substitution anions (LU 2005).

Considering cationic substitutes, Mg ion is the most abundant, amounting typically around 6 mol%, in cartilage and bone tissue during the initial phases of osteogenesis (Landi *et al.* 2008).  $\text{Mg}^+$  is the fourth most abundant cation in the human body, with an estimated 1 mol of magnesium stored in the body of a normal 70 kg adult, with approximately half of the total physiological magnesium stored in bone tissue (Staiger *et al.* 2006).

In order to improve HA coating features, nHA coatings can be doped with small amounts of Mg ions found in natural bones as cited above. Magnesium is believed to be integral for bone formation, and some researchers demonstrated its importance of Mg in early-stage bone development through in-vivo tests. A study by Landi *et al.* (2008) exposed improved response of cells adhesion, proliferation and metabolic activation, and found that synthetic HA powder containing 5,7% Mg substituting for calcium is the best and the most biocompatible Mg-HA composition due to its better chemico-physical feature.

Yajing *et al.* (2014) demonstrated also that HA coatings bond strength, bioactivity and corrosion resistance were enhanced by with  $\text{Mg}^{2+}$  incorporation. Besides, coatings with 6,6 mol% of Mg showed good biocompatibility and no adverse effect in cell culture tests.

All these findings are useful to develop Mg-doped nHA coatings which is an active area of research investigated in this work too. Synthesis of HA thin films with incorporation of magnesium through USP is reported in the chapter 4 of this thesis.

## **1.6. Antimicrobial Coatings**

### **1.6.1. Orthopedic implant infections**

Healthcare-Associated Infections (HAI), also called nosocomial infections, are considered to be the biggest healthcare related complication worldwide. Orthopedic Implant Infections (OII), a major sub-populations within the multifactorial group of HAI (Jim *et al.* 2013), still remain one of the most serious complications associated with orthopedic surgery, which can lead to prolonged hospitalization, complex revision procedures, complete failure of the implant and the need for secondary surgery for its removal, increasing the economic burden and mortality rate (Lyndon *et al.* 2014).

The major problem in orthopedic implant infection is the growth of massive mattes or biofilms of infectious bacteria which can form over the metal surface, especially roughened areas. This biofilm protects the microorganisms from the host immune system and antibiotic therapy. The treatment often necessitates surgical removal of the device in addition to prolonged courses of antibiotic therapy, both systemic and local. Thus OII is a substantial healthcare burden, and leads to prolonged patient suffering, and substantial morbidity and even mortality (Goodman *et al.* 2013).

Various infections strike roughly 2 million people annually in the U.S. Orthopedic implant infection rates range from 0.3% to 8.3% (Le 2013) without taking trauma implants into account: Trauma implants or implants for fracture fixation and stabilization, like plates, screws and stabilizing frames, have been described to have an even the highest risk for infection (Jim *et al.* 2013) . Wounds from modern

high-energy blast trauma mechanisms are unique: Blast trauma wounds are characterized by severe composite tissue damage, large zones of injury, complex injuries, open fractures, the high rate of bacterial contamination in war zones and extensive devitalization (Kumar *et al.* 2010). Patients with these open fractures are at higher risk of deep wound infections, with rates ranging from 6 to 33% , this risk increases with the severity of soft tissue injury and fracture severity (Fuchs *et al.* 2011).

### **1.6.2. Use of antibiotics**

Since the discovery of antibiotics, (implant) infections have been reduced and implant infections have become less lethal and can even be cured, the use of antibiotics has been shown to dramatically reduce the incidence of implant related infections (Jim *et al.* 2013; Goodman *et al.* 2013).

Systemic administration of antibiotics is accepted as standard practice to control bacterial contamination and prevent infection after surgery, however, it may have limited efficacy: as cited before, bacteria can colonize the surface of an implant, forming a biofilm of an extracellular polysaccharide matrix (glycocalyx) that protects the bacteria from the antimicrobial action of systemic antibiotics. Furthermore, systemically delivered antibiotics might not reach the medullar canal of long bones when blood flow has been disrupted by trauma. Therefore, implant-related infection often requires aggressive treatment including long-term antibiotic therapy (Fuchs *et al.* 2011) which can cause toxicity and increase resistance, thus, may lead to drug resistance systemic and local toxicity, and potentially compromise bone growth, immune system surveillance and implant osseointegration (Goodman *et al.* 2013).

Various systems have been developed for the local delivery of antibiotics at the tissue-implant interface to benefit from several advantages over systemic drug therapy (Lyndon *et al.* 2014):

1. Low doses required
2. Greater control over toxicity and bioavailability of dose
3. Less susceptibility to promoting antibiotic resistance
4. Controlled release from surfaces of combination devices directly to site
5. Avoidance of systemic drug exposure

Thanks to these advantages, Antibacterial coatings have attracted wide attention as a technique to release antimicrobial agents (Stigter *et al.* 2004a; Zhang 2013; Lyndon *et al.* 2014). The problem is that biomaterial surfaces that facilitate host cell adhesion, spreading, and growth are also favorable to microorganisms that share many of the same adhesive mechanisms as host cells. On the other hand, surfaces and coatings designed to prevent bacterial colonization and biofilm formation may not effectively integrate with host tissues. Thus, the challenge is to develop infection-resistant coatings without impairing local host immune competence or the potential for tissue integration (Goodman *et al.* 2013).

Other important point that has to be considered is the optimal release kinetics: the system should deliver those drugs for the time period required for maximal and complete effect, and concentrations below the minimum therapeutic dose must be avoided as extended exposure of bacteria to sub-therapeutic drug concentrations can lead to the development of resistance (Lyndon *et al.* 2014).

Early stage infection occurs after implantation when the host local defense system is impaired due to surgical trauma. At this critical time, bacteria may colonized on implant surface (Kazemzadeh-Narbat *et al.* 2012). Thus, delivery system must exhibit initially high release rates to counter increased infection risk immediately following surgery, followed by an extended long period of lower concentration drug release conforming to therapeutic efficacious dose to prevent latent infection (Lyndon *et al.* 2014).

### **1.6.3. Multi Drug-Resistant (MDR) bacteria**

Another challenge that faces the antibacterial coatings in specified to war injuries (mostly military ones) is the presence of multidrug-resistant (MDR) bacteria in extremity wounds. Most frequently identified resistant strains are methicillin-resistant *Staphylococcus aureus* (MRSA), *Klebsiella pneumoniae* (KP), *Pseudomonas aeruginosa* (PA), and *Acinetobacter baumannii* (AB) ( Mody *et al.* 2009; Kumar *et al.* 2010; Yin *et al.* 2013). AB is referred to as 'Iraqibacter' due to its seemingly sudden emergence in military treatment facilities during the Iraq war ( Davis *et al.* 2005; Anand R. Kumar *et al.* 2010). Carbapenem-resistant enterobacteriaceae (CRE) has been found to be carried by Syrian patients wounded in the country's civil war (Rana 2014), and *Enterobacter cloacae* infections are seen commonly in burn victims (Adam 2013). This is the main reason why antimicrobial coatings, based on disinfectants or non-traditional antibiotics must have great interest in the research and development of such coatings.



#### **1.6.4. Use of Antimicrobial Peptides (AMP)**

After more than two decades of research and development, antimicrobial peptides (AMP) are non-traditional antibiotics and are now well recognized as promising novel agents against MDR pathogens. They often have broad-spectrum bactericidal activity against both Gram-negative and Gram-positive bacteria, and due to the complex mechanisms of AMPs; bacteria are killed more rapidly than with conventional antibiotics and it is extremely difficult for bacteria to develop resistance (Anand *et al.* 2010; Kazemzadeh-Narbat *et al.* 2012, 2013).

In a very recent study made by Kazemzadeh-Narbat *et al.* (2012, 2013) a short cationic AMPs with high antimicrobial activity, namely HHC36 (KRWWKWWRR) has been loaded into some implant coatings, and showed that it could effectively kill *S. aureus*, and *P. aeruginosa* bacteria without negatively affecting osteoblast cells, and did not impair *in vivo* bone growth onto the implants. A substantial amount of HHC36 was loaded on CaP coating, this was attributed to the affinity between the positively charged side groups of HHC36 and negatively charged phosphate groups in the CaP and the porous structure of the coating.

#### **1.6.5. Limitation of AMP use in implant coatings**

Despite their efficiency in preventing orthopedic implants from infections, or even in healing infection caused by MDR bacteria, AMP have major disadvantages that limit their use as antimicrobial agents in implant coatings:

Firstly, AMP cannot be incorporated into coatings prepared by techniques that use high processing temperatures (Stigter *et al.* 2004b; Lyndon *et al.* 2014).

Secondly, even if AMP can be loaded through immersion process (dip coating) by physical adsorption into HA coatings –thanks to HA high porosity- after coatings synthesis at high temperature, the amount loaded is very limited and its release kinetics found to be much burst:

- In the previously mentioned Kazemzadeh-Narbat *et al.* (2013) study, HHC-36 was loaded into TiO<sub>2</sub> nanotubes via vacuum-assisted physical absorption and demonstrated excellent functionality. However, the technique is considered complicated and the release is still quick.

- In another recent research carried out again by Kazemzadeh-Narbat *et al.* (2010) HHC-36 was loaded into CaP via immersion process (physical adsorption), yet the elution kinetic is very fast (71.2% of AMP was eluted in the first 30 min; and 90.8% after 1-day).

Another approach of synthesizing antimicrobial coatings by sol-gel method was also investigated and antibiotic release from the biodegradable thin films prepared could be controlled and even became slower than that from HA coatings. Layer-by-layer self-assembly coating technique can also significantly slow the release of antibiotics (Goodman *et al.* 2013). Although, sol-gel method can lead to amorphous coatings and self-assembly technique has the disadvantage of time consuming (Zhang 2013).

Finally, AMP are very expensive which made their use very costly and unavailable especially for developing countries and war regions where the risk of orthopedic infections and MDR bacteria development are the highest. The very elevated price of AMP (for example 1 mg of the antimicrobial peptide LL-37 costs 413 Euro (Sigma-Aldrich)) is affected to their very complicated biological synthesis way which is considered the biggest problem that limit AMP use in antimicrobial orthopedic implants.

#### **1.6.6. Honey as a promising antimicrobial agent in antimicrobial coatings**

As a very interesting and new alternative to Antimicrobial peptides to prevent the infection by MDR bacteria, we propose to incorporate honey in nHA coatings; in fact, honey has good antibacterial activity against numerous microorganisms of many different genera, moreover, no honey-resistant phenotypes have been detected, different studies proved its impact on biofilm formation and concluded that it represents an attractive antimicrobial treatment with great potential to be used to treat wound infection with multidrug-resistant bacteria in future (Maddocks and Jenkins 2013).

Honey as a wound dressing has re-emerged into medical practice, and particularly into management of acute and chronic wounds. Today, medical honey wound dressings are widely used for management of a large number of wound types; among others, these also include treatment of burns that occur very highly in wars (Goerdts *et al.* 2013).

According to different studies, honey shows very high activity and resistant-isolation against MDR bacteria developed in war wound injuries such as MRSA (Goerdts *et al.* 2013), *Staphylococcus aureus*, *Pseudomonas aeruginosa*, *Enterobacter cloacae*, and

*Klebsiella oxytoca* that were killed within 24 h by 10%–40% (vol/vol) honey (Kwakman *et al.* 2008), also *Enterobacter cloacae* and *Acinetobacter baumannii* were found to be extremely sensitive to honey at concentrations 50% and 100 % (Adam 2013). Therefore, a great recent interest in the antimicrobial activity of honey against important antibiotic-resistant human pathogens is perceived (Ratcliffe *et al.* 2014) .

For this reason, we proposed to investigate honey in our study to innovate very good antimicrobial coatings for war wound implants. To the best of our knowledge, no one has investigated the use of honey in antimicrobial implant coatings which makes this initiative very attention-grabbing, however it requires further works: this research should be pursued by carrying out in-vitro and in-vivo tests in the aim of studying bone growth analysis, cell attachment and -most essentially- antimicrobial activity, to confirm the great potential of these antimicrobial coatings to be used in future in trauma wound treatment.

#### **1.6.7. Stainless steel as implants based-material in trauma surgery case**

Titanium implants are actually standard in trauma surgery. One main argument for its use is supposedly better biocompatibility and reduced infection rates predominantly on the basis of less potential corrosion. These suppositions arise from in-vitro and in-vivo studies, but not from clinical evidence as reported by Dr. Sebastian Weckbach who carried out with his colleagues a retrospective study to challenge the dogma on inferiority of stainless steel implants for fracture fixation. By evaluating data -obtained from a trauma center in the United States- of patients had fractures fixated with stainless steel plates, it was found that surgical revision and complication rate of the fractures treated

with stainless steel plates is less than those treated with titanium plates, this result led implants Weckbach *et al.* (2012) to conclude that steel implants for fixing fractures would be a “safe and economically viable alternative to the widespread use of titanium.

In the light of these considerations, stainless steel is chosen in the present research to be used as metal implant material coated first with  $\text{TiO}_2$  buffer layer that inhibits its corrosion and also enhances nHA coating formation on its surface. The resulted HA/ $\text{TiO}_2$ /Stainless steel system with incorporating honey as an antimicrobial agent is expected to be an excellent system for traumatic bone injuries application.

## **2. PREPARATION OF TITANIUM OXIDE BUFFER LAYER BY SPRAY PYROLYSIS TECHNIQUE**

### **2.1. Introduction to the Second Chapter**

This chapter explains the method used to prepare TiO<sub>2</sub> buffer layer that is Spray Pyrolysis Technique (SPT), its basics, equipment and parameters. It also gives the experimental details from the substrate cleaning to the formation of TiO<sub>2</sub> thin films. Under “Results and Discussions” section, effects of different process parameters are studied. Finally, in “Conclusion” section, the optimized factors to get the best buffer layer are determined.

### **2.2. Materials and Methods**

Comparing to physical methods, chemical methods are more economical and easier and have some advantages. However, they have also some drawbacks. In fact, there is no ideal method to prepare thin films which will satisfy all the requirements. Of all, we chose the Spray Pyrolysis Technique, one of the chemical methods, to synthesize TiO<sub>2</sub> layers, because it is a simple, practical and low-cost technique largely used for the preparation of oxide thin films.

#### **2.2.1. Spray Pyrolysis Technique (SPT)**

##### **Basics of SPT**

Among various chemical methods, SPT is very popular because of its applicability to produce variety of materials (Perednis and Gauckler 2005). The principle of SPT is the pyrolytic (endothermic) decomposition of salts of a desired compound to be deposited (Shinde 2012).

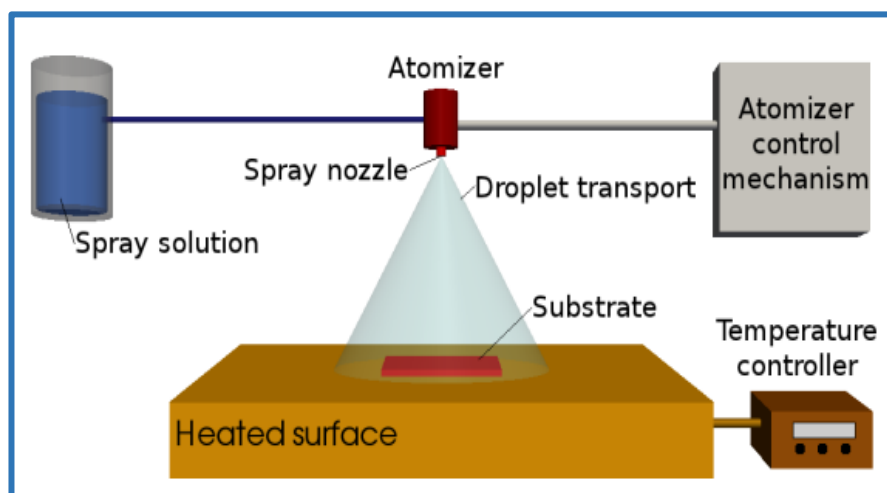


**Figure 2.1.** General schematic of a spray pyrolysis deposition process (Filipovic *et al.* 2013)

Because of the thermal energy provided by simultaneous heat treatment of the substrate, sprayed droplets undergo a pyrolytic decomposition and forms a single crystalline or cluster of crystallites when reaching the surface of the substrate heated. The solvent and other volatile by-products escape in the vapor phase. The heat treatment provides also subsequent recombination of constituent species, sintering and crystallization of the clusters on the substrate surface, which results in a coherent film.

### **Advantages of SPT**

Apart from its simplicity, spray pyrolysis technique has a number of advantages (Shinde 2012; Chourashiya 2013; Filipovic *et al.* 2013):

- 1- Spray pyrolysis is low-cost technique
- 2- It can prepare oxide thin films with large area, high quality adherence and uniform thickness.
- 3- Substrates with complex geometries can be coated.
- 4- It is a very simple method: it does not require high quality targets and /or substrates nor does it require vacuum at any stage, which is a great advantage if the technique is to be

scaled up for industrial applications.

5- The deposition rate and the thickness of the films can be easily controlled over a wide range by changing the spray parameters. Thus eliminating the major drawbacks of chemical methods such as sol-gel which produce films of limited thickness.

6- A major advantage of this method is operating at moderate temperature (100-500°C)

7- It can produce films on less robust materials. It offers an extremely easy way to dope films with virtually any elements in any proportion, by merely, adding it in some form to the spray solution.

8- By changing composition of the spray solution during the spray process, SPT can be used to make layered films and films having composition gradients throughout the thickness.

8- Unlike high power methods such as radio frequency magnetron sputtering (RFMS), it do not cause local over-heating that can be harmful for materials to be deposited. There are virtually no restrictions on substrate material, dimension or its surface profile.

Spray pyrolysis technique has been largely used to fabricate coating on different substrates (glass, ceramic or metallic..), and thanks to its simplicity and its good productivity on a large scale, it offered the most attractive way for the formation of thin films of metal oxides (Shinde 2012). For this reason, it has been chosen in different applications (solar cells, anti-reflection coatings, and gas sensors, solid oxide fuel cells..), studied in details and comprehensively reviewed by Mooney and Radding (1982), Albin and Risbud (1987), and recently by Perednis and Gauckler (2005) and Guild *et al.* (2014). Therefore, we chose Spray Pyrolysis Technique to prepare Titanium Oxide layers, and we have changed the process parameters to find the optimized ones that give full crystalline and uniform nano-coating of TiO<sub>2</sub>.



### **SPT process aspects**

The SPT process aspects such as: precursor solution, its atomization, transport and decomposition strongly affect the structural and morphology of thin films synthesized.

#### **a) Precursor solution**

The true solutions, colloidal dispersions, emulsions, and sols can be used as aerosol precursors. Aqueous solutions are usually used due to ease of handling safety, low-cost, and availability of a wide range of water-soluble metal salts. The solute must have high solubility, which increases the yield of the process (Shinde 2012).

In general, due to their high solubility in water, metal chlorides and oxy-chlorides are used for industrial production. Nitrates, acetates and sulfates are also water-soluble metal salts but can introduce impurities, which adversely affect the film properties. Because of their high decomposition temperature, the use of metal sulfates is limited. Therefore, hybrid systems in which one of the components is added via a solution have also been reported (Shinde 2012).

#### **b) Precursor solution atomization**

The first essential step of SPT is the generation of uniform and fine droplets by the nozzle which depends on the type and the geometry of the spraying nozzle and also on the pressure of the carrier gas. Three important atomization methods have been used: pneumatic, ultrasonic, and electrostatics (Perdnis 2003). Every atomizer differs in droplet size and velocity, and in rate of atomization:

- The importance of droplet velocity resides in influencing the heating rate and the residence time of the droplet during spraying.

- Getting small droplets is preferable to obtain thin films in good quality. When using pneumatic nozzles, the droplets size decreases by the increase of carrier gas pressure. But a very high pressure leads to rapid splashing of droplets which causes the substrate temperature to drop. On the other hand, if the carrier gas pressure is too small, larger droplets fall onto the substrates. Hence, it is important to optimize the carrier gas pressure. Noting that droplets characteristics depend not only on the type of atomizer, but also on the solution proprieties (density, viscosity, and surface tension).

### c) Aerosol transport

The result of evaporating the droplets transported by the carrier gas delivered by the nozzle is called aerosols. The pyrolytic decomposition that follows the transport of these aerosols is strongly dependent on the substrate temperature, thus its optimization is critical in the aim of obtaining of thin films with desired properties.

The influence of forces that determine droplets trajectory and evaporation was examined by Sears and Gee (1988) who investigated the mechanism of SnO<sub>2</sub> trajectory film growth. Gravitational, electric, thermophoretic and Stokes forces were taken into account:

1) Gravitational force: it pulls the transported droplets downward and depends on their mass. For small droplets the force of gravity is too small, so droplets have the time to be fully evaporated before arriving to the substrate surface. For larger particles, the force of gravity is the driving force behind the droplets transport and may not allow them to evaporate before reaching the surface.

2) Electrical force: it is applicable to spray pyrolysis systems which include an additional electrical source governing the droplet's trajectory.

Ultrasonic atomizers are electrically driven, whereby an electric generator is vibrated at ultrasonic frequencies through a titanium nozzle. Increasing the frequency can result in smaller droplet sizes. Electric spray deposition (ESD) atomizers use a strong electric field at the liquid-gas interface to generate charged droplets. Hence, there are no additional contributions from an electrical force in the case of air blast atomization systems and the droplets transport is driven downwards only by the gravitational force and the initial velocity, while for spray pyrolysis deposition using ultrasonic or ESD atomizers, the electrical force is the main component which drives the droplets downwards.

3) Stokes force: It is caused by the air friction of droplets during their transport. So they experience a drag due to the air resistance. The Stokes force is a factor of the particle's velocity and size. For large droplets which move with a high velocity, this experience retarding force is very high.

4) Thermophoretic force: it pushes the droplets away from the substrate hot surface, because the gas molecules from the hotter side of the droplet rebound with higher kinetic energy than those from the cooler side. It was then concluded that the film grows from the vapor of droplets passing very close to the hot substrate.

This thermophoretic force depends on the thermal gradient in the transport environment and begins to dominate several millimeters away from the substrate in case of pressure spray deposition. More than pushing away the aerosols, the increased temperature has additional effects on the droplets size that is reduced due to droplet evaporation.

#### d) Decomposition of precursor

The precursor vaporization and decomposition occurs after solvents evaporation and precipitate formation. These steps may happen before arriving to the substrate or in its surface depending on the droplets size and the adjusted temperature.

Figure 2.2 describes the main 4 processes that may take place (Fiddes 1993):

A- The larger the droplets, the greater the likelihood that the solvent will not have evaporated before reaching the substrate and the precursor material approaches the substrate as a solute in solvent, so the droplets splash onto the substrate.

B- If the droplets sizes are smaller, then a larger proportion of the solvent is vaporized before impinging on the surface, so that the precursor lands as a dry precipitate where decomposition occurs.

C- For even smaller droplets sizes, not only does the solvent vaporizes but also the precursor or precursors, and these species diffuse to the substrate surface as vapors. This vapor diffusion to the substrate surface results in subsequent decomposition/oxidation and a CVD-like process.

D- Finally for very small droplets sizes all three steps, solvent evaporation, precursor volatilization and precursor pyrolysis all occur soon after the spray leaves the gun. This will result in films with low adherence to the substrate.

It is important to know that these process can be carried out for a fixed droplets size but by varying the adjusted temperature (Figure 2.2).

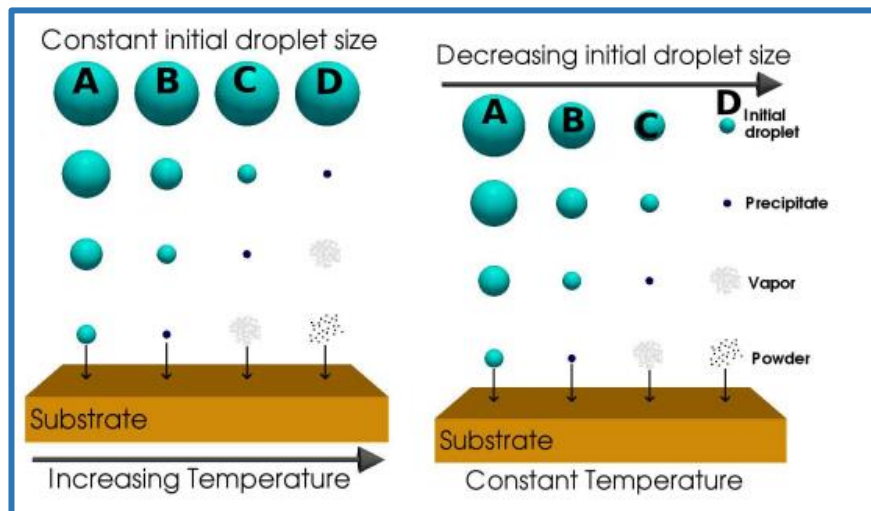


**Figure 2.2.** Spray pyrolysis droplets modifying during their transport (Filipovic *et al.* 2013)

The CVD-like deposition (C process in Figure 2.2) is the most desired one because it yields to a high quality film. This process happens as it is previously explained when the droplets evaporate and the precipitate forms early, and when this precipitate reaches the immediate vicinity of the substrate and subsequently converted into a vapor state and undergoes a heterogeneous reaction through the following steps (Filipovic *et al.* 2013):

- 1) Reactant molecules diffuse to the surface.
- 2) Adsorption of some molecules at the surface.
- 3) Surface diffusion and a chemical reaction, incorporating the reactant into the lattice.
- 4) Diffusion of the product molecules from the surface.

The next figure recaps the processes that can happen depending on the substrate temperature, where the CVD-like deposition can be reached by keeping the temperature between intermediate to high.

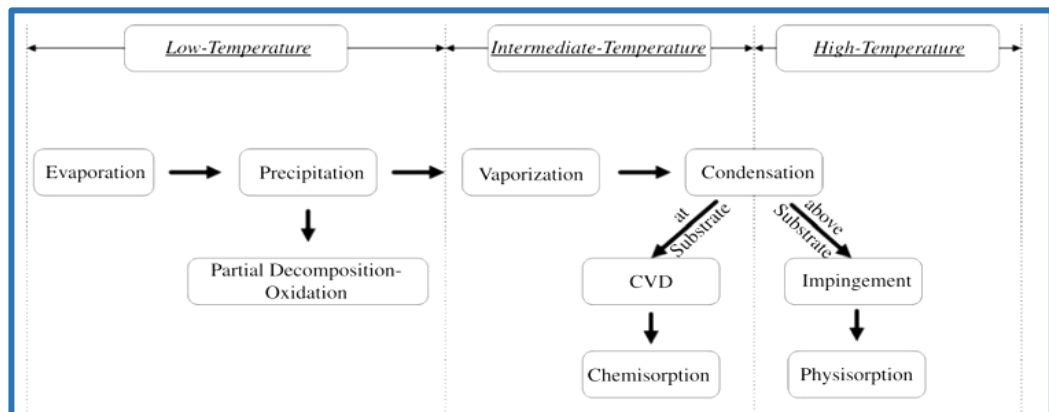


**Figure 2.3.** Summary of SPT processes as a function of temperature (Nakaruk and Sorrell 2010)

### SPT process parameters

The thin film formation by SPT and film properties depend significantly on the next parameters: carrier gas flow rate, nozzle-to-substrate distance, droplet radius, solution concentration, solution flow rate, chemical composition of the carrier gas and/or environment, and, most importantly, substrate temperature. An ideal deposition can be carried out when the droplets approach the substrate just as the solvent is fully evaporated. So it is very crucial to well control the process parameters in order to get coatings with desired structural and morphological properties. Noting that a desired film thickness can be obtained by changing the distance between the nozzle and substrate, solution concentration and quantity, and finally substrate temperature.

### 2.2.2. Spray Pyrolysis Equipment

Figure 2.4 illustrates the schematic diagram of the SPT equipment used in this work.

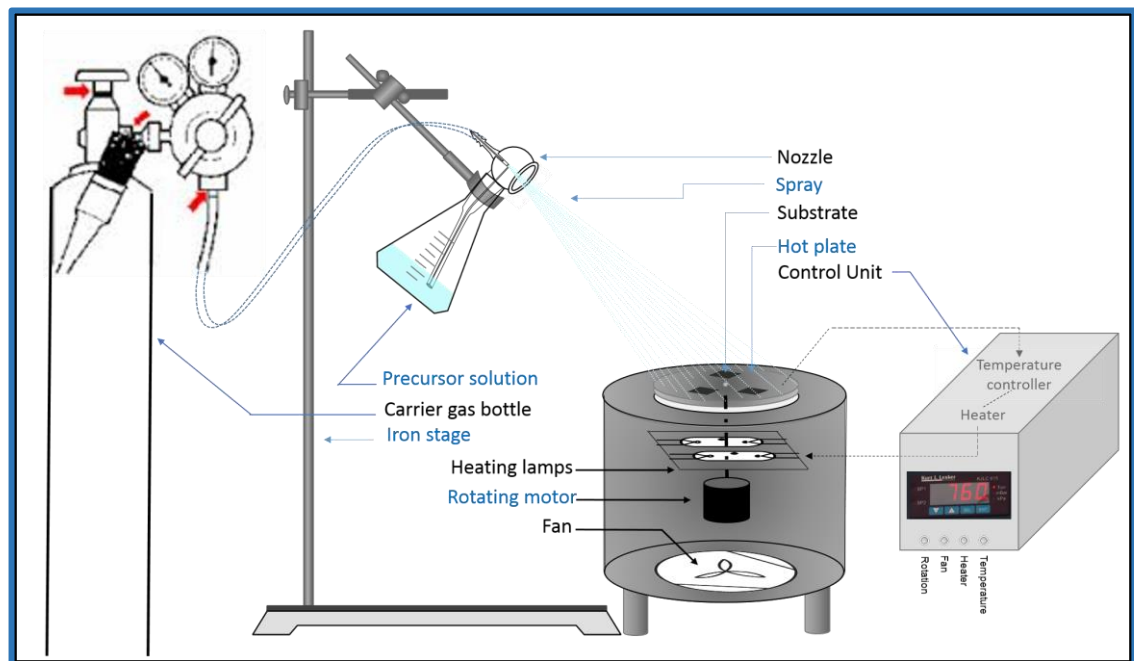


**Figure 2.4.** Schematic diagram of the home-made SPT equipment used

The main constituents of this equipment are:

a) Spray nozzle

Made up of glass with a precise geometry to create fine droplets. When delivering the carrier gas with good pressure, the vacuum will be created at the nozzle tip, and the precursor solution will get automatically sucked in the fine tube, when arriving to the tip it starts to be sprayed in fine droplets carried by the pressed gaz.

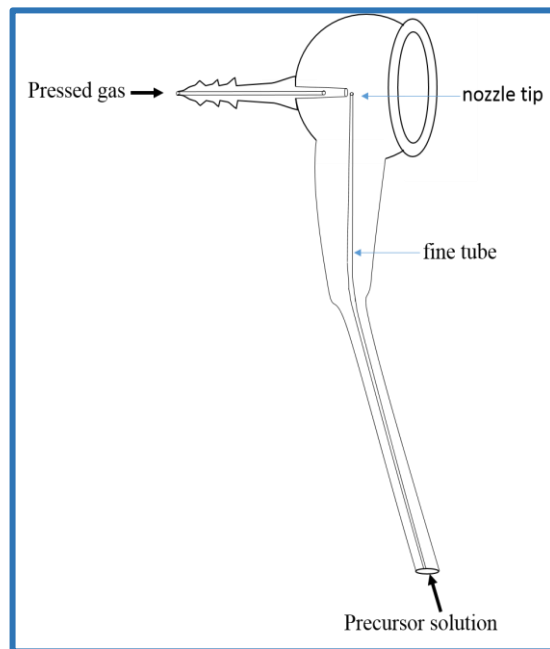


**Figure 2.5.** Pneumatic atomizing nozzle used

b) Iron stage

It is used to adjust the spraying nozzle position to ensure the direction of the droplets from the nozzle to the substrates.

c) Hot plate with temperature regulation arrangement

Heating the substrates surface is very important aspect in PST as it is explained before. It is ensured in our system by heating the substrates porter (the plate) using halogen lamps. The temperature should be kept constant during deposition. Thus, it is regulated by connecting the halogen lamps to a temperature controlling unit that:

- Determines the hot plate temperature using a thermo-couple.
- Receives its signal which is proportional to the temperature read.
- Switches on/off the power supply delivered to the lamps according to the temperature read, in the aim adjusting it at the set point (the desired temperature).



This cycle is repeated during the whole deposition time. After finishing, the temperature is regulated to fall down slowly, to conserve the lamps and to avoid quick cooling of substrates.

d) Rotating motor

Used to rotate the plate in the aim of providing a homogenous substrates temperature, equal distribution of aerosols, and therefore almost identical thin films formation.

e) Laboratory Fume Hoods

Since several gases are emitted after precursor decomposition, it is necessary to fix the SPT system inside an Airtight Chamber or a Laboratory Fume Hoods. The outlet of chamber is fitted to exhaust fan to remove the gases evolved.

### **2.2.3. Preparation of TiO<sub>2</sub> thin films**

#### **Substrates cleaning**

The purpose of this step is to remove contaminants (grease, oil particles, air dusts..) from substrates surface without damaging it. In thin film deposition process, substrates cleaning is an important factor to get reproducible films as it affects the smoothness, uniformity, adherence and porosity of the films (Shinde 2012).

The stainless steel piece was cut in small specimens with dimensions of (1 cm x 1 cm x 0,127 cm). The specimens were used as substrates and ultrasonically cleaned in methanol for 10 minutes, rinsed with deionized water, ultrasonically cleaned again for 10 minutes but with acetone, rinsed again with deionized water but this time in the ultrasonic bath for 10 minutes. The substrates are then dried in air under normal atmosphere conditions.

### **Precursor solution preparation**

The precursor solution is composed of:

- Titanium (IV) Isopropoxide (TTIP) as a titanium source. ( $\text{Ti}[\text{OCH}(\text{CH}_3)_2]_4$ , molecular weight= 284.22 g/mol, Sigma-Aldrich, India)
- Acetylacetone (AcAc) as a stabilizer. ( $\text{C}_5\text{H}_8\text{O}_2$ , molecular weight= 100.12 g/ mol, Merck Schuchardt OHG, Germany)
- Ethanol as solvent ( $\text{CH}_3\text{CH}_2\text{OH}$ , molecular weight= 46.07 g/mol, Sigma-Aldrich, India)

The concentration of the precursor solution is 6 vol.% of TTIP, and TTIP:AcAc volume ratio is 1:2. For every essay, 100 ml of the precursor solution is prepared by mixing the previous ingredients, stirred (which forms a yellowish colored solution) and then put down in the conical flask to be sequentially sprayed through the nozzle.

Even if TTIP is completely dissolved in Ethanol, AcAc should be added to the solution otherwise the nozzle tip can be closed off by a weight powder formed due to the intimate contact between TTIP and the environmental humid air when spraying.

### **Formation of $\text{TiO}_2$ buffer layers**

After placing the substrates in the plate, heating it till the desired temperature, installing the flask that contains the precursor solution and rotating the plate by increasing the rotating motor voltage, the spray process can be started by opening the carrier gas valve and its flow rate is controlled also using flow meter.

In order to find the optimized SPT process to get the best TiO<sub>2</sub> layer, the substrate temperature was varied from 320, 350, 380, 400 until 420°C when keeping the other parameters constant (concentration of solution (6%), quantity of the spraying solution (100 ml), distance (35 cm)). The compressed dry air was used as carrier gas at a flow rate of about 7 LPM. Deposition was carried out in some experiments under a flow of oxygen directed to the substrates to study its adding effect. After optimizing the temperature, the nozzle-to-substrate distance was varied (30 and 35 cm). It is worth noting that a post-heat treatment of all the prepared films was carried out at 700°C for one hour in normal atmosphere using a 3 Zone-Tube Furnace (PZE 12/50/500, Protherm Furnace, Turkey).

#### **2.2.4. Coatings characterization methods**

The evaluation of crystallinity and composition of the prepared buffer layers and also for the synthesized nHA coatings in the next chapters (chapter 3 and 4) was carried out using an X-Ray Diffractometer (Cu K<sub>α</sub> radiation ( $\lambda=0.154$  nm), GNR APD 2000 PRO, Ataturk University) ( $\lambda=0.154$  nm). Data were collected from  $2\Theta=20^\circ$  to  $70^\circ$  with a scanning step of 0,05.

The morphology and cross-section of the coatings was examined by a high resolution Field Emission Scanning Electron Microscope (Quenta 450 FEG FE-SEM; Erzincan University). Elemental analysis was carried out by energy dispersive X-ray spectroscopy (EDS) detector connected with SEM.

## 2.3. Results and Discussions

### 2.3.1. Effect of post-deposition heat treatment

The crystallinity of  $\text{TiO}_2$  deposited films, before and after heat treatment, was compared through their XRD patterns shown in Figure 2.6.

The as-deposited films prepared at substrate temperature below  $400^\circ\text{C}$  are amorphous since there are no titanium dioxide peaks appeared in their XRD graphs, however they become crystallized after being annealed at  $700^\circ\text{C}$ .

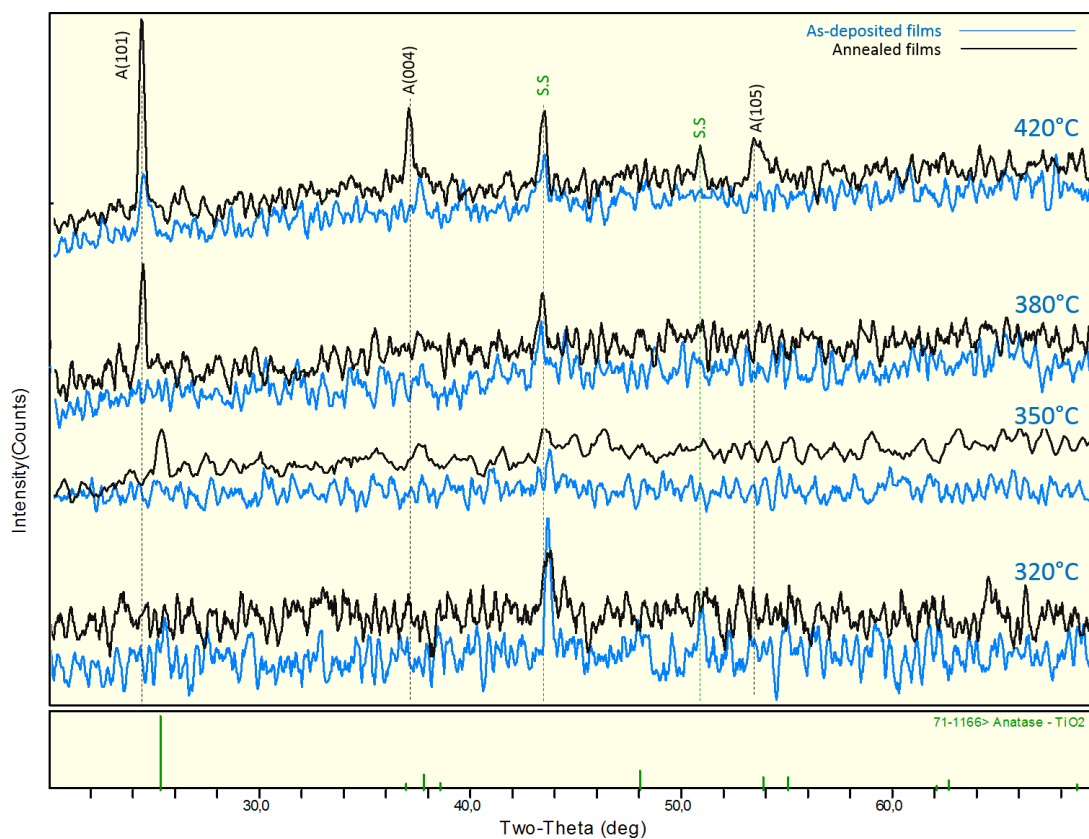


**Figure 2.6.** XRD patterns of films before and after heat-treatment ( $D=35\text{cm}$ , with  $\text{O}_2$ )

On the other hand, the as-deposited films at temperature equal or above 400°C under oxygen-rich atmosphere were already crystallized but TiO<sub>2</sub> characteristic peaks intensities has been augmented, which indicates that their crystallinity degree has been enhanced thanks to the heat treatment. In fact, heat treatment provides the energy necessary for the diffusion of film molecules and for their rearrangement in more ordered and stable form which is the crystalline form.

The identification of TiO<sub>2</sub> crystalline phase formed was done using the software: *Materials Data - Jade XRD pattern processing, version 6*. It was found according to the Standard JCPDS card no:71-1166 that TiO<sub>2</sub> crystalline phase formed is the anatase which its peaks are clearly detected at 25,3°, 37,6° and 48° corresponding to (101), (004) and (200) diffraction planes respectively.

An exception is observed for the films deposited without adding O<sub>2</sub> at temperature above 400°C, of which other peaks corresponding to the rutile phase appeared after annealing at 700°C, this case will be discussed in details in a next section about the effect of oxygen.

### **2.3.2. Effect of substrate temperature**

Figure 2.7 illustrates the XRD patterns of films deposited at a distance equal to 35cm, under O<sub>2</sub>-rich atmosphere, at different temperatures after their post heat treatment.

In all the XRD spectra -except the spectra of the film deposited at 320°C- the main characteristic peak of TiO<sub>2</sub> corresponding to the (101) crystal plan of the anatase phase is observed. Additional minor peaks along (004), (200) and (105), planes are also observed with the rise of the substrate temperature.

Intensities of (101) anatase peak and the other minor peaks increase progressively as the substrate temperature increases, which illustrates the improvement in films crystallinity. Similar results are reported by other writers (Castañeda *et al.* 2003; Oja *et al.* 2004; Nakaruk *et al.* 2010; Shinde 2012). This can be explained by explaining the different processes that take place by virtue of temperature:

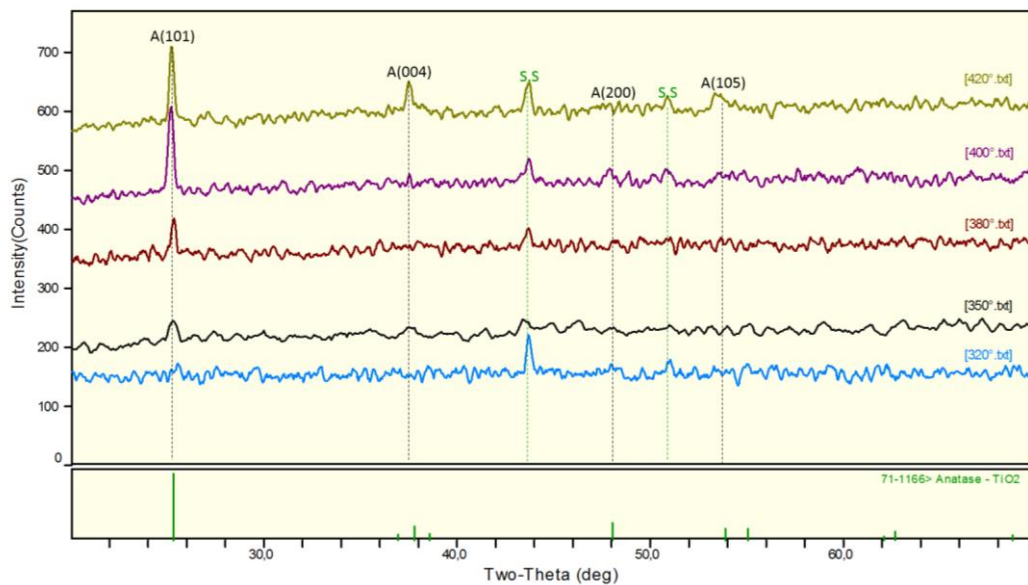


**Figure 2.7.** XRD patterns of  $\text{TiO}_2$  thin films deposited at different temperatures

For the films deposited at  $320^\circ\text{C}$  which is considered low, the thermal gradient is not sufficient to miniaturize the droplets which approach the substrate in their big form and precipitate in its surface as an amorphous salt ( $\text{Ti}[\text{OH}]_4$ ) (Process A).

For the films deposited at  $350^\circ$  and  $380^\circ\text{C}$ , the droplets are greatly evaporated and the aerosols formed precipitate before arriving to the surface, then the formed precipitates oxidize partially when arriving to the substrate surface (Process B). Consequently,  $350^\circ$ - $380^\circ\text{C}$  temperatures are considered intermediate and hence not suitable to establish a perfect deposition process.

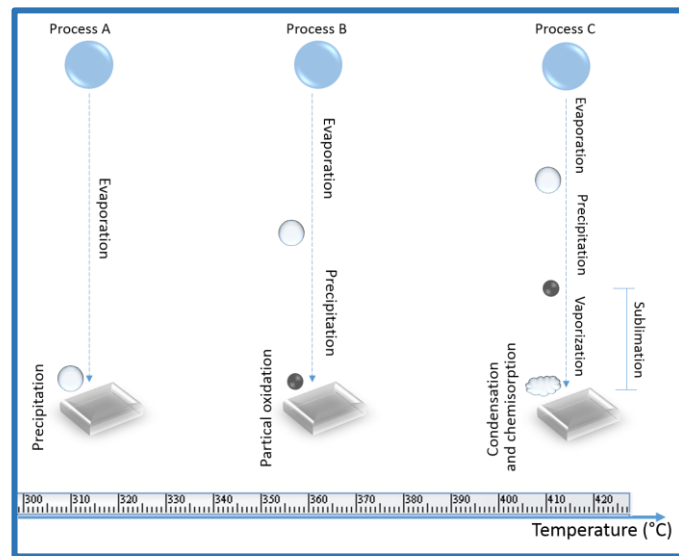


**Figure 2.8.** Effect of substrate temperature on SPT processes

For the films deposited at 400° and most importantly 420°C, thermal gradient is adequate to diminish the droplets size and to extensively evaporate them, and to cause an early precipitation of their aerosols. The precipitates obtained sublime immediately just before touching the substrate surface, and when their vapor come into collision to the surface, it oxidize subsequently and be chemically adsorbed (CVD-like process, process C in Figure 2.2). In conclusion, substrate temperature nearly equal to 420°C is considered in our case an intermediate to high temperature, necessary to carry out the most desired CVD-like mechanism that provides the synthesis of well crystallized and highly adhered TiO<sub>2</sub> films.

Nakaruk and Sorrell (2010) have summarized in Figure 2.9 the different processes discussed above and the proprieties of the resulted TiO<sub>2</sub> films deposited in glass. In this illustration, the third process is the favorite one (which takes place in our case at 420°C) that insures the best thin film proprieties (crystallinity, hardness..etc).

Process	Aerosol Spraying I (liquid only)	Aerosol Spraying II (liquid → precipitate)	Chemical Vapor Deposition (liquid → vapor)	Dried Spray (liquid → sublimate)	
<b>Coating Process</b>	Entrained droplet (initial)				
	Entrainment temperature (radiant and convective heat from substrate)	low	low to intermediate	intermediate to high	high
	Entrained particle (during transit)				
	Depositing particle (during impingement)				
	Form	<b>liquid aerosol (solution)</b>	<b>solid aerosol (salt)</b>	<b>vapor (Ti / OH)</b>	<b>sublimate (solid)</b>
	Particle immediately after impingement				
	Cooling effect of droplet on substrate	high			low
<b>Annealed Film</b>	After annealing (high-temperature)				
	Final thickness	thick		thin	n/a
	Bonding to substrate after short-term heating (low-temperature)				
<b>As-Deposited Film</b>	Degree of oxidation/decomposition at substrate	low		high	n/a
	Type of bonding	<b>hydrogen &gt; covalent</b>	<b>hydrogen / covalent</b>	<b>Covalent (chemisorption)</b>	<b>van der Waals (physisorption)</b>
	Bonding strength	weak		strong	very weak
	Crystallinity	amorphous			crystalline
	Initial thickness	thick		thin	friable
	Thickness growth rate	low		high	n/a
	Roughness	high		low	friable
	Film Parameters				

**Figure 2.9.** Different SPT processes and formed thin films proprieties according to substrate temperature (Nakaruk and Sorrell 2010).



It is unlikely that our films deposited at 420°C are formed through the last process where the sublimation occurs so early and the solid is impinged in the surface which results in weakly adhered film. The reason of excluding such process is that our films formed at 420°C are so thin, and their bonding strength is high since they are firmly attached to the stainless steel (S.S) substrate and could not be scraped off with a metal chip. However this should be confirmed by measuring their thickness and by determining their hardness through nano-indentation test.

### **Study of Films Morphology**

Through the XRD patterns obtained, the average crystallite size was calculated using the famous Scherrer's formula:

$$D = \frac{K \lambda}{\beta \cos \theta}$$

D is mean grain size of nanoparticles, K=0.9, the diffractometer used is with CuK $\alpha$  radiation so  $\lambda= 1,5406\text{\AA}$ ,  $\beta$  is the full width at half of the peak maximum (FWHM) in radians and  $\Theta$  is Bragg's angle.

FWHM values correspond to A(101) peak were obtained by the software: *Materials Data- Jade XRD pattern processing*.

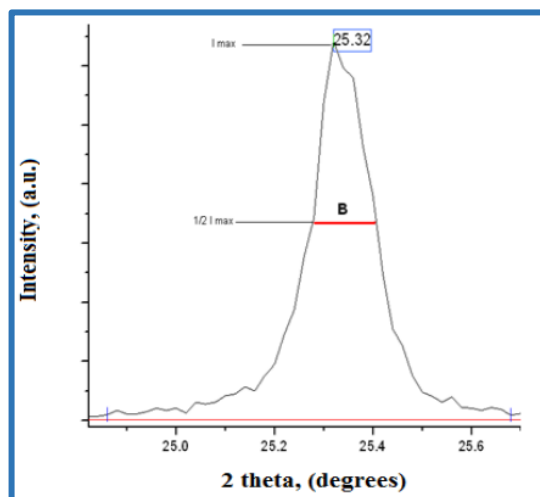


**Figure 2.10.** Procedure of FWHM values determination

**Table 2.1.** Values of crystallite size (D) and dislocation density ( $\delta$ ) for TiO<sub>2</sub> deposited at different temperatures

T	2-Theta	d(Å)	Height	FWHM	D (nm)
350°	25,301	3,5172	19	0,268	30,380
380°	25,342	3,5116	38	0,255	31,932
400°	25,194	3,5319	95	0,239	34,060
420°	25,206	3,5303	97	0,171	47,605

Crystallite size varies from 30 to 48 nm with the rise of substrate temperature. This confirms the nanocrystallinity of the deposited films.

The surface morphology of the film prepared at the optimized temperature (420°C) was investigated by field emission scanning electron microscopy (FESEM) which give the next representative image (Figure 2.11). This illustration shows that the substrate is well covered with large number of grains and film surface is almost homogenous with compact growth. Grains growth occurs because the inter-grain pore channels which provide effective grain boundary pinning have disappeared due to the sintering at 700°C.

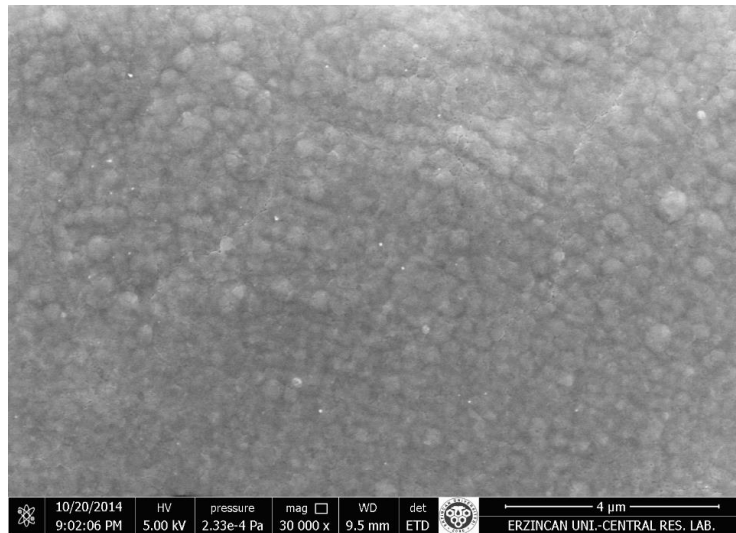


**Figure 2.11.** Representative FESEM image of the film deposited at 420°C and annealed at 700°C

The Figure 2.12 displays an EDAX pattern of the same film and shows that its stoichiometry (1,37 w/w) is smaller than the typical TiO<sub>2</sub> one (1,50 w/w) because of the high quantity of O<sub>2</sub> detected. This may be due the adsorption of O<sub>2</sub> (delivered to the films during their formation) in the grain boundaries. There are also very small peaks that proclaim the presence of very small quantities of iron and nickel, the main constituents of the substrate used (stainless steel).

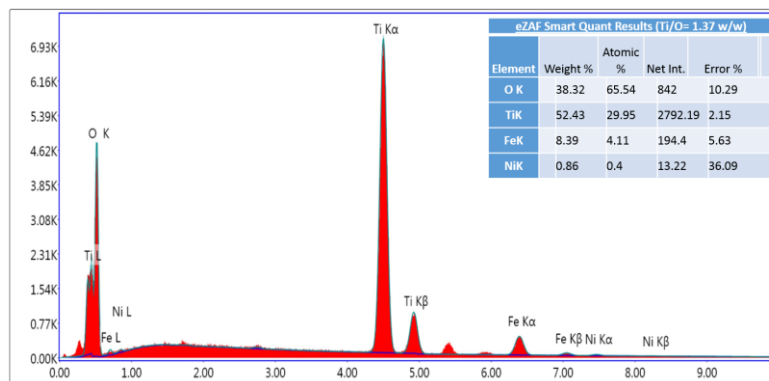


**Figure 2.12.** Energy dispersive X-ray analysis (EDAX) of the film deposited at 420°C and annealed at 700°C

### 2.3.3. Effect of nozzle-to-substrate distance

After optimizing the temperature, the effect of nozzle-to substrate distance is studied by synthesizing TiO<sub>2</sub> coatings at 420°C under oxygen-rich atmosphere, but at different distances from the nozzle (30 and 35 cm).

According to XRD patterns presented in Figure 2.13, coatings deposited at a distance equal to 30 cm have the best crystallinity interpreted by the highest TiO<sub>2</sub> peaks intensities. This may be justified by the quantity of titanium dioxide deposited and crystallized. The shorter the distance, the smaller the coated area and the larger fraction of precursor that riches the surface. The effect of convection forces coming off the substrate (tend to keep the aerosols away from the substrate) is also minimized by minimizing the distance.

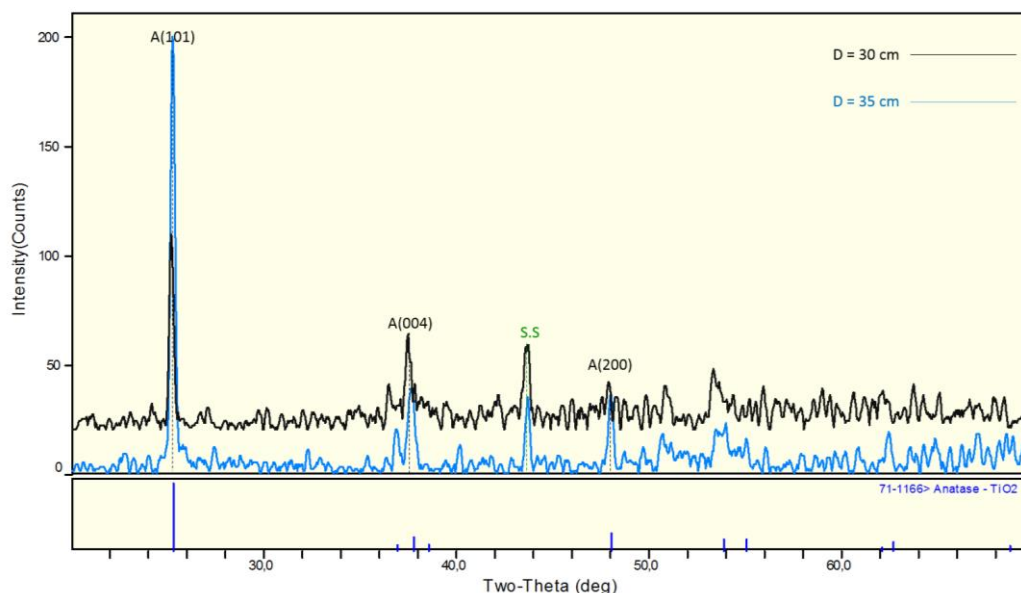


**Figure 2.13.** XRD patterns of TiO<sub>2</sub> thin films deposited at 30 and 35 cm

Another explanation can be valid if the flow rate of precursor solution is taken into account. To focus on the substrates holder from a short distance (30 cm), we tried to

reduce the carrier gas flow rate a little bit. Even if the flow rate is considered to have a minor effect on the film properties (Filipovic *et al.* 2013), reducing it has led to extend the experiment time and therefore to slow the deposition process, which provides a long exposition to the simultaneous heat treatment and by consequence good formation of TiO<sub>2</sub> crystallized coating.

### 2.3.4. Effect of adding oxygen to the deposition atmosphere

In order to accomplish this study, TiO<sub>2</sub> coatings have been synthesized under the previously optimized parameters (substrate temperature of about 420°C, and nozzle-to-substrate distance equal to 30 cm), under high-pressure oxygen-enriched atmosphere, low-pressure oxygen-enriched atmosphere, or without adding oxygen to the deposition atmosphere.

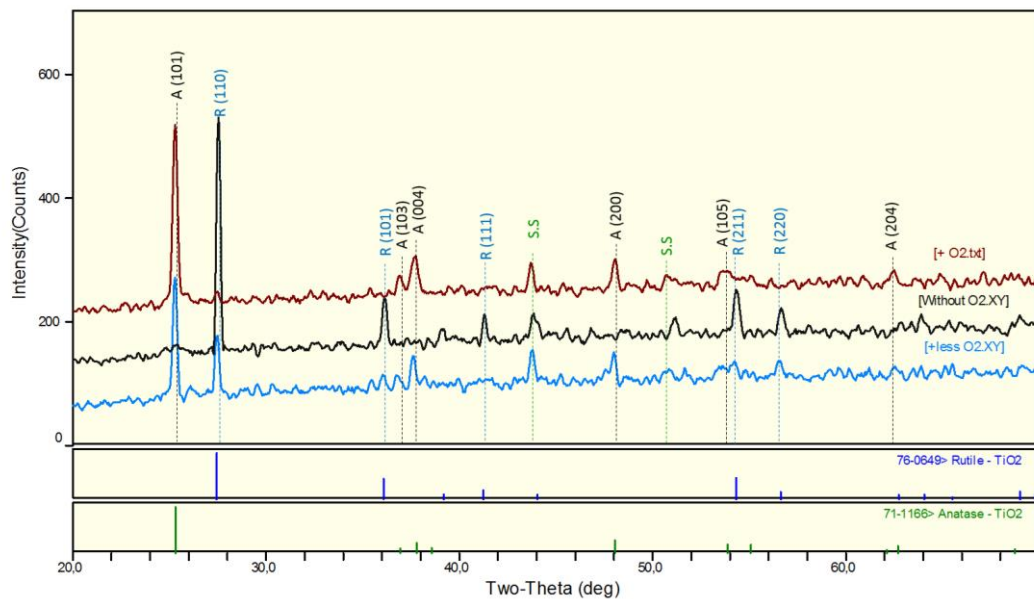


**Figure 2.14.** XRD patterns of TiO<sub>2</sub> films deposited under different atmospheres, after annealing at 700°C

XRD patterns of the resulted coatings, annealed at 700°C for one hour, shown in Figure 2.14 demonstrate that oxygen-rich atmosphere has a great influence in the crystalline phase formed:

Films deposited under a high oxygen pressure exhibit XRD peaks at 25,3°, 37,6° and 48°..etc correspond to a pure TiO<sub>2</sub> anatase phase according to the Standard JCPDS card no:71-1166. In contrast, films obtained without using O<sub>2</sub> in the SPT process, exhibit peaks at 27,5°, 36,1° and 54,4° ..etc which coincide with TiO<sub>2</sub> rutile phase peaks as it is given by JCPDS card no:76-0649. Whereas coatings deposited under low-pressure O<sub>2</sub>-enriched atmosphere exhibit peaks of both phases with a remarked drop in their intensities which means that these coatings are composed of a mixture of anatase and rutile.

All the as-deposited films consist of pure anatase phase whatever is the degree of oxygen-enrichment (Figure 2.15). This is reasonable since the surface Gibbs free energy of anatase phase is lower than that of rutile phase, so TiO<sub>2</sub> initially prefers to nucleate into anatase phase rather than into rutile (Choudhury and Choudhury 2013)

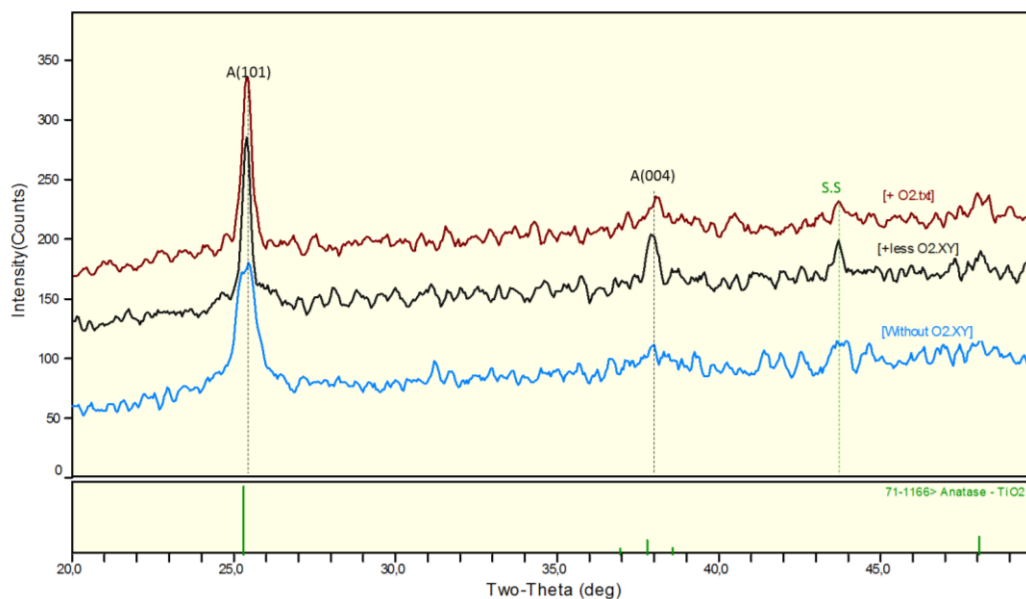


**Figure 2.15.** XRD patterns of TiO<sub>2</sub> films as-deposited under different atmospheres

Per contra, some coatings exhibit new rutile phase after being annealed at 700°C in the case of being synthesized in normal atmosphere (Figure 2.14). This signifies that a phase transformation occurs due to the heat treatment of these coatings.

Some articles about TiO<sub>2</sub> films prepared by SPT in normal conditions (without adding oxygen) reported similar results:

- Oja *et al.* (2004) found that films prepared at 435°C and at 500°C and annealed at 700°C in air have a mixture of anatase-rutile and rutile respectively. However Castañeda *et al.* (2003) remarked that heat treating films at 650°C and 750°C give pure anatase TiO<sub>2</sub> films and only 850°C annealing temperature give rutile crystalline structure.

- Nakaruk *et al.* (2010) noted that films prepared at 400°C and annealed at 600°C consist of single-phase anatase, whereas a phase transformation occur if the films are annealed at 800°C or 1000°C which give both phases.

It was reported in the review of the anatase to rutile phase transformation made by Hanaor and Sorrell (2011) that pure anatase is considered widely to begin to transform to rutile in air at 600°C, however, it may vary owing to the use of raw materials and processing methods.

The same review recorded that the most important factor affecting the phase transformation is the presence and amount of defects on the oxygen sublattice: the increased presence of oxygen vacancies (oxygen defects on the surface and on the grain boundaries) will cause positive strain in anatase lattice. The heat treatment will provide the activation energy necessary for removing these defects which leads to release the strain, relax the lattice and rearrange it to the rutile state (Hanaor and Sorrell 2011; Choudhury and Choudhury 2013).

Rutile has more appropriately the formula  $\text{TiO}_{2-x}$  because it exhibits oxygen deficiency. High level of oxygen vacancies in anatase enhances the transformation to rutile due to the ease of ions rearrangement. Conversely, filling those vacancies by  $\text{O}_2$  will strongly inhibit the transformation (Hanaor and Sorrell 2011). This information explains very well our results obtained when depositing  $\text{TiO}_2$  under  $\text{O}_2$ -rich atmosphere: anatase phase could be conserved and prevented from being transformed to rutile even after its heat treatment at high temperature, because the  $\text{O}_2$  has been greatly absorbed at grain boundaries. As well, anatase is partially transformed if less oxygen quantity is delivered to the films during the spray process (Figure 2.14) because lower amount of oxygen vacancies has been filled.



This explanation is confirmed by different studies:

- In the study of Iida and Ozaki (1961), heat treatment of TiO<sub>2</sub> powder was affected under different atmospheres where the rate of rutile to anatase transformation decreases with an increase in O<sub>2</sub> partial pressure.
- Thin films of Co-TiO<sub>2</sub> were deposited by Ali *et al.* (2009) using Pulse Laser Deposition (PLD) technique at various oxygen partial pressures. At higher oxygen partial pressure the dominant phase was anatase inhibited to be transformed to rutile.
- Another innovative way to keep the anatase phase even under high temperature was achieved by Etacheri *et al.* (2011). High temperature stable and oxygen rich anatase phase nanocrystalline titania was successfully synthesized by the reaction of amorphous titanium dioxide with hydrogen peroxide (H<sub>2</sub>O<sub>2</sub> - TiO<sub>2</sub>) and the calcination of the complex produced above 400°C. At a high calcination temperature of 900°C, the control converted to 100% rutile and oxygen rich 16 H<sub>2</sub>O<sub>2</sub> -TiO<sub>2</sub> remains as 100% anatase. The other modified compositions with smaller molar ratio of H<sub>2</sub>O<sub>2</sub> gave anatase-rutile mixtures at this temperature.

To the best of our knowledge, there are no systematic studies reported the synthesis of high temperature stable anatase TiO<sub>2</sub> thin films by spray pyrolysis technique without using any dopants. So we report in this work new, easy and economical route to synthesize stable and high crystalline anatase nanocoatings deposited under O<sub>2</sub>-rich atmosphere by SPT method.

The average sizes of crystallites that compose the previous coatings were determined through their XRD patterns obtained, FWHM values correspond to the main peaks (A(101) peak for anatase phase, and to R(110) peak for rutile phase).

**Table 2.2.** Values of crystallite size (D) and dislocation density ( $\delta$ ) for TiO<sub>2</sub> deposited at 420°C under different atmospheres, annealed at 700°C

deposition atmosphere	2-Theta	d(Å)	Height	Phase ID	FWHM	D (nm)
normal atmosphere	27,541	3,236	519	Rutile	0,158	51,768
low-pressure O <sub>2</sub> -enriched atm	25,293	3,5183	223	Anatase	0,19	42,852
	27,455	3,246	137	Rutile	0,185	44,205
high-pressure O <sub>2</sub> -enriched atm	25,299	3,5175	326	Anatase	0,25	32,568

Qualitative assessment reveals that the film deposited under high-pressure O<sub>2</sub>-enriched atmosphere is composed of anatase crystallites with ~33 nm in size. Oppositely, the film deposited under normal atmosphere consists of rutile phase which its grains size is about 52 nm. This film was first composed of anatase and after anealing at 700°C it was completely transformed to rutile where the crystallite size increases along due to the remove of structural defects (oxygen vacancies, grain boundaries..).

In contrast, film deposited under low-pressure O<sub>2</sub>-enriched atmosphere shows mixed sizes between ~43 nm anatase and ~44 nm rutile grains. In this case, a partial transformation of anatase to rutile happened and was accompanied by grain growth, which results in a film constituted of large rutile grains and small anatase grains, the amount of anatase phase that does not be transformed is determined using Spurr equation:

$$F_A = \frac{1}{1 + 1,26\left(\frac{I_r}{I_a}\right)}$$

$F_A$  is the anatase amount an anatase-rutile mixture,  $I_a$  and  $I_r$  are the intensities of anatase and rutile main peak, ie (101) and (110) respectively.

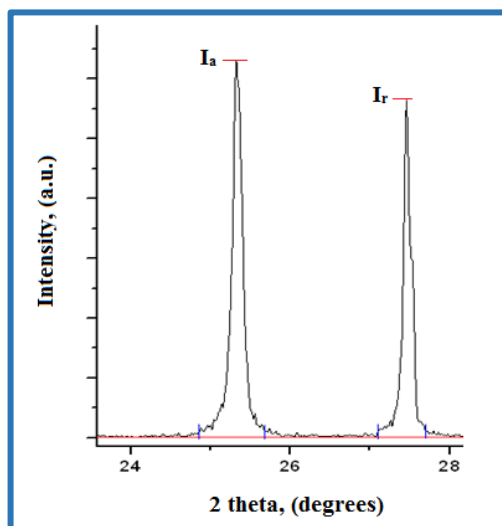


**Figure 2.16.** Anatase amount determination using Spur–Meyer’s equation

Using this equation, it is found that the coating deposited in an environment partially rich of oxygen approximately contains about 56% of anatase and 44% of rutile.

To a better study of the results obtained, Scanning Electron Microscopy (SEM) images of the synthesized films were presented in Figure 2.17 and were compared. All the films look like they uniformly cover the substrate surface, but the difference in grain sizes is clearly observed:

The first image shows the morphology of the film deposited in an environment rich on O<sub>2</sub>. This film is fully dense composed of aggregates which are primary small particles. In contrast, the film deposited without enriching the deposition atmosphere consists largely of showed square-based pyramidal individual grains with narrow size distribution. These grains size is relatively large comparing to the first film.

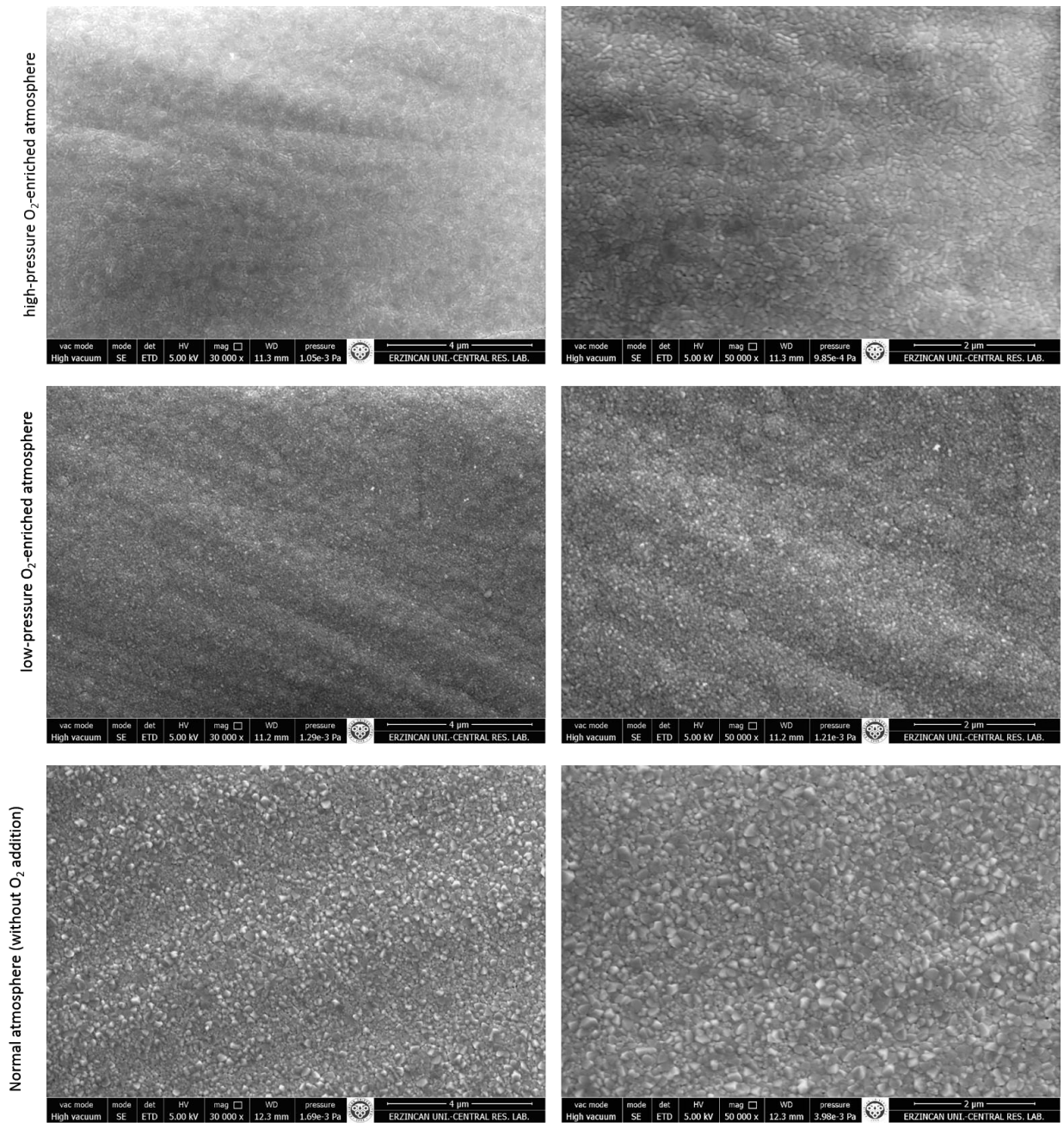


**Figure 2.17.** Representative FESEM images of the films deposited at 420°C under different atmospheres, annealed at 700°C

Deposition of Titania in a partially  $O_2$  rich atmosphere results in the film presented in the second image. The structure of this film exhibits a mixture of individual grains and agglomerated small particles. These results confirm those obtained by XRD: rutile grains that constitute the third film are bigger than the anatase ones that constitute the first film, and the second film is a mixture of both phases with near grain sizes according to SEM morphology exactly as it was concluded from XRD pattern.

Figures 2.18, 2.19 and 2.20 display the EDAX patterns of the previous films, these graphs demonstrate again the given explanation about  $O_2$  effect: films deposited in an oxygen rich environment have higher  $O_2$  percentage which is due to its filling of oxygen vacancies and the formation of interstitial oxygen. While the film deposited without any enrichment by oxygen has lower composition of  $O_2$  and a Ti/O report of about 1,54 w/w that means film is composed of  $TiO_{1,94}$  (comply with the rutile formula  $TiO_{2-x}$  with  $x=0,06$ ).

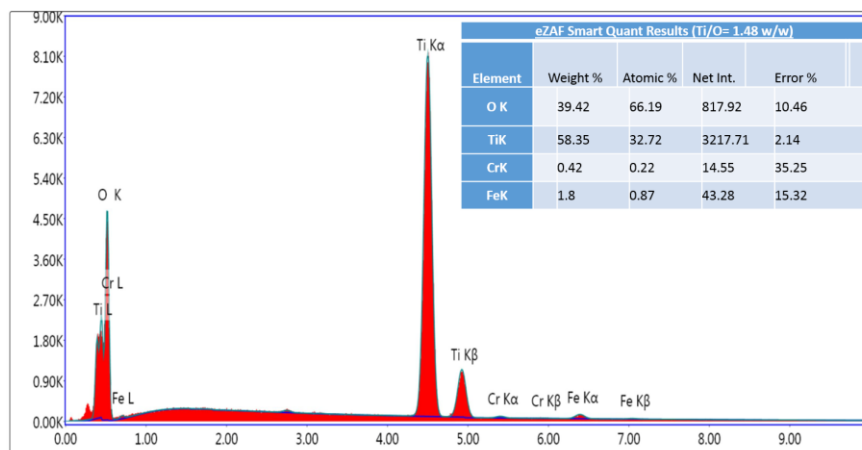


**Figure 2.18.** EDAX of the film deposited under high-pressure  $O_2$ -rich atmosphere

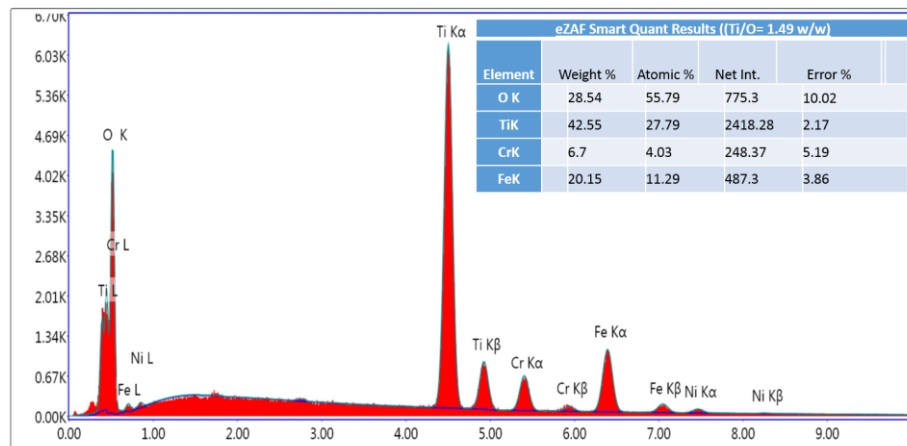


**Figure 2.19.** EDAX of the film deposited low-pressure O<sub>2</sub>-rich atmosphere

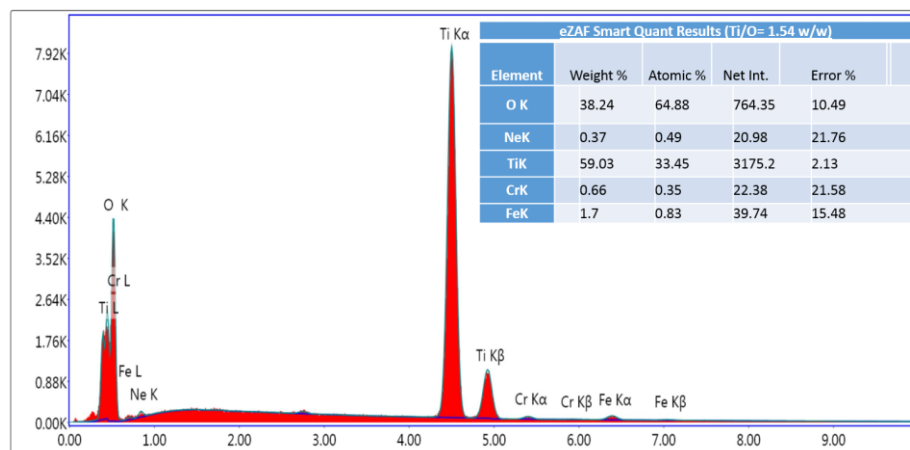


**Figure 2.20.** EDAX of the film deposited under normal atmosphere

### 2.3.6. Thickness of the prepared buffer layers

The cross-section configuration of a representative TiO<sub>2</sub> film, presented in Figure 2.21, demonstrates that the buffer layers prepared are very thin, continuous and smooth with a uniform thickness of 414 nm approximately. This thickness is considered very suitable since these films will be used as buffer layers for nHA nucleation in their surface

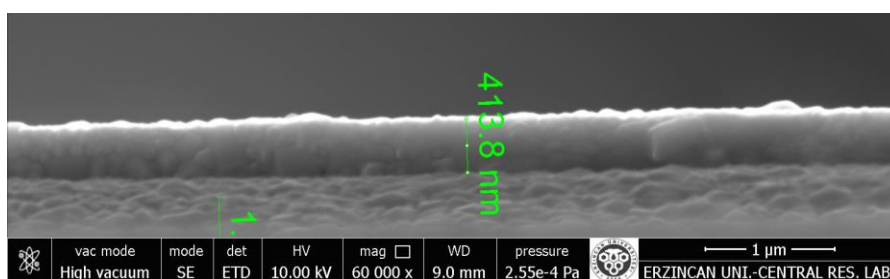


**Figure 2.21.** Cross-section of TiO<sub>2</sub> (R) buffer layer prepared in normal environment

## 2.4. Conclusion of the Second Chapter

The optimized parameters which ensure the preparation of nano TiO<sub>2</sub> buffer layers with good properties are determined in this study (substrate temperature 420°C, nozzle-to-substrate distance 30 cm with post heat-treatment at 700°C). High crystalline, very thin and continuous anatase and rutile buffer layers have been successfully prepared by just carrying out the spray experiments under high-pressure oxygen-enriched atmosphere (to get anatase), or in normal environment without O<sub>2</sub> addition (to get rutile). Both types of TiO<sub>2</sub> buffer layers were used in the next studies to prepare nHA coatings by RF-MS method (Chapter 3) or USPT (Chapter 4).

### **3. PREPARATION OF HYDROXYAPATITE COATINGS BY RF-MS TECHNIQUE**

#### **3.1. Introduction to the Third Chapter**

The purpose of this chapter is first to explain the basic concept of sputtering and especially RF Magnetron sputtering method, to justify why this technique is used by exploring its advantages without neglecting its limits, also to illuminate some previous works about RF-MS used to prepare HA coating and its parameters. Then experimental details about the equipment used, target preparation and coating synthesis are given. Finally, the results of experiments are detailed and discussed through studying different parameters impact on the HA films crystallinity and morphology.

#### **3.2. Materials and Methods**

##### **3.2.1. Fundamentals of sputtering**

Sputtering is a physical vapor deposition technique and non-thermal vaporization process in which target atoms are physically ejected from the surface by momentum transfer from an energetic bombarding species of atomic/molecular size (Reidenbach 1994). When ions or neutral gas atoms with a high energy collide with the target surface, and when the collision energy is higher than the material lattice energy, some target atoms or clusters are ejected (sputtered) and re-deposited onto the substrate surface.



## **Sputtering systems**

### a) Direct current (dc) sputtering

Direct Current (DC) sputtering is the simplest sputtering technology that can be used to synthesize nano-coatings, however it necessitates a conductive target material to be sputtered. A target and a substrate are placed in a deposition chamber generally made of steel evacuated to a base pressure in the range of  $10^{-6}$  Torr then filled with an inert gas, generally argon at a pressure between 1 to 200 mTorr. A highly negative DC voltage is applied across the target, typically hundreds to thousands of Watts, making it the cathode in the electrical system and the substrate material is attached to an electrically grounded anode completing the circuit. This causes electrons to be ejected from the cathode which then act to ionize argon atmosphere producing positive argon ions. These ions are then attracted to the cathode at energies dependent on the voltage applied. As these ions travel towards the target material, some target atoms are sputtered, and commonly some ions recombine with electrons thus producing energetic neutrals. As the system is in a vacuum, target material will be deposited everywhere in the chamber and eventually in the substrate surface. The colored glow is caused by neutralization of positive ions. In the cathode (target) dark space, electrons are energized to the point where they begin to ionize neutrals. This dark region commonly referred as “the cathode sheath”. The resultant electric field acts to accelerate ions towards the cathode (Wasa *et al.* 2004; Coe 2008).

### b) Radio Frequency (RF) Sputtering

DC-MS cannot be used to sputter an insulating material because a positive charge will accumulate on the target surface and cause arcing. To solve this problem, there are two possible ways:



- Pulse the DC current between + and – voltages, which will dissipate the cumulative charge on the target surface.

-Or use a radio frequency (RF) power supply with generally 13.56 MHz frequency which is the most popular solution. In this case, target surface is neutralized by the alternation of target potential. Noting that this potential should be optimized to stay negative for long periods of time to sputter the target atoms, and be a positive voltage for a small time just to dissipate the accumulated positive charge.

The RF diode sputtering system requires an impedance-matching network between the power supply and discharge chamber (Wasa *et al.* 2004).

#### c) Magnetrons

When adding a magnet (magnetron) under the target, the electric potential combined with the magnetic field will direct secondary electrons in a cycloid path which will keep the glow discharge near to the target. This will increase the ionization and the impact with the target, and by consequence provide higher deposition compared with sputtering alone.

As the 'magnetic trapping' increased, the path length and residence time of the electrons in the near-cathode plasma region is multiplied and so is the probability to undergo ionization collisions which in turn increases the sputtered flux by up to ten times and therefore increasing the deposition rate (Schneider *et al.* 2000).

Here is a recap to re-explain the basic concept of RF-MS in a simplified way (Figure 3.1):

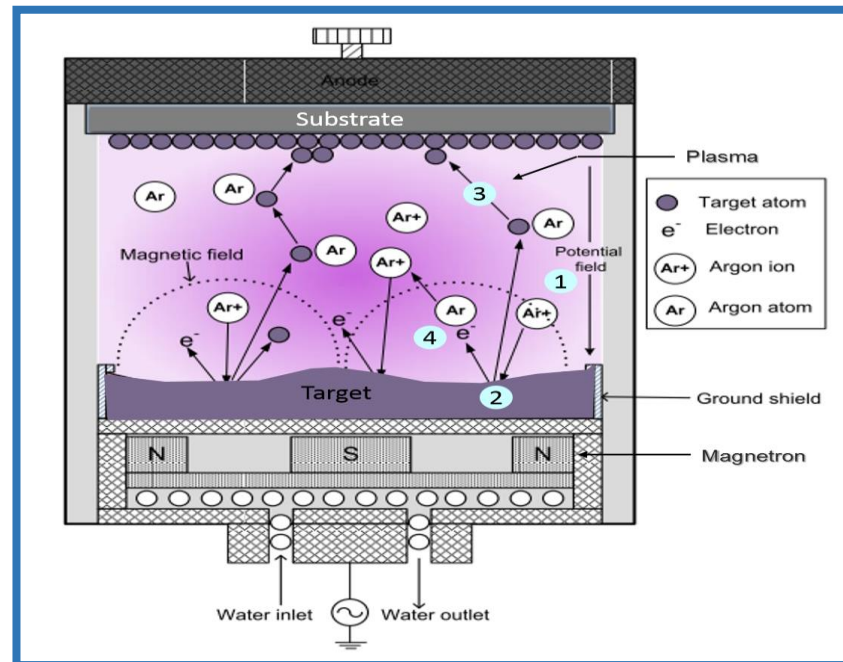


**Figure 3.1.** Basic concept of RF-MS

1- An RF power is applied between target (cathode) and substrate (anode) which will create an electric field in the central area. As the argon gas fills the chamber kept under vacuum, argon atoms will get ionized and create a plasma (glow discharge).

2- Argon ions are accelerated causing collisions with (ion bombardment of) the target surface, which leads to the ejection of secondary electrons and some target atoms.

3- Released target atoms are scattered by argon atoms until they arrive and condense on the substrate surface which will form a thin film layer.

4- Released secondary electrons collide with neutral argon atoms and lead to double the ionization of argon atoms, the magnetic field provided by the magnetron keeps the

electrons confined with the target surface and restricts their movement in that region. Thanks to this confinement, the efficiency of target surface sputtering is augmented, and the formed thin film in the substrate surface is kept far away from being bombarded.

### **3.2.2. Advantages and disadvantages of RF-MS**

The most important advantage of sputtering -which make it a very attractive technique- is the high quality of films produced: very homogeneous coatings with uniform thickness, high purity and strong adhesion can be synthesized. Moreover, RF-MS is a versatile coating method because it can coat a variety of substrates with thin films of electrically conductive and nonconductive materials. Furthermore, multi-component films can easily be deposited using a co-sputtering system. It is also possible to coat substrates without requiring high temperature. However, in this case, the films formed risk of being amorphous and need post-heat treatment.

Though these interesting advantages, sputtering technique has some limitations: because it uses a line of sight process, it is enable to coat complex shapes. Even it synthesizes films of high quality, its low deposition rate and the necessity of vacuum system make RF-MS a time consuming and low energy efficiency method. What is more is that the initial cost of such systems is higher than nearly all other coating systems. This problem is solved in our work by using a home-build system instead of purchasing a very expensive RF-MS equipment.

A final limitation of this technique is that it is extremely hard to use some materials which outgas in vacuum environment as targets (polymers), and it is in some cases difficult to control film stoichiometry due to preferential sputtering (Ca/P ratio in HA coatings for example) which needs to be overcome by an adequate control of process parameters.

### 3.2.3. RF magnetron sputtering of hydroxyapatite thin films

Many researchers have investigated RF magnetron sputtered HA films over two decades ago and continue to investigate them. HA coating produced by RF-MS is further developed by using of interlayers and dopants (Titanium (Desai 2007), Silicon (Chaikina *et al.* 2013)) which improve film bioactivity, stability and mechanical properties. Adding silver (Jamuna-Thevi *et al.* 2011) by RF-MS is also a matter of research in order to provide antimicrobial propriety to the implants. The next section gives more details about RF-MS but with particular regard to HA thin films.

#### Sputtering Parameters

Discharge power, pressure, gas composition and target material are all important parameters which can affect resultant thin films (Coe 2008) are discussed below.

##### a) RF Power

RF power influences the composition and the deposition rate of HA thin films. When power density rises, the flux of positive ions colliding with the target rises too, and by consequence sputtering yield (Y) and deposition rate become higher.

There is a strong relation between increasing power density and calcium to phosphate ratio (Ca/P), Ca is more probable to reach the substrate than P due to its higher atomic mass (when the target is positioned above the substrate). Furthermore, when Ca on the surface of the growing film is less likely to be removed, P is known to be re-sputtered from the film. As the power is increased these events occur more frequently with net effect of more Ca present in the film and less P. Other factors are also responsible of Ca/P ratio change such as target purity and sputtering consistency (Van-Dijk *et al.* 1995).

#### b) Sputtering Pressure

Gas pressure affects coating thickness and composition. At low pressures, collisions distance between electrons-gas atoms is long and the cathode sheath is large. At higher pressure the distance between collisions is smaller which leads to more generation of electrons and thus higher efficiency. At very high pressure, collisional scattered ions number increases which limits the sputtering and so the deposition rate.

#### c) Gas Composition

The sputtering yield increases with the atomic mass of the sputtering gas. Non-reactive sputtering is generally carried out in argon atmospheres as this inert gas is readily available and inexpensive (Coe 2008).

Some studies have found that for HA thin films the Ca/P ratio in HA coating can be diminished by adding a flow of oxygen to the argon atmosphere (Van-Dijk *et al.* 1997). The theoretical explanation of this result is that oxygen undergoes reactive sputtering with phosphorus and forms heavier phosphate species  $(\text{PO}_4)^{-3}$  which decreases P re-sputtering effect from the substrate, and by consequence improves films stoichiometry that becomes closer or almost equal to HA of natural bones.

Despite of this, oxygen is an electron scavenger which reduces the number of electrons available for ionization and therefore lowers the sputtering yield, which overall decreases the deposition rate of sputtered material (Coe 2008).

#### d) Substrate Temperature

It is obvious that substrate temperature is critical for the resultant HA thin films. Even if the process is carried out without any external heat treatment, the substrate become hot

due the heat generated by bombardment of high energy secondary electrons. The use magnetron lowers the substrate temperature since it confines electrons near to the target cooled using a water circulation system.

Even if the substrate is heated as it is explained above, as-deposited films are almost amorphous due to the decomposition of the HA structure into individual atoms or clusters and their random deposition in the substrate. To induce recrystallization, it is necessary to provide a post-heat treatment. Yang *et al.* (2003) who heat treated the coatings for 1 h at 350°C, found that films were still amorphous, and not until temperatures of 500 and 600 °C crystalline HA structure was observed. It was also observed that Ca/P ratio increased with rising heat treatment temperature. Anyhow, this temperature may vary according to coating thickness, composition, film residual stress and substrate material.

Another way to get films with better crystallinity is to simultaneously heat the substrate during deposition. This annealment affects also the coating adhesive strength because thermal expansion coefficients (TEC) of the substrate material and the coating are different knowing that TEC of HA is  $\sim 14 \times 10^{-6} \text{ K}^{-1}$  (Pichugin *et al.* 2013).

#### e) Target density

Sometimes powder targets are used in experimental setup due to the simplicity of their use. However, the process suffers from low deposition rate and requires longer time, therefore becomes more costly process (RF power, vacuum..). This is why targets of very high density are adopted because they ensure the more elevated deposition rate.



f) Target-substrate distance

A shorter target-to-substrate distance helps to get higher deposition rate, but lower film uniformity. Re-sputtering of deposited atoms may also occur if the substrate is positioned very close to the bombardment area.

### **3.2.4. Components of RF-MS equipment used**

Figure 3.2 shows the home-build RF-MS system used in this work, and Figure 3.3 presents its schematic diagram.

The first component of our system is a cylindrical, domed end vacuum chamber made of glass (Pyrex), and isolated from the surrounding atmosphere. To evacuate the air from the chamber, this last is connected to two pumps: a rotary pump that creates primary vacuum (80 mTorr), and a turbo pump that brings the pressure to  $10^{-5}$  mTorr, thus achieves a high vacuum. Argon gas (necessary to create the plasma) and oxygen (necessary in case of reactive sputtering) are delivered with precaution into the chamber, thus the chamber is connected through different valves to argon and oxygen gas cylinders.



**Figure 3.2.** The home-build RF-MS system used

Inside the chamber, a nHA target of 50,8 cm diameter is placed inside its holder above the magnetron that is linked to a water cooling system and most importantly to a 13,56MHz RF power generator (Advanced Energy-Dressler Cesar 1330 with 3kW matching network, 50  $\Omega$  load impedance).

A substrate holder is placed on the obverse side of the target. This holder is attached to an electrically grounded anode necessary to complete the circuit and obtain the plasma, and linked to an external temperature controller necessary to regulate its temperature during sputtering. The substrate can also be heated in situ until 450°C using a lamp of 250W, 24V. Substrate holder-to-target distance can be modified but it is fixed in our work at 4 cm.

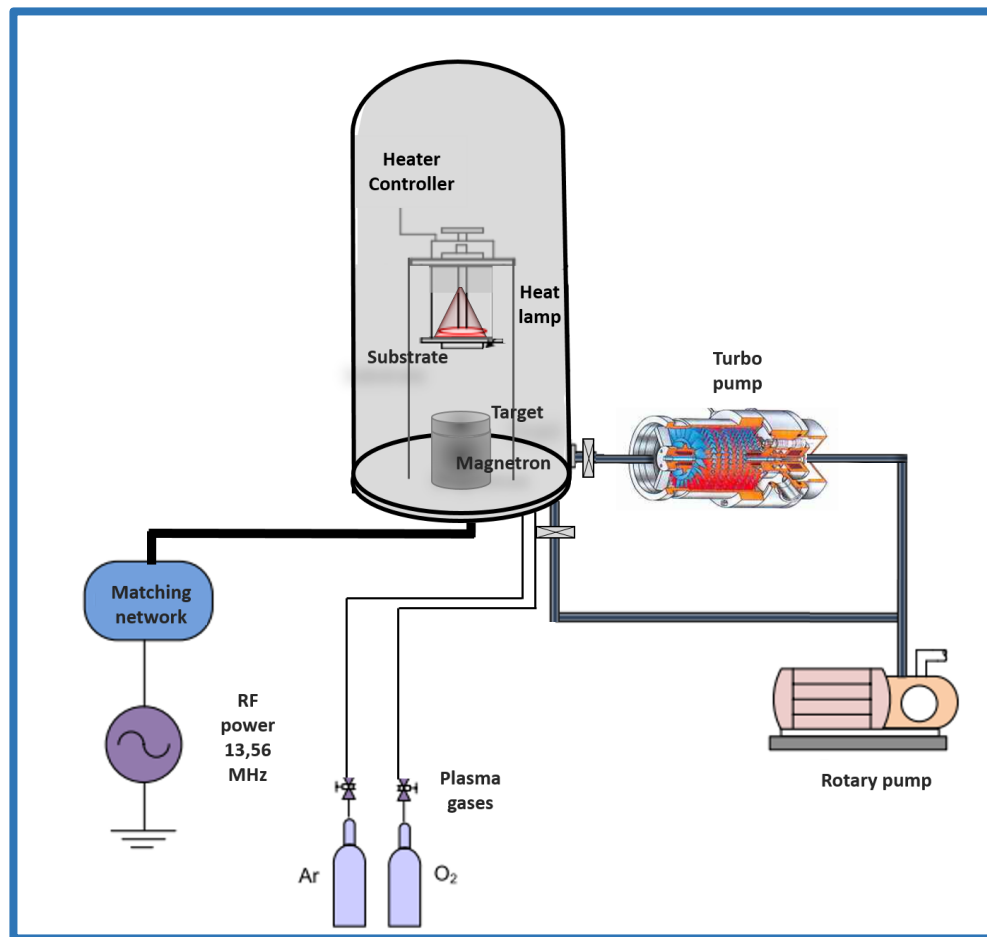


**Figure 3.3.** Schematic diagram of RF-MS system used

### 3.2.5. Preparation of hydroxyapatite target

Perquisite HA targets for sputtering are not yet commercially available products. Thus, a suitable nHA target for RF-MS has been prepared according to Lai *et al.* (2014) who studied in details different ways to fabricate HA targets in the aim of determining the most successful method that insures the best target proprieties.

Lai *et al.* (2014) produced hydroxyapatite parts through cold pressing followed by sintering in vacuum and air. They found that some proprieties such as index of crystallization, density, and hardness were more favorable for parts sintered in air than

those sintered in vacuum, furthermore the parts sintered in vacuum could crack or break. Second, they performed HA sputtering using hot targets produced through isostatic pressing and cold pressing, their results show that no cracking occurred in the cold pressing–produced HA targets at the best sintering temperature that is 1050 °C.

In our work, produced HA sputtering target of 50,8 mm diameter were produced. HA was purchased from Sigma-Aldrich, USA and was cold-pressed at 12 ton then slowly ejected upward (Figure 3.4). The filled-powder weight was 12 g.

The sintering of the compacted HA powder was performed in air for 2 hours at 1000°C to avoid phase transformations to b-TCP/a-TCP/TTCP that may occur if the sintering temperature exceeds 1000 °C. The resulted target was 3mm in thickness.

Using a silver glue as an adhesive layer, HA target prepared was bonded at 100°C for 120 min to a copper back-plate to achieve favorable electric conduction.

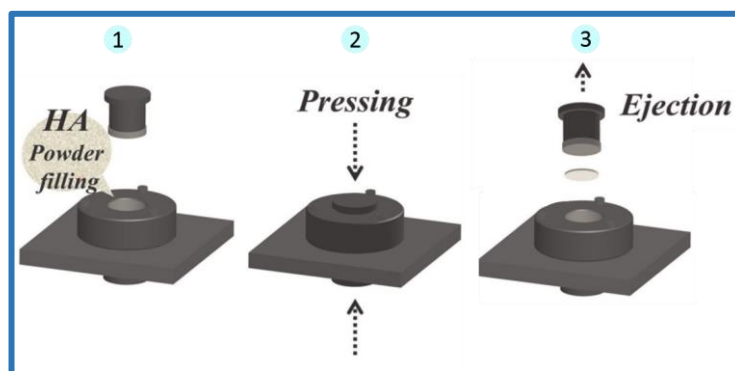


**Figure 3.4.** Schematic representation of the compacting process

### 3.2.6. Experimental details about HA nano-coatings synthesized by RF-MS

The substrate and the target that have previously prepared were first loaded in the sputtering system with a distance of 4 cm. The substrate is a stainless steel specimen coated with TiO<sub>2</sub> buffer layer prepared as it is explained in the second chapter.

Before sputtering took place, the deposition chamber was closed and evacuated till a pressure of  $1,8 \cdot 10^{-5}$  Torr. High-purity argon (Ar) gas was then back-filled into the chamber, bringing the pressure to 4,5 mTorr, followed by introducing oxygen in the aim of reducing Ca/P ratio, the quantity of oxygen added is controlled by controlling the total pressure that arrived to 5 mTorr which means that  $P_{O_2}/P_{total}$  was equal to 10%.

The further step was the start-up of cooling water circulation and RF power supply. The RF power delivered to the system was first 50 Watt reflected completely due to absence of plasma, a quick closing and opening of the turbo pump valve is a simple astuteness just to temporarily increase the internal pressure in order to generate the plasma, the plasma generation causes the drop of reflected power to zero. Once the plasma was established and stabilized, RF power was increased gradually in steps of 10 W until the specific required power. This slow power elevation is necessary to avoid target cracking.

A series of depositions were carried out by RF-MS as follows:

First, the electric RF power was adjusted at 150W to deposit HA in different substrates (anatase buffered stainless steel, rutile buffered stainless steel, and stainless steel without any buffer layer). Second, the RF power effect was studied by comparing the previous results with those obtained by changing plasma discharge power from 150W, 200 to 250W, while target-to-substrate distance, chamber pressure and finally sputtering duration were kept constant (4 cm, 5 mTorr and 10,5 hours respectively). Finally a

post-heat treatment of all the synthesized coatings was carried out in air at 700°C for 1 hour using a 3 Zone-Tube Furnace (PZE 12/50/500, Protherm Furnace, Turkey).

### **3.3. Results and Discussions**

#### **3.3.1. Effect of substrate /buffer layer**

Crystallinity and morphology of HA Films deposited on different type of substrates using 150W RF power was studied by comparing their XRD patterns and FESEM images.

First, a comparison is made between the use of anatase or rutile buffer layers. Unfortunately, XRD patterns do not exhibit any HA peak but only TiO<sub>2</sub> sharp peaks.

Figures 3.6 shows that the specimen with R buffer layer has higher CaP amount formed in its surface compared to that with A buffer layer. Furthermore, Ca/P ratio of HA/TiO<sub>2</sub>(R)/S.S is closer to 1,67 than that of HA/TiO<sub>2</sub>(A)/S.S according to EDX graphs.

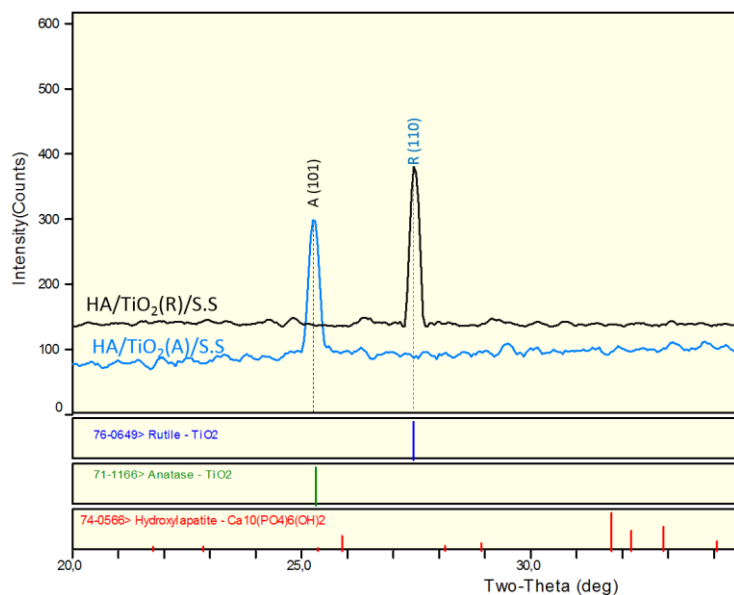


**Figure 3.5.** XRD patterns of HA deposited onto A or R buffer layer by RF-MS

The small amounts of Ca and P compared to Ti amount detected are due to the very small thickness of HA films formed: EDX analyses a large proportion of the film ( $\sim 3 \mu\text{m}$ ) which is greater than our coatings thickness. Hence, Ca/P value may not be representative of the coating stoichiometry and further analysis with X-ray Photoelectron Spectroscopy (XPS) should be done since XPS analyses the composition corresponds to the very top surface of the coating (nearly 10 nm in thickness).

At a high magnification ( $\times 30000$  and  $\times 100000$ ), the ultrafine grain morphology of HA layer was revealed. Interestingly, the grain sizes of the HA crystals appear to reflect that of the underlying  $\text{TiO}_2$  films: HA grains formed in rutile buffer layer are bigger than those formed in anatase buffer layer since anatase crystals have smaller grain size (see the paragraph 2.3.4).

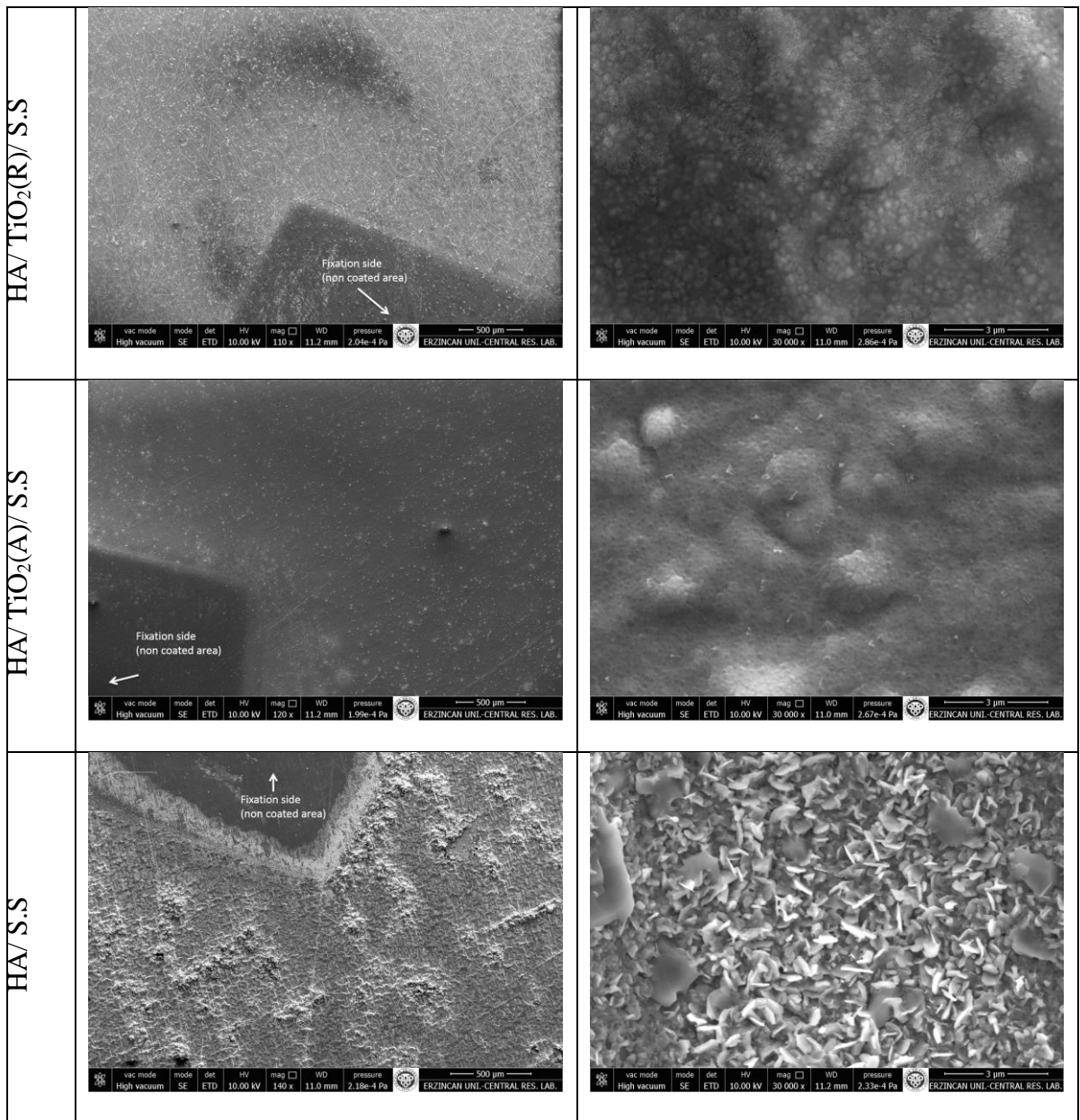


**Figure 3.6.** Representative FESEM images of the HA films deposited onto different substrates at 150W



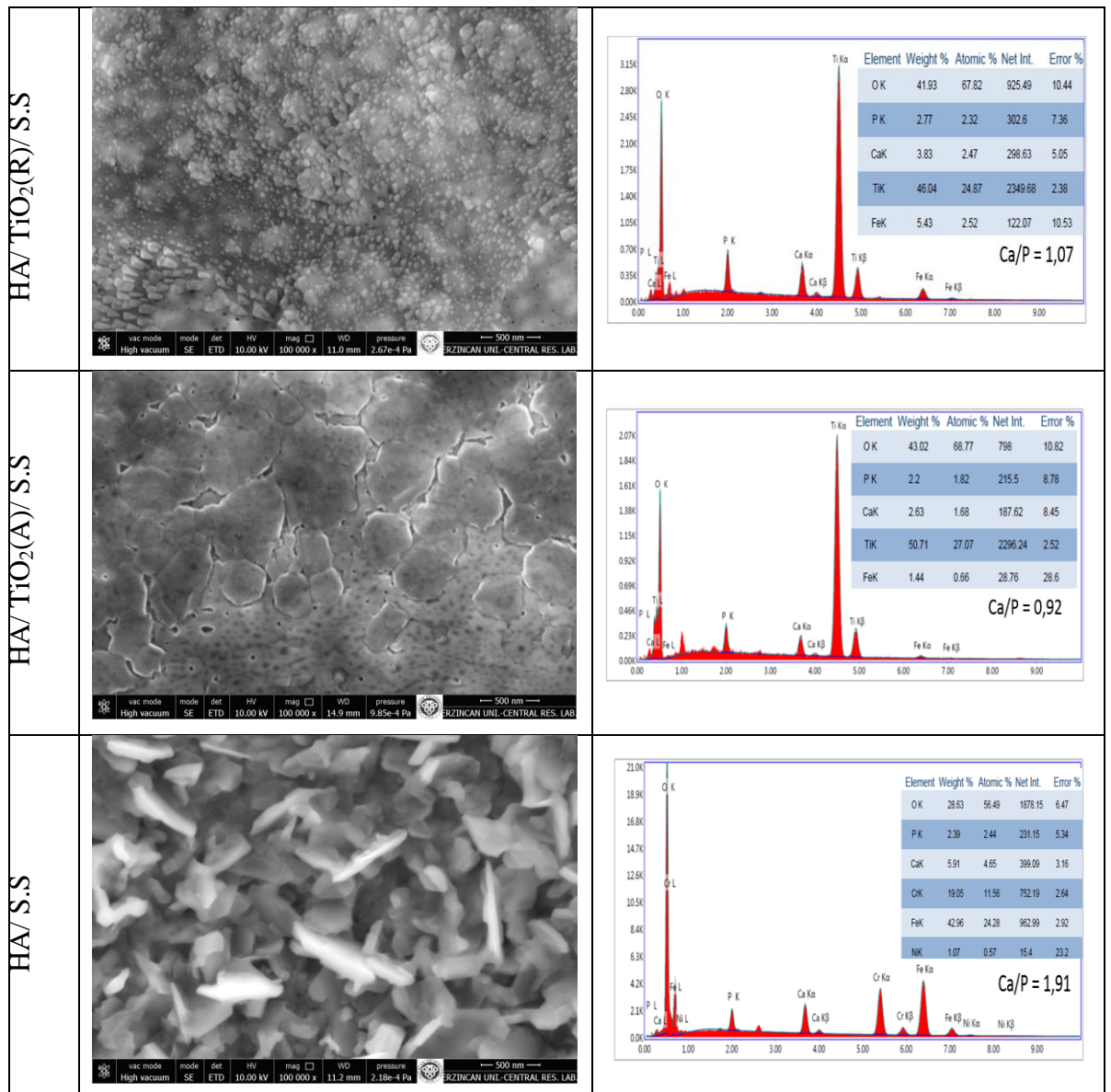


**Figure 3.7.** Representative high magnified FESEM images and their EDX analysis of HA films deposited onto different substrates at 150W

A non-expected result was obtained from HA deposited directly into stainless steel substrates, HA has been very well formed, even better than its formation above TiO<sub>2</sub> under layers. HA crystalline grains were well grown as (300), (301) and (113) planes peaks were detected by X-Ray diffractometer (Figure 3.8). Rod-like apatite nano-crystals were homogeneously formed in austenite surface. What is more, the Ca/P ratio is acceptable since it is closer to that of HA (1,67) (Figure 3.7). This may be due to a variation of another parameter (such as pressure) during sputtering.

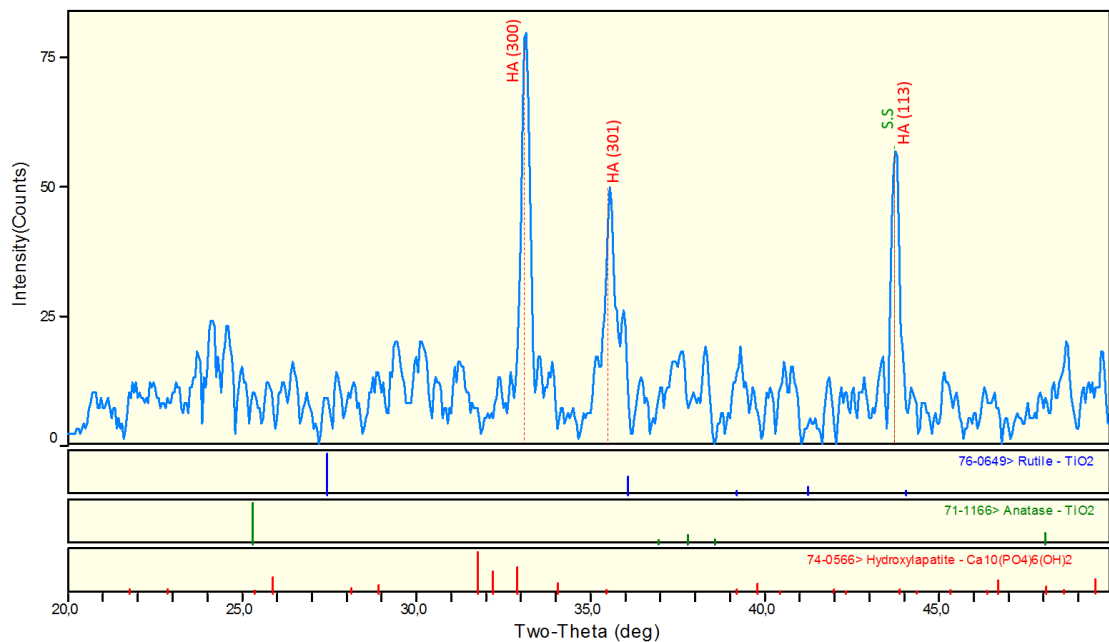


**Figure 3.8.** XRD patterns of HA deposited onto stainless steel substrate by RF-MS

### 3.3.2. Effect of RF-MS sputtering power

The impact of RF power used to deposit HA into rutile buffered stainless steel specimen was studied by power supply adjustment at 150, 200 and 250 W.

The presence of HA in the coatings formed was not improved by XRD since no HA peak was detected. However, intensity of the characteristic peak of rutile under layer was reduced. This reduction was more pronounced for film deposited using RF power equals 200W which may indicate that HA deposited amount is the highest in this specimen.

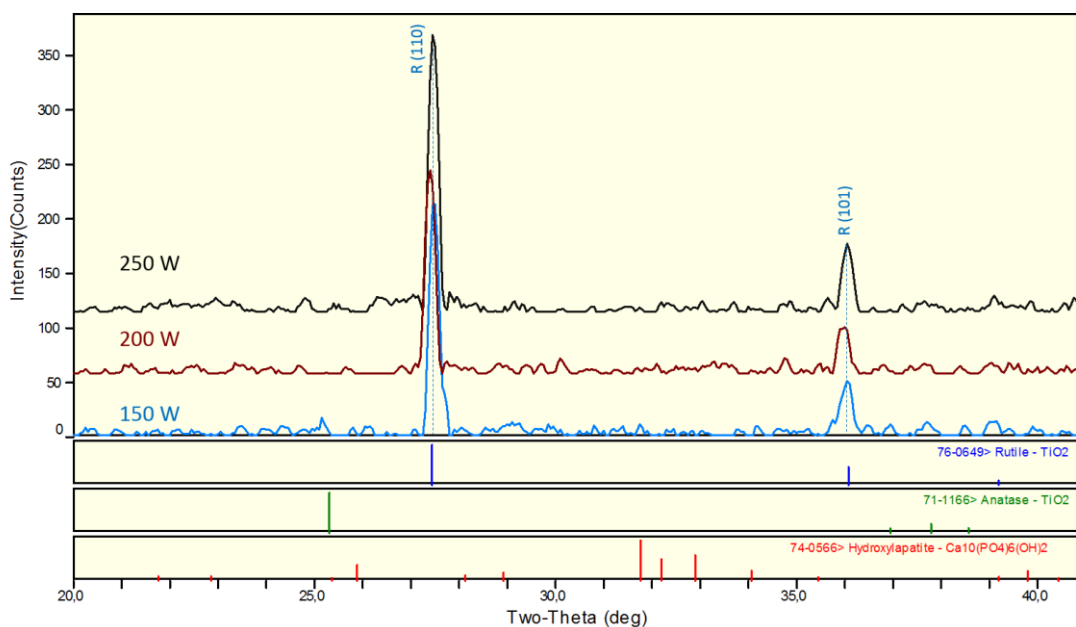


**Figure 3.9.** XRD patterns of HA/TiO<sub>2</sub> (R)/S.S using different RF powers

As it is shown in the next figures, the film deposited using 200 W is the most dense and its stoichiometry is identical to that of HA (Ca/P=1,67) (Figure 3.10 and 3.11). When power density increases, the number of positive ions colliding with the target increases and leads to higher sputtering yield, therefore to greater HA deposition amount. However, film synthesized using the highest discharge power (250W) has lower HA amount compared to that obtained with 200W. This may be due to a re-sputtering phenomena that perhaps happened, or to certain anomalies in the equipment used or the experiment made.

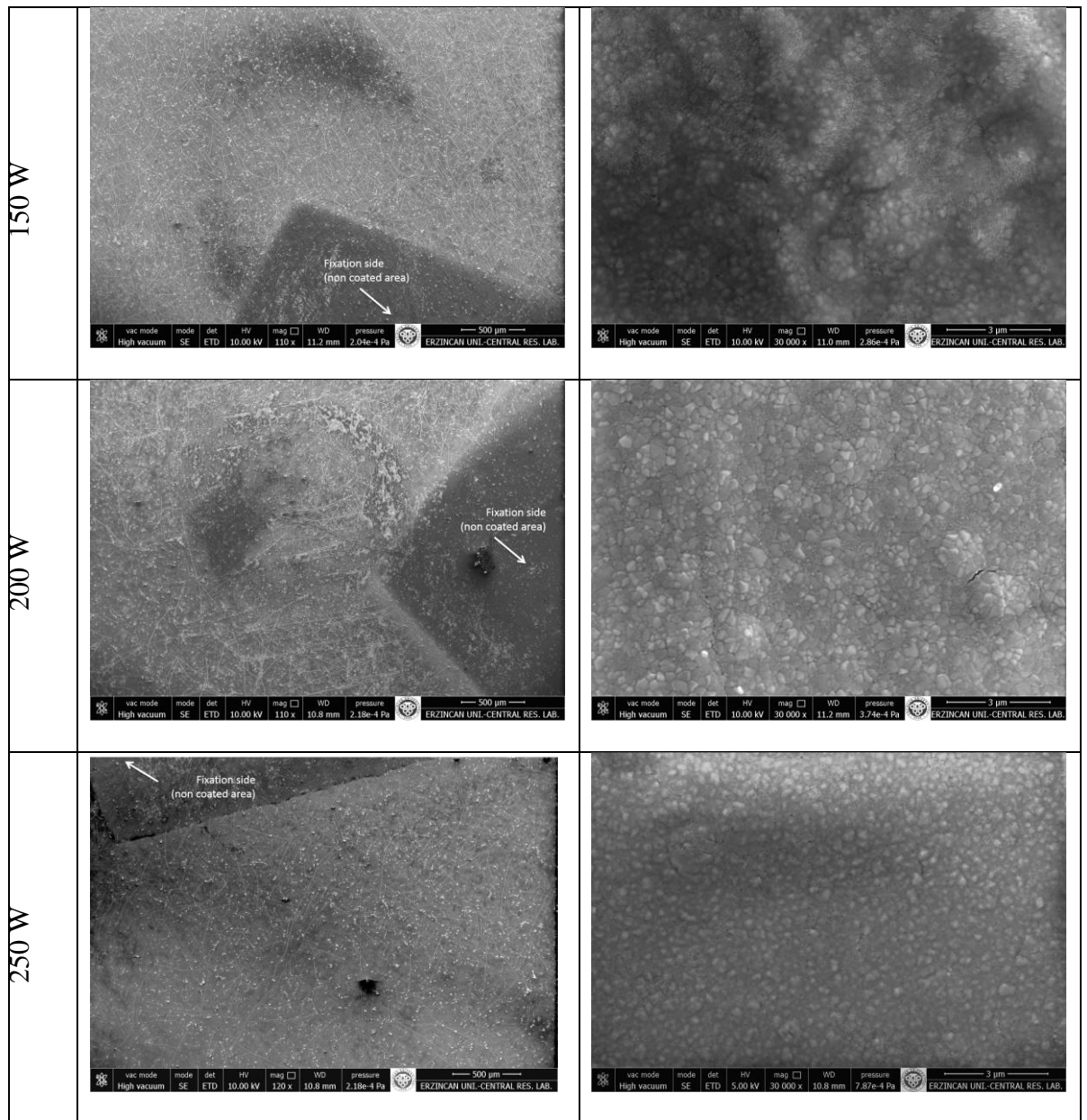


**Figure 3.10.** Representative FESEM images of the HA/TiO<sub>2</sub>(R)/S.S films deposited using different RF-MS discharge powers

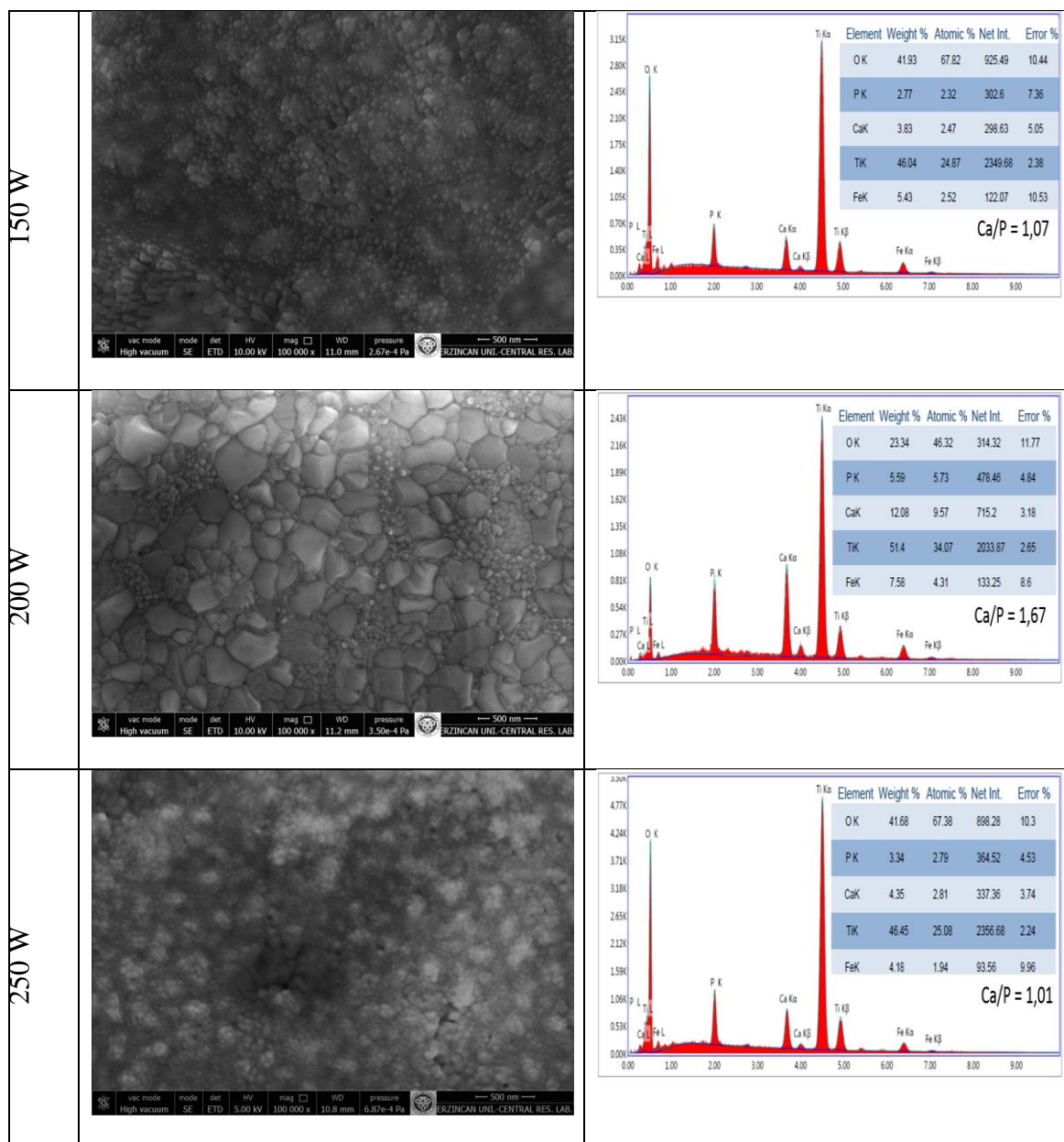


**Figure 3.11.** High magnified FESEM images and their EDX of the HA/TiO<sub>2</sub>(R)/S.S films deposited using different RF-MS discharge powers

### 3.3.3. Thickness of the nHA coatings synthesized by RF-MS

The cross-section of a HA coating synthesized using an RF sputtering power equals 200W onto TiO<sub>2</sub> rutile buffer layer is presented in Figure 3.12. This figure proves that the coatings prepared by RF-MS prepared are so thin, continuous and dense with a uniform thickness of 1,3  $\mu\text{m}$  approximately.

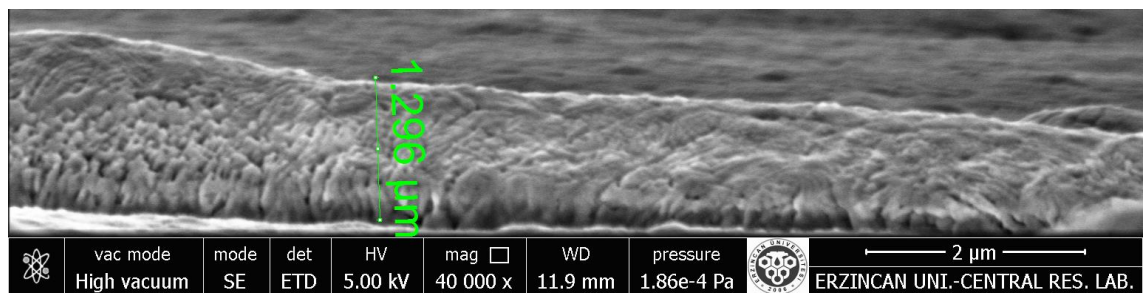


**Figure 3.12.** Cross-section of HA/TiO<sub>2</sub> (R)/S.S deposited using 150W RF-MS power

## **4. PREPARATION OF HYDROXYAPATITE COATINGS BY ULTRASONIC SPRAY PYROLYSIS TECHNIQUE**

### **4.1. Introduction to the Forth Chapter**

After using RF-MS technique to synthesize HA coatings, another more practical and cost-effectiveness technique was used and its results were compared to those obtained by RF-MS. This alternative method is Spray Pyrolysis Technique (SPT) used previously to prepare TiO<sub>2</sub> buffer layers, but with small modification in the type of atomizer: instead of using air blast nozzle, an ultrasonic one related to an ultrasonic oscillator were used to generate smaller droplets. In the second chapter, generalities about SPT and its advantages were already given, so this chapter adds only an explanation about the modification made and the reason of making it, then reports the results achieved with their discussion, finishing by an appropriate conclusion about nHA coatings synthesis.

### **4.2. Materials and Methods**

#### **4.2.1. Ultrasonic Spray Pyrolysis Technique (USPT)**

Before deciding to adopt ultrasonic SPT instead of the previously air blast SPT used, several experiments were effectuated in the aim of preparing nHA coatings with good proprieties. However, all the coatings obtained were neither homogeneous nor nanostructured films despite changing several parameters to improve their morphology. The problem of air blast method is that due to its large nozzle diameter (500-800 $\mu$ m), big droplets are generated and cannot undergo –in case of hydroxyapatite precursor solution– all the steps of evaporation, precipitation and sublimation before reaching the substrate surface, which leads to the formation of HA coatings with modest microstructure. A

solution proposed is to increase the substrate temperature to more than 500° in the aim of reducing droplets size by the crossed high thermal gradient. However, this solution is not suitable due to a system limitation (heating power) and also to its impracticality.

A better way to diminish droplets size is the use of an ultrasonic atomizer: in this case, an electromechanical device vibrates at high frequency generated by an RF ultrasonic oscillator, its vibration causes the precursor solution to be broken down into tiny and uniform droplets sprayed from the nozzle tip. The higher the frequency used the smaller the droplets size.

#### **4.2.2. The equipment used**

The USPT equipment used to prepare HA coatings -displayed in Figure 4.1- is the same used to prepare TiO<sub>2</sub> buffer layers but after changing the nozzle by an ultrasonic one (Lechler Ultraschall-Zerstäuber US1– 710.070.16.60.00.0; Metzingen/Germany; 100 kHz; 8 W; opening angle 30°). Typically, droplet size generated by this nozzle is specified to be 22±1,7 μm. The nozzle is covered by a metallic cylinder to protect it from external exposition.



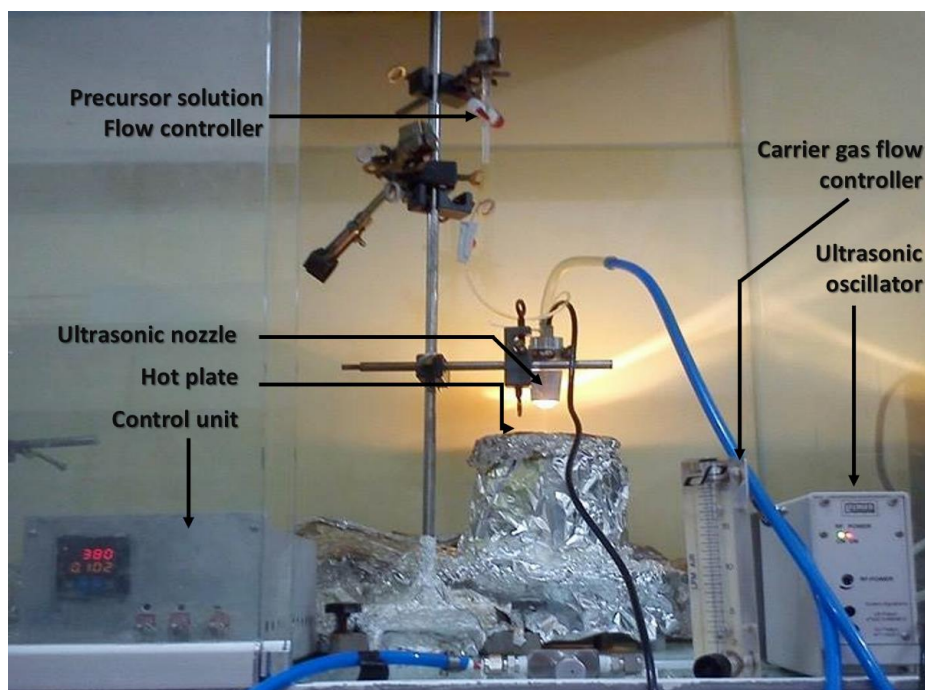


**Figure 4.1.** Ultrasonic SPT system used

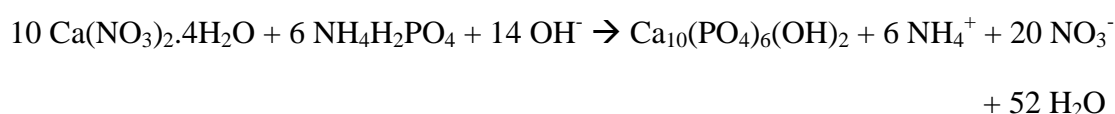
### 4.2.3. n-HA precursor solution preparation

The precursor solution of nHA is composed of:

- Calcium nitrate tetrahydrate  $\text{Ca}(\text{NO}_3)_2 \cdot 4\text{H}_2\text{O}$  (>99%, Sigma-Aldrich, Germany)
- Ammonium dihydrogen phosphate  $\text{NH}_4\text{H}_2\text{PO}_4$  (98%, Carlo Erba reagent, Spain)
- Nitric acid ( $\text{HNO}_3$ , Assay 68%, Carlo Erba reagent, Spain)

nHA precursor solution is in fact a mixture of calcium and phosphor precursor solutions of which concentrations are determined in the way that Ca/P molar ratio equals 1,67: 11,801 g of  $\text{Ca}(\text{NO}_3)_2 \cdot 4\text{H}_2\text{O}$  was dissolved in 50 ml deionized water to form a solution with  $\text{Ca}^{2+}$  concentration equal to 1 mol/l. Similarly, 3,45 g of  $\text{NH}_4\text{H}_2\text{PO}_4$  was dissolved in 50 ml deionized water which forms a solution with  $\text{P}^{5+}$  concentration equal to 0,6 mol/l. The second solution was added drop wise to the first one under vigorous stirring to avoid

HA precipitation. Only 10 ml of much diluted nitric acid (10%) was then added to the mixture. The chemical reaction which takes place and results in HA production is:



The solution obtained was diluted before being sprayed, because a weak solution will generate more homogenous and smooth films in spite of taking longer time for film growth.

### 4.3.3. Formation of nHA coatings

For each essay, 100 ml of HA precursor of 0,005 mol/l concentration is sprayed into the substrates heated at the desired temperature. The carrier gas used is atmospheric air compressed using a compressor.

First of all, the substrate temperature which is the most critical parameter of SPT was varied from 350, 380 to 420 in order to find the optimal one that ensures good HA films growth. In this first step, the substrates used are the same (stainless steel specimens coated first with TiO<sub>2</sub> anatase buffer layer as it is detailed in chapter 2). Nozzle-to-substrate distance as well as carrier gas and precursor solution flow rates were kept constant (8 cm, 3 LPM, 2,26 ml/min respectively). The films prepared were then heat treated for 1 hour at two temperatures (600°C and 700°C) under normal atmosphere using a 3 Zone-Tube Furnace (PZE 12/50/500, Protherm Furnace, Turkey).

After determining the best substrate temperature and annealing temperature, these temperatures were used but for 3 types of substrates: stainless steel specimens, stainless

steel specimens with TiO<sub>2</sub> anatase buffer layer, and thirdly with TiO<sub>2</sub> rutile buffer layer prepared earlier.

To study the influence of doping magnesium, the previous experiment was repeated but by spraying a HA precursor solution containing Mg molar fraction  $X_{Mg} = Mg/(Mg+Ca) = 0,15$ . This Mg molar fraction is chosen according to Landi *et al.* (2008) study where  $X_{Mg}$  of the starting solution equal to 0,15 was found to give powders with 5,7 (Mg/Ca) mol % which is found to be the best and the most biocompatible MgHA composition.

### **4.3. Results and Discussions**

#### **4.3.1. Effect of substrate temperature**

Figure 4.2 displays the XRD patterns of HA films deposited on stainless steel specimens with TiO<sub>2</sub> anatase buffer layer, simultaneously heated at different temperatures and post heat treated at 700°C for one hour.

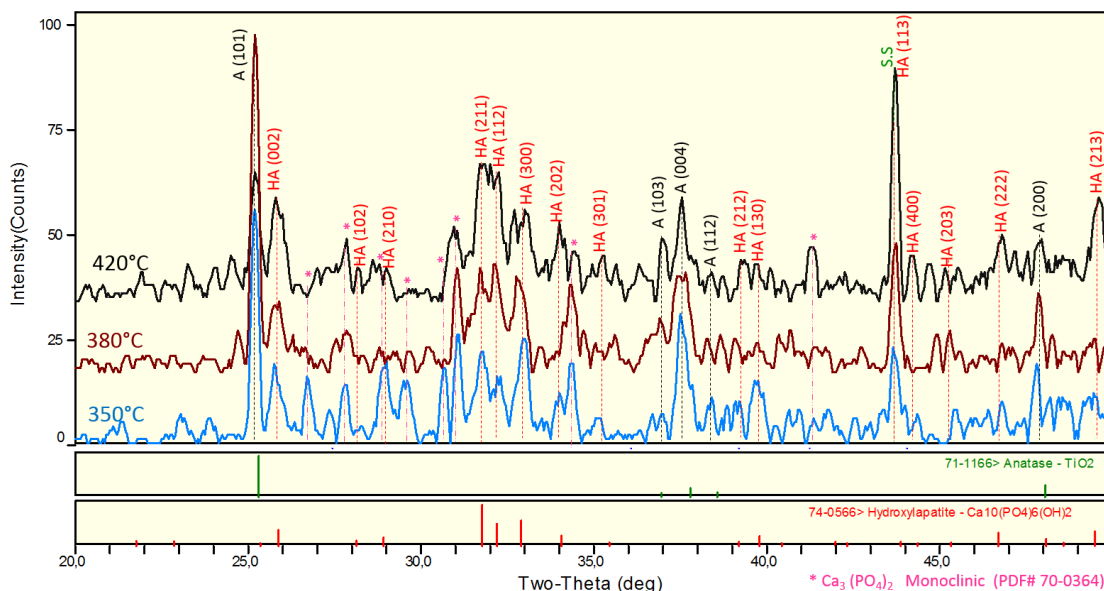


**Figure 4.2.** XRD patterns of HA/TiO<sub>2</sub> (A)/S.S thin films deposited at different temperatures

This graph confirms the formation of well crystalline HA coatings with different planes: (002), (221), (112), (300), (113) and (213) approved by the peaks detected at 25,88, 31,75, 32,23, 32,89, 43,91, and 49,45 (Standard JCPDS card no:74-0566).

Anatase peaks were also detected, this may mean that HA films formed have not completely coated the specimens, or perhaps due to the small-thickness of HA coatings. This last supposition is more probably the correct one because A peaks intensities have significantly reduced if we compare them with those of A buffer layer only. The rightness of this supposition is confirmed by morphology and composition analysis where the films look continuous (Figure 4.3) and no titanium EDX peak is observed (Figure 4.4).

These patterns illustrates also that the coatings formed are composed of another calcium phosphate ceramic which is tricalcium phosphate Ca<sub>3</sub>(PO<sub>4</sub>)<sub>2</sub> according to the card

no: 70-0364. This was also observed in previous works where HA coatings were prepared by USPT (Ye and Troczynski 2008).

The effect of simultaneous heat treatment is not so clear, but it seems that the crystallinity of HA increases with the increase of substrate temperature since the intensities of peaks correspond to (002), (221), (113) and (213) have risen. The purity of HA coatings has been likewise improved as the intensities of tricalcium phosphate peaks have been decreased.

It is worth noting that during spraying at substrate temperature equal to 350°C, we observed that droplets arrive to the substrates before being evaporated which results in a wet state of the substrates then to their drying. This means that at 350°C is for sure not an appropriate temperature because the film growth is identical to the first process (A) illustrated in the second chapter (see paragraph 2.3.2). This was also confirmed by the weak film adhesion observed.

Through XRD results, 420°C is considered the best temperature between the three temperatures used, in which the CVD-like process takes place (calcium and phosphor precursors sublime then arrive as vapor to the substrate surface where they react to produce HA). This conclusion was checked by comparing the microstructure of the films formed (Figure 4.3): the coating prepared at 420°C look continuous, denser and more homogeneous. Furthermore, EDX results shows that Ca/P ratio of this film (1,59) is the closest to that of pure HA (1,67) compared to films prepared at 380° and 350° (1,55 and 1,19 respectively). This last reduced value of Ca/P ratio is due to tricalcium phosphate presence which causes the deviation from stoichiometric hydroxyapatite. Ca/P value has

increased with increasing substrate temperature thanks to tricalcium phosphate quantity diminution, thus film purity improvement, as it was pre-concluded from XRD patterns.

These synthesized HA coatings are observed to be extremely nanostructured as illustrated in Figure 4.5 where the specimens scanning images are magnificated to 100 000x.

It is also important to notice from FESEM images that these nHA films grown by USPT are highly porous with micro and nano internal pores (Figure 4.5), in the addition to the external porosity developed by the deposition of multiple layers with different levelness (Figure 4.3). This is considered a great advantage since these films will be used to load honey through physical/chemical adsorption to synthesize antimicrobial coatings.

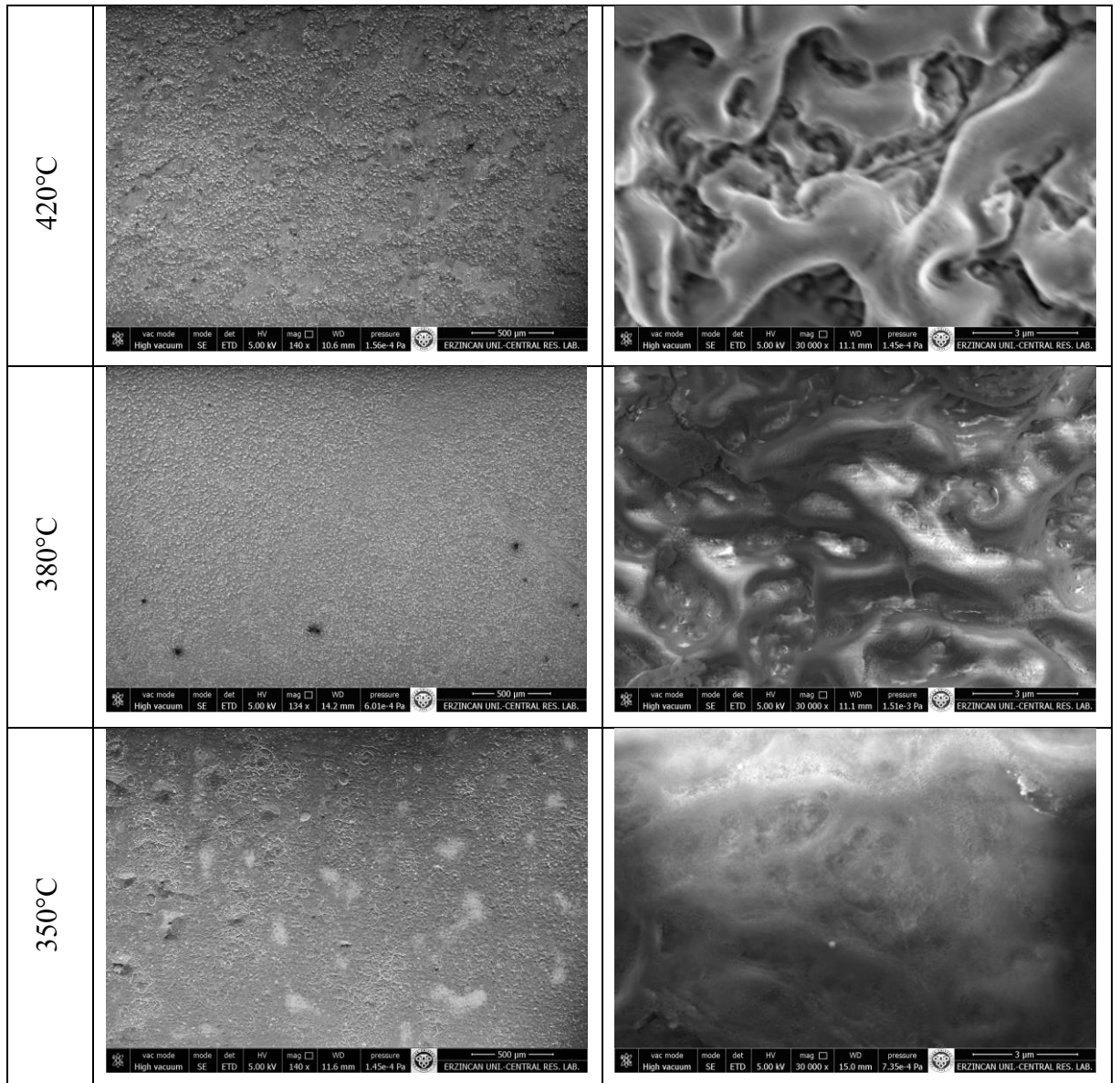


**Figure 4.3.** Representative FESEM images of the HA/TiO<sub>2</sub>(A)/S.S films deposited at different temperatures and annealed at 700°C

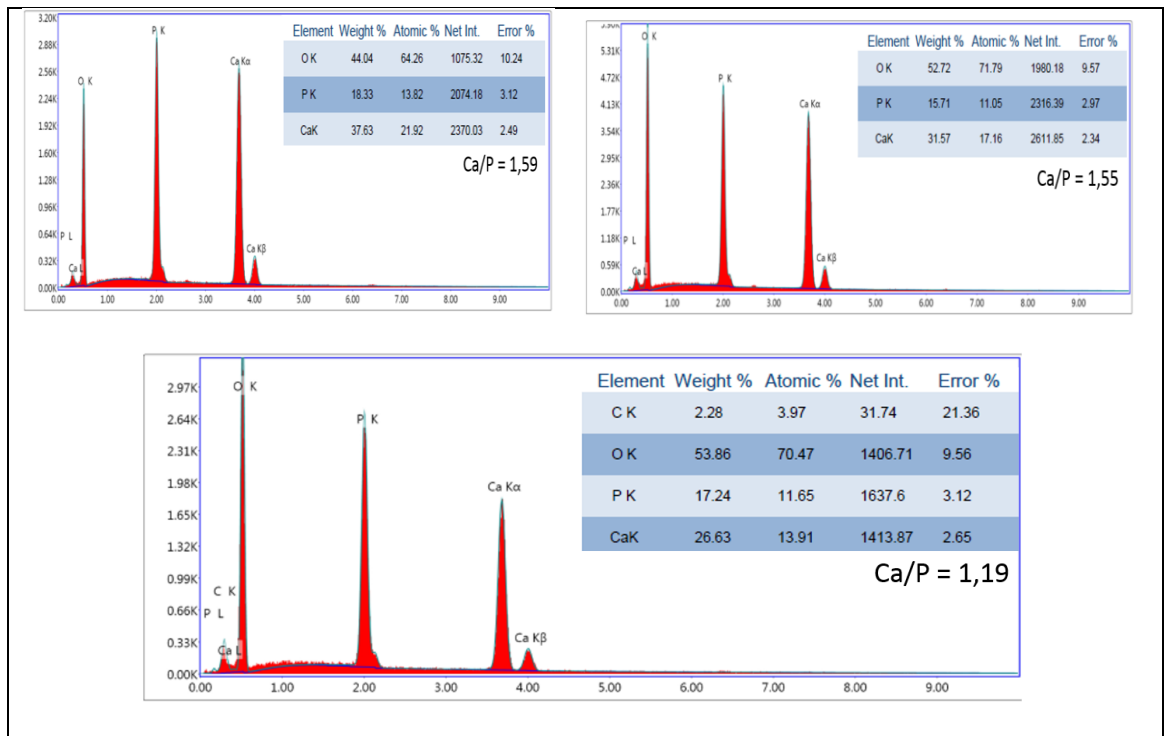


**Figure 4.4.** EDX analysis of the HA/TiO<sub>2</sub>(A)/S.S films deposited at 420°, 380° and 350°C respectively.

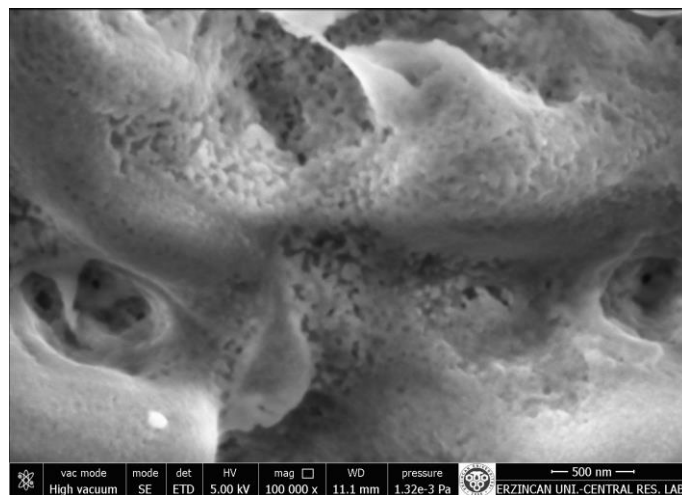


**Figure 4.5.** Representative FESEM images of typical HA/TiO<sub>2</sub>(A)/S.S films



### 4.3.2. Effect of post heat-treatment temperature

nHA coatings prepared at the optimal substrate temperature (420°C) were heat treated for 1 hour at two temperatures (600°C and 700°C). It can be concluded from their XRD patterns presented in Figure 4.6 that annealing temperature of 700°C is better than 600°C because it induces the crystallinity of nHA coatings prepared (clarified by HA peaks intensities augmentation). Therefore, all the next heat treatments were effected at 700°C.

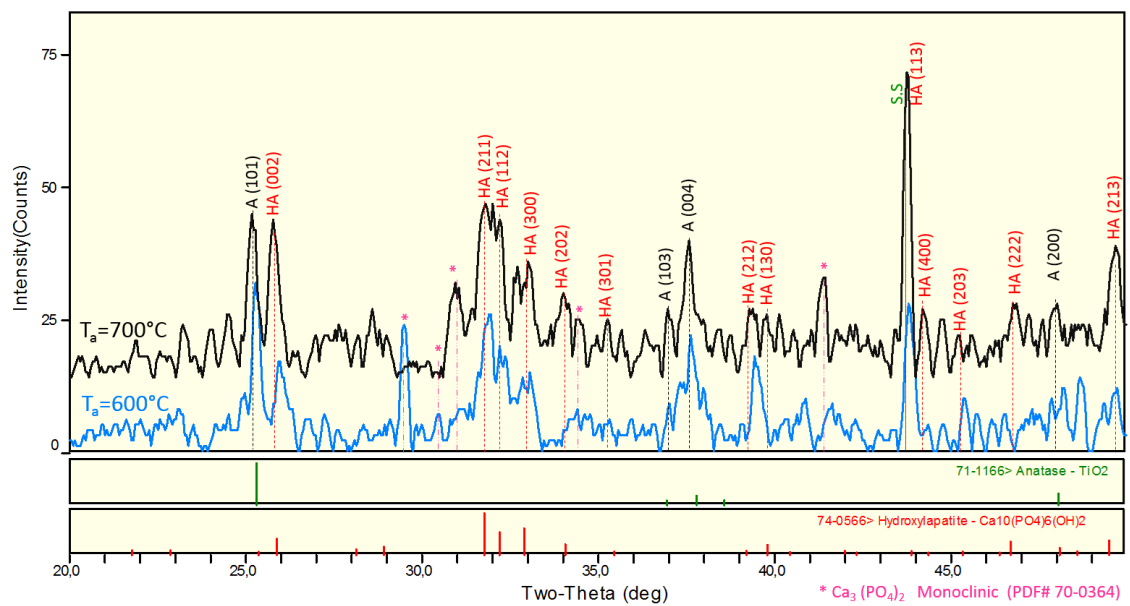


**Figure 4.6.** XRD patterns of HA/ TiO<sub>2</sub> (A)/S.S thin films deposited at 420°C and annealed at 600°C and 700°C

### 4.3.3. Influence of substrate and buffer layer

Examination of XRD patterns of coatings deposited on different substrates show that HA films have been successfully formed either if a buffer layer of TiO<sub>2</sub> exists or not. However, the existence of TiO<sub>2</sub> buffer layer appears to slightly enhance films crystallinity and purity, since some HA peaks intensities have been somewhat augmented (peaks of (300), (212)) and tricalcium phosphate peaks intensities have been reduced (at 2 $\Theta$  equal to 25,8, 29,9 and 29,7° approximately).

It is hard to determine if TiO<sub>2</sub> anatase or rutile buffer layer is better for HA film formation from XRD results, because the preferred crystallographic growth orientations are different: some HA peaks have larger intensities in case of rutile buffer layer (peaks of (102), (212), (130) planes) whereas other HA peaks were sharper in case of anatase buffer layer (peaks of (202), (113) and (213)). Both anatase and rutile have enhanced the crystalline HA formation because they both possess lattice match with HA, with compared mismatch:  $|X_{HA} - X_A| = 1,0\%$ ,  $|Y_{HA} - Y_A| = 1,4\%$ ,  $|X_{HA} - X_R| = 2,5\%$ ,  $|Y_{HA} - Y_R| = 0,5\%$ . In our case anatase did not lead to favorable HA formation comparing to rutile for the reason that Ti-OH groups did not exist. Ti-OH can only exist in wet methods where hydrogen bond can be established between Ti-OH groups of TiO<sub>2</sub> gel and OH<sup>-</sup> of HA (see the paragraph 1.4).

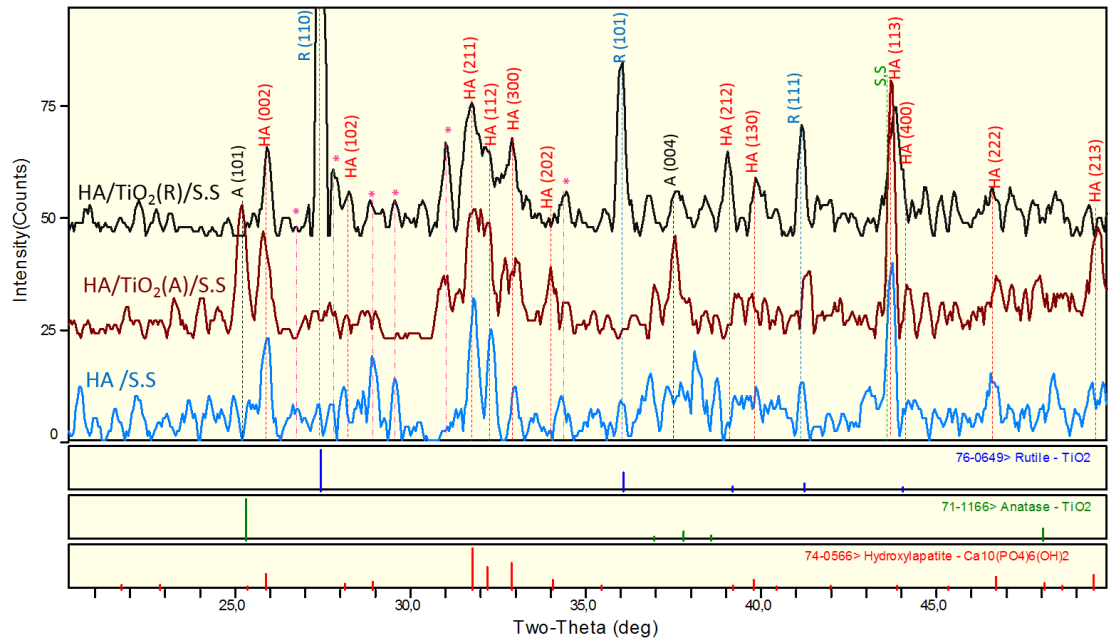


**Figure 4.7.** XRD patterns of nHA coatings deposited at 420°C on different substrates.

The analysis of coatings surface using FESEM (Figure 4.8) showed great enhancement of HA formation if TiO<sub>2</sub> buffer layers exist. HA coatings are in this case more homogeneous and more continuous, moreover they possess more porous structure compared to HA/S.S coatings.

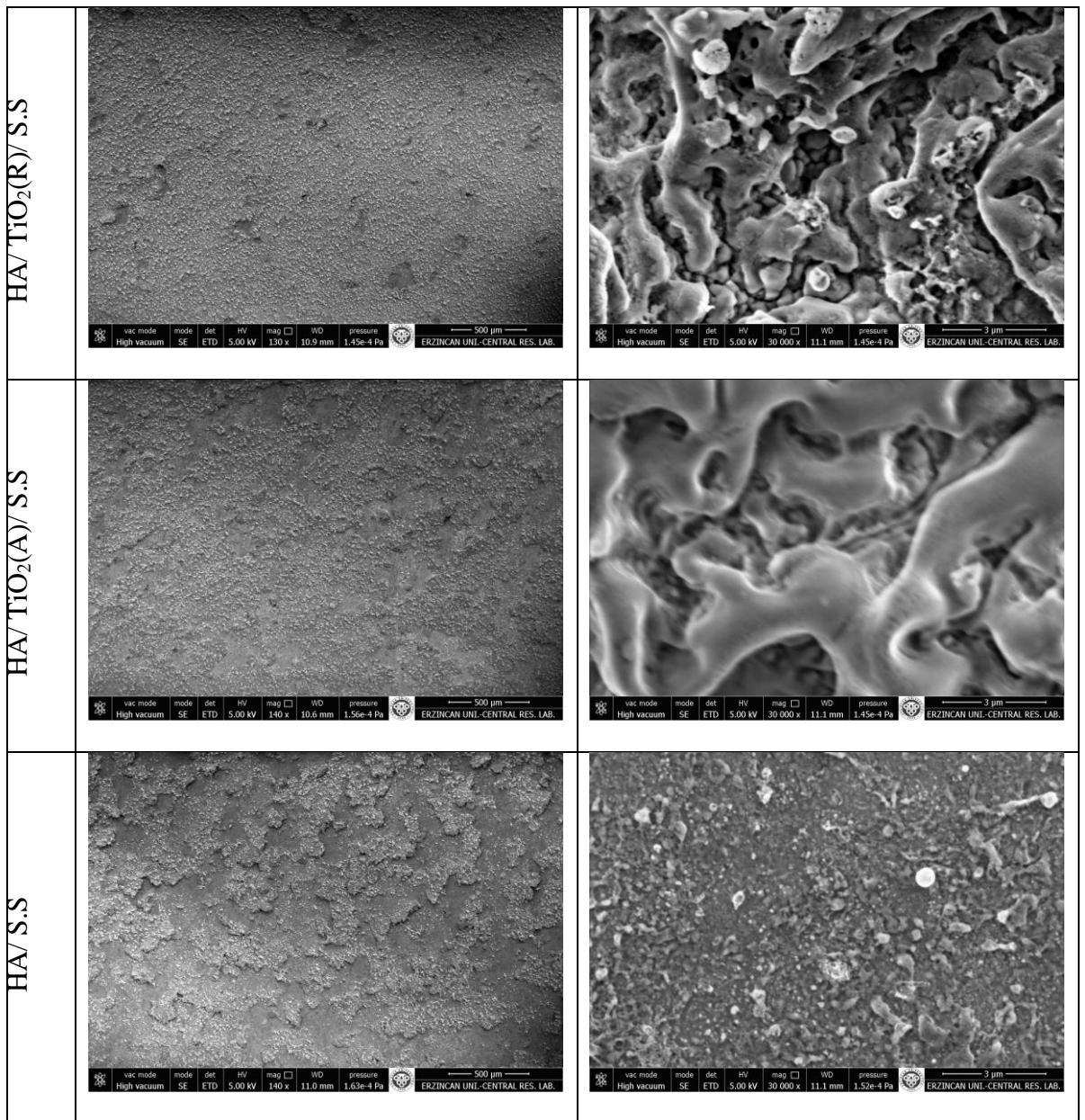


**Figure 4.8.** Representative FESEM images of the HA films deposited in different substrates.

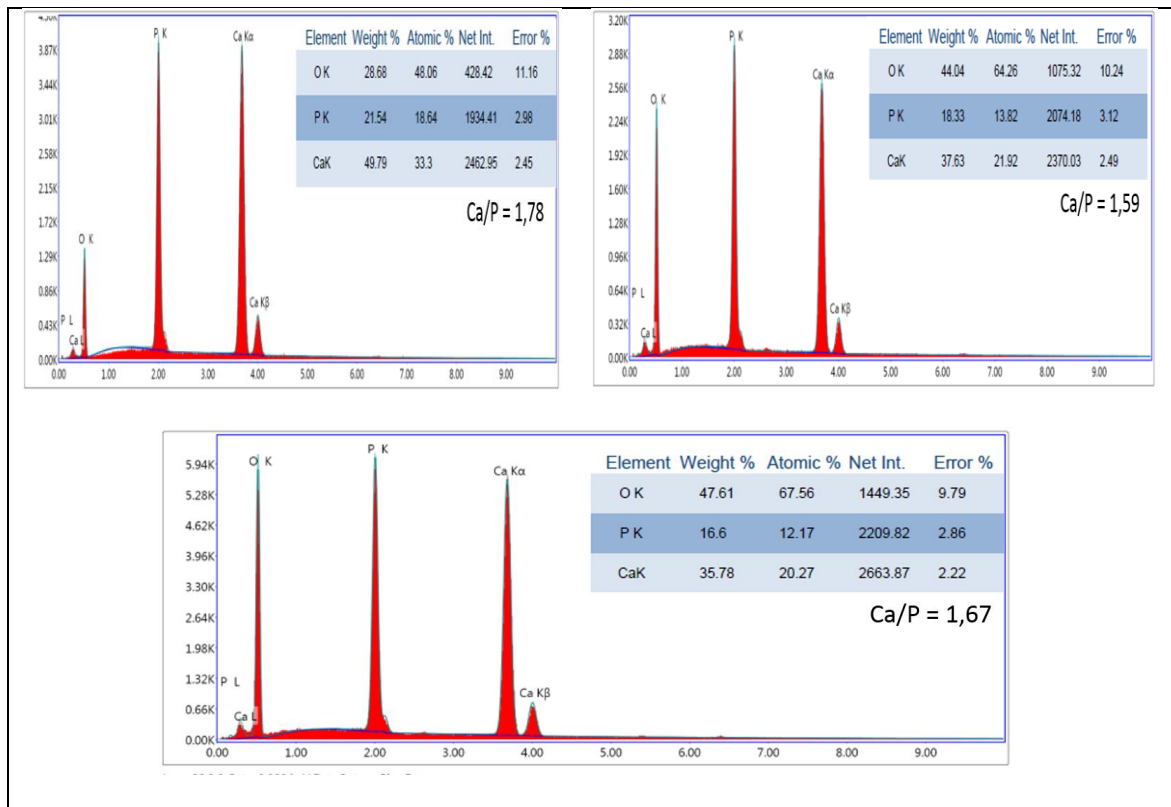


**Figure 4.9.** EDX analysis of the HA films deposited at 420° on rutile, anatase and stainless steel respectively

EDAX graphs of these films (Figure 4.9) indicate that rutile buffer layer leads to the formation of HA films with better stoichiometry compared to anatase buffer layer. Even though HA/TiO<sub>2</sub>(R)/SS films were calcium-rich with Ca/P = 1,78 bigger than (Ca/P)<sub>HA</sub> = 1,67, these films are considered better than those calcium-deficient HA/TiO<sub>2</sub>(A)/SS (Ca/P = 1,59). This consideration was taken according to the proprieties required in orthopedic implants application (see paragraph 1.3.2), and because its Ca/P ratio is closer to that of bone apatite ((Ca/P)<sub>bone</sub> = 1,71).

#### 4.3.4. Thickness of the nHA coatings synthesized by USPT

A cross-section of a typical HA coating -synthesized using USPT deposited onto TiO<sub>2</sub> rutile buffer layer- is displayed in Figure 4.10. This figure shows that the coatings prepared by USPT are thin but thicker than that prepared by RF-MS. This nHA film is continuous with a thickness of 4,7 μm approximately.

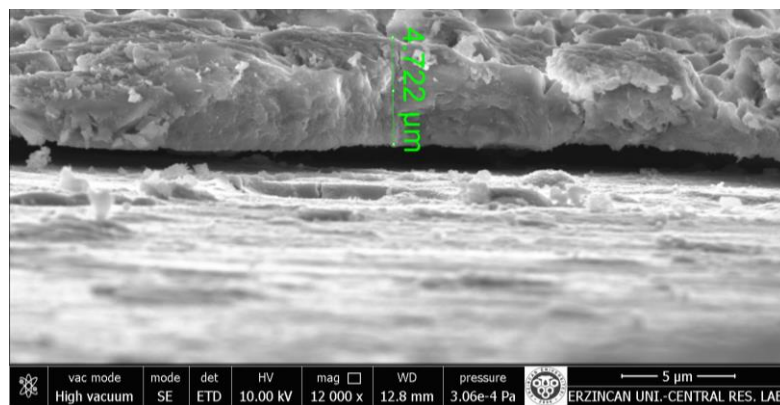


**Figure 4.10.** Cross-section of HA/TiO<sub>2</sub> (R)/S.S deposited at 420°C using USPT

#### 4.3.5. Effect of doping magnesium

Doping magnesium has highly influenced the crystalline composition of the coatings formed (Figure 4.7): Mg has substituted the calcium of tricalcium phosphate that exhibits peaks of Ca<sub>2,81</sub>Mg<sub>0,19</sub>(PO<sub>4</sub>)<sub>2</sub>.

The patterns in the next figure show that HA diffraction characteristics were the same of those before adding Mg, but with very slight shift of (002) peak to a higher angle (from 25,88 to 25,99 from HA/TiO<sub>2</sub>(R)/S.S pattern). Thus, the lattice parameters of Mg-doped HA have been reduced due to the replacement of some Ca<sup>2+</sup> by Mg<sup>2+</sup> that has smaller ionic radius. This result was also obtained by Yajing *et al.* (2014).

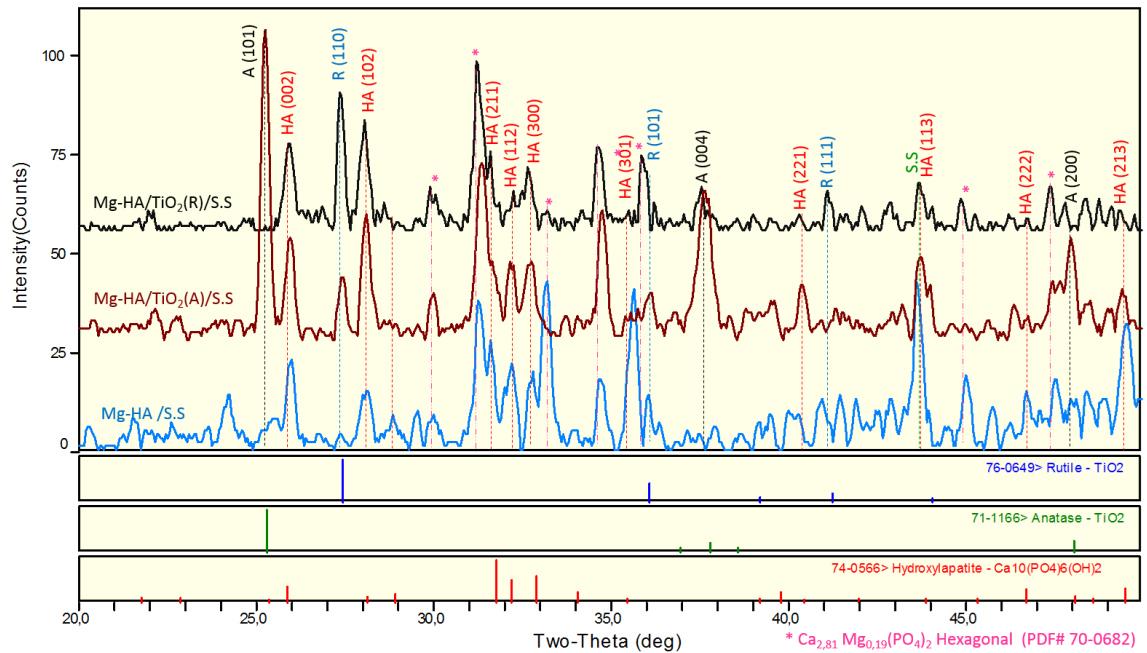


**Figure 4.11.** XRD patterns of Mg doped-nHA coatings deposited at 420°C in different substrates.

No big difference was observed in Mg-doped HA coatings microstructures (Figure 4.12 and 4.13). However their EDX exhibit new peak of Mg due to its incorporation with different grades: films with rutile buffer layer show high Mg loading (Mg/Ca=0,32) compared to films with anatase buffer layer (Mg/Ca=0,16) (Figure 4.14).

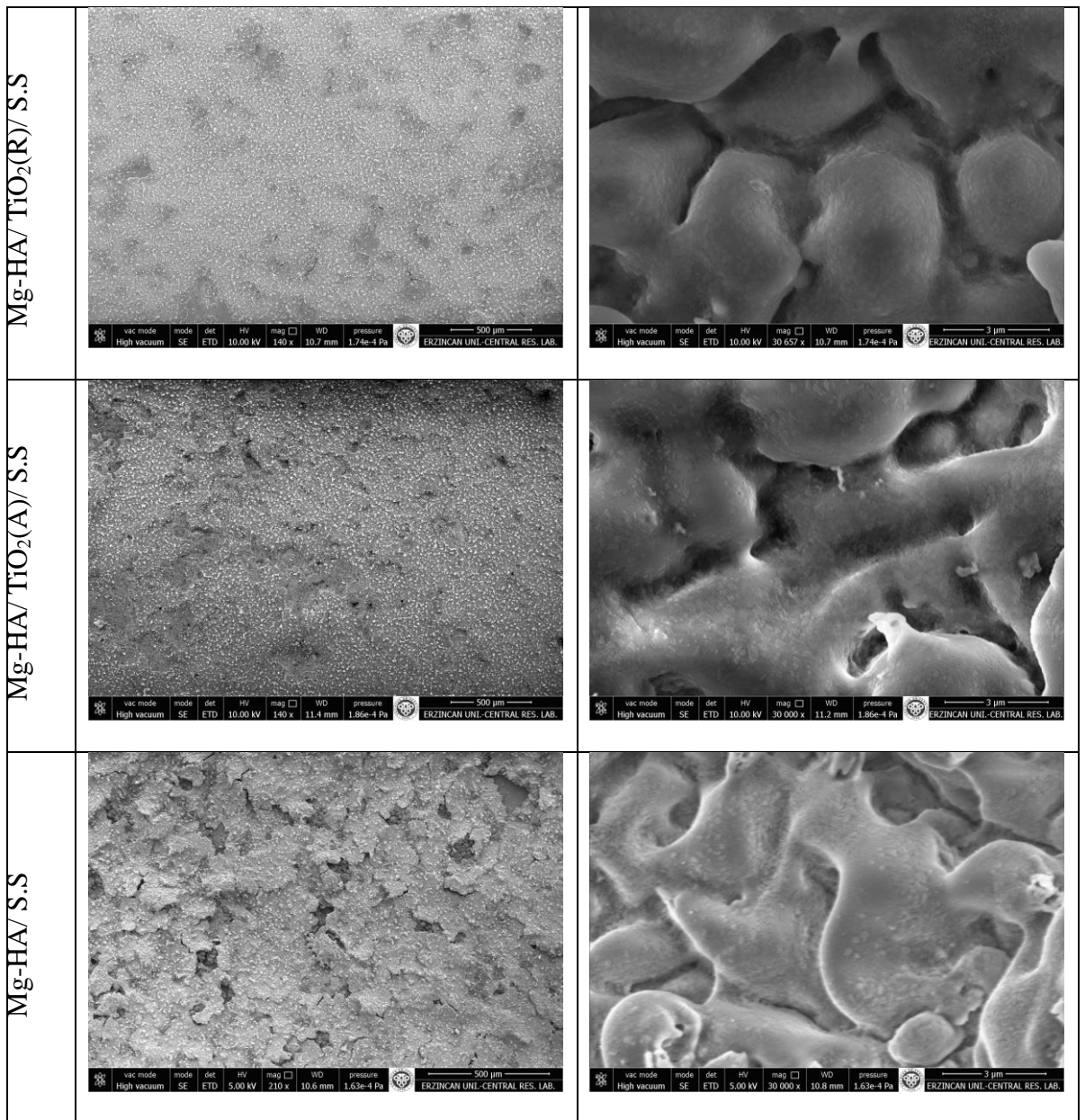


**Figure 4.12.** Representative FESEM images of the Mg doped-HA films deposited on different substrates.



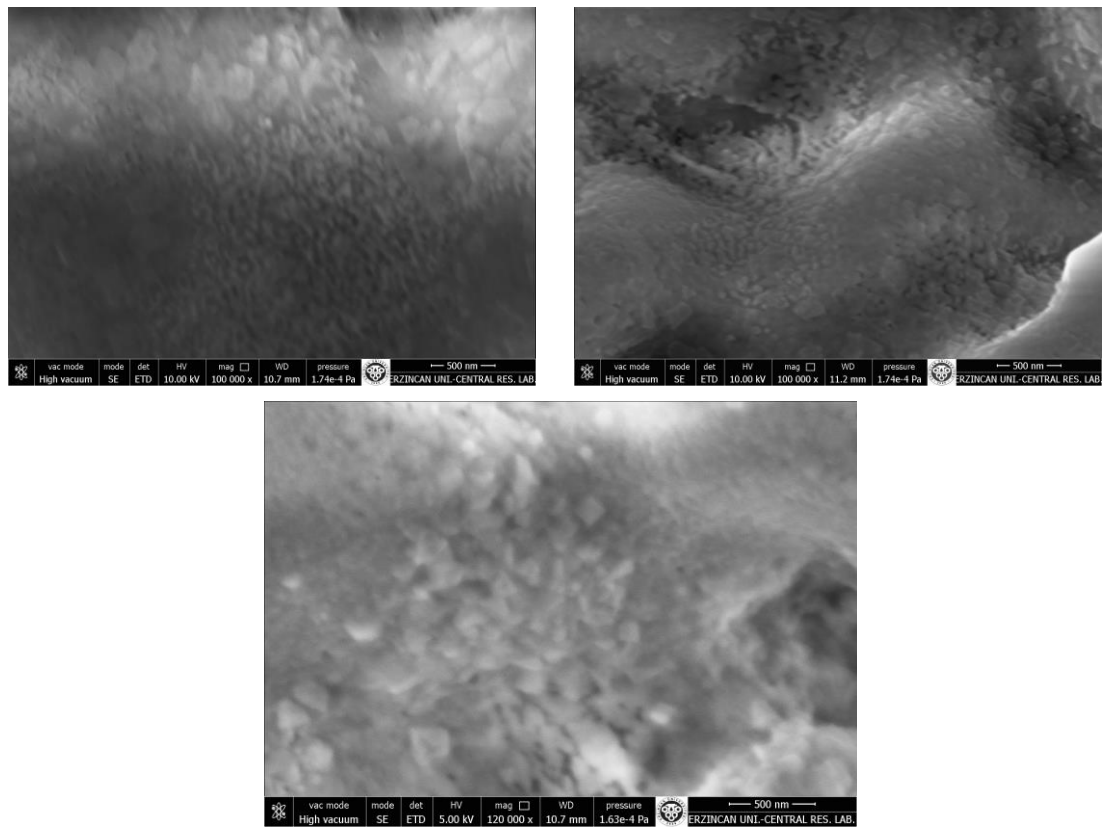


**Figure 4.13.** High magnificated FESEM images of the Mg doped-HA films deposited on rutile, anatase and S.S respectively

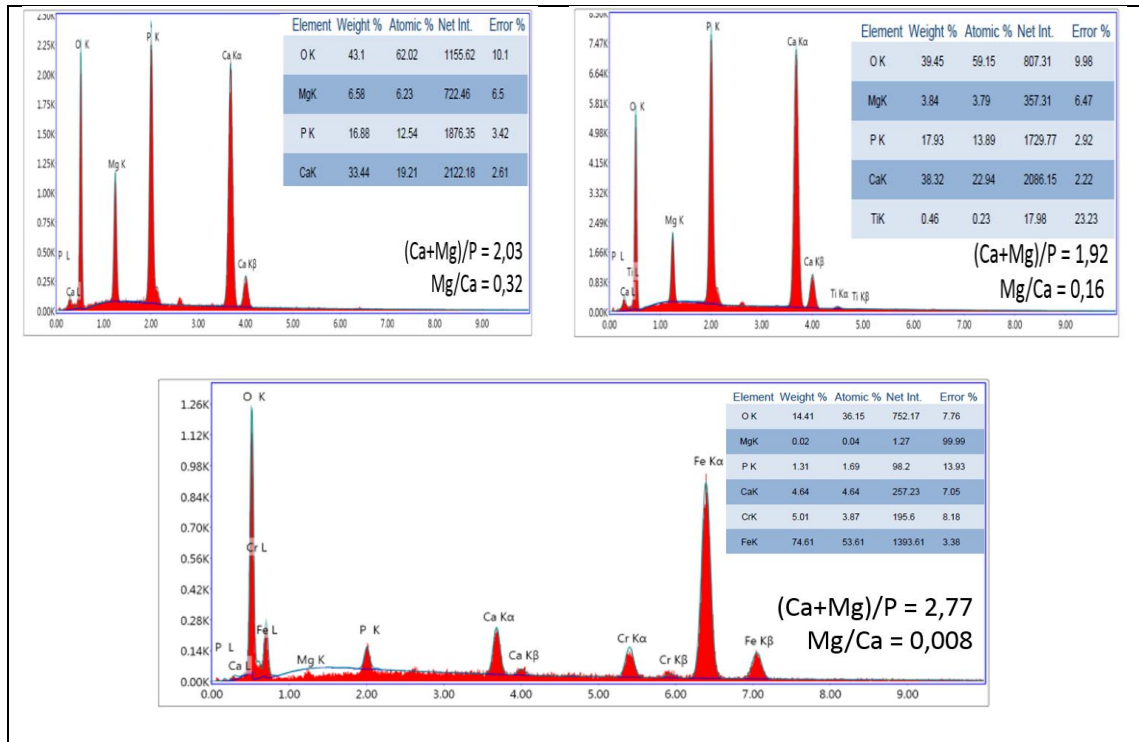


**Figure 4.14.** EDX analysis of the Mg-doped HA films deposited at 420° on rutile, anatase and stainless steel respectively.

#### **4.3.6. Honey incorporation into nHA coatings**

nHA films prepared at 420°C and annealed at 700°C with anatase or rutile buffer layers were selected to prepare antimicrobial coatings by incorporating honey into their vast porous structure through physical/chemical adsorption.

The geographic origin of honey used is Pazar village, Rize –Turkey, this honey was mostly collected from chestnut trees that were not treated with any pesticides or chemicals. Furthermore, there was no addition of any natural or non-natural ingredient to the honey collected.

Each HA/TiO<sub>2</sub>/S.S specimen was simply immersed in 0,5 ml honey during one hour to allow its adsorption by hydroxyapatite, then it was taken out and conserved at room temperature. The extra quantity of honey that remained in the surface was removed by rotating the specimen at 3600 RPM for 10 seconds using a spin coating device. In fact, more than being adsorbed in nHA pores, honey formed also a thin film above the specimen surface. This superficial layer will be quickly released when immersed in body fluid, which provides the antimicrobial propriety for coatings for a short time after implantation. On the other hand, the quantity of honey adsorbed will ensure the antimicrobial propriety of our coatings for long time.

As perspectives of this research, several characterizations should be made to determine the quantity of honey incorporated and to measure its release kinetics in simulated body fluid (SBF). Furthermore, antimicrobial activity testing and cell study should be carried out to approve the potential of the antimicrobial coatings prepared and the feature of their use in trauma wound treatment.

## 5. CONCLUSION

The purpose of this performed thesis was the synthesis of antimicrobial nHA coatings. Thus, several sub-topics have been first explored to provide knowledge on different aspects of orthopedic implants, hydroxyapatite, its desired proprieties and coating techniques, its formation enhancement through TiO<sub>2</sub> buffer layer, and also by doping magnesium to mimic bone appetite and to improve some HA coating proprieties.

TiO<sub>2</sub> buffer layers were then prepared using spray pyrolysis technique. Very homogeneous and high crystalline anatase and rutile thin films have been successfully deposited after determining SPT optimized parameters and spray conditions.

Subsequently, two methods (RF-MS and USPT) have been used for nHA thin films formation, and have been attentively studied. nHA coatings have been successfully synthesized with both RF-MS and USPT onto stainless steel with and without anatase or rutile TiO<sub>2</sub> buffer layer. Nevertheless, these two methods have provided films with different proprieties and structures: nHA coatings prepared with USPT were more crystalline, highly porous, furthermore possess good Ca/P ratio compared to those obtained by RF-MS. The thickness of these films was also considered optimized since it is neither small nor big.

The effect of TiO<sub>2</sub> buffer layer was more pronounced for the coatings obtained by USPT, where rutile phased under layer has ensured better nHA deposition with good stoichiometry and with high magnesium incorporation. Moreover, high porosity of films obtained by USPT provides great benefit for antimicrobial honey incorporation. As conclusion, USPT is considered very good and promising method to produce nHA

coatings with interesting proprieties, in addition to its simplicity, practicality and cost effectiveness.

Honey incorporation was finally performed via simple immersion process of nHA coatings synthesized. To the best of our knowledge, no one has used honey as an antimicrobial agent for developing antimicrobial implant coatings. Further works should be performed such as in-vitro and in-vivo tests, antimicrobial activity tests..etc in order to study the potential of the synthesized antimicrobial nHA coatings especially in traumatic bone injuries treatment.

**BIBLIYOGRAPHY**

- Adam, M. E., 2013. Antimicrobial activity of bee honey, black cumin oil and green tea against multi-drug resistant pathogenic bacteria. *Int. J. Curr. Microbiol. App. Sci.*, 2(12), 58–63.
- Ali, B., Rumaiz, A. K., Ozbay, A., Nowak, E. R. and Ismat Shah, S., 2009. Influence of oxygen partial pressure on structural, transport and magnetic properties of Co doped films. *Solid State Communications*, 149(47–48), 2210–2214.
- Anand R. Kumar, Raymond H. and Barry M., 2010. *Plastic Surgery Challenges in War Wounded. Advances in Wound Care: Volume 1.* Mary Ann Liebert, Inc., publishers, 65–69.
- Bai, Y., Park, I. S., Park, H. H., Lee, M. H., Bae, T. S., Duncan, W. and Swain, M., 2011. The effect of annealing temperatures on surface properties, hydroxyapatite growth and cell behaviors of TiO<sub>2</sub> nanotubes. *Surface and Interface Analysis*, 43(6), 998–1005.
- Boyd, A., Akay, M. and Meenan, B. J., 2003. Influence of target surface degradation on the properties of r.f. magnetron-sputtered calcium phosphate coatings. *Surface and Interface Analysis*, 35(2), 188–198.
- Byd, A. R., Meenan, B. J. and Leyland, N. S., 2006. Surface characterisation of the evolving nature of radio frequency (RF) magnetron sputter deposited calcium phosphate thin films after exposure to physiological solution. *Surface and Coatings Technology*, 200(20–21), 6002–6013.
- Castañeda, L., Alonso, J. C., Ortiz, A., Andrade, E., Saniger, J. M. and Bañuelos, J. G., 2003. Spray pyrolysis deposition and characterization of titanium oxide thin films. *Materials Chemistry and Physics*, 77(3), 938–944.
- Catledge, S. A., Fries, M. D., Vohra, Y. K., Lacefield, W. R., Lemons, J. E., Woodard, S. and Venugopalan, R., 2002. Nanostructured ceramics for biomedical implants. *Journal of Nanoscience and Nanotechnology*, 2(3-4), 293–312.
- Jim C.E., Tim J.M., Welting J.CH.I.M. Walenkamp, G. and J., P., 2013. Modern Orthopaedic Implant Coatings — Their Pro's, Con's and Evaluation Methods. in M. Aliofkhazraei (ed.), *Modern Surface Engineering Treatments.* InTech, New York, 45-73.
- Choudhury, B. and Choudhury, A., 2013. Local structure modification and phase transformation of TiO<sub>2</sub> nanoparticles initiated by oxygen defects, grain size, and annealing temperature. *International Nano Letters*, 3(1), 55.

- Chourashiya, M. G., 2013. Studies on synthesis and characterizations of gadolinium doped ceria solid electrolyte.
- Coe, S. C. , 2008. The deposition, characterisation and biocompatibility of hydroxyapatite and silicon doped hydroxyapatite thin film coatings for orthopaedic applications. PhD thesis, University of Nottingham, UK.
- Davis, K. A., Moran, K. A., McAllister, C. K. and Gray, P. J., 2005. Multidrug-resistant *Acinetobacter* extremity infections in soldiers. *Emerging infectious diseases*, 11(8), 1218–1224.
- Desai, A. Y., 2007. Fabrication and Characterization of Titanium-doped Hydroxyapatite Thin Films. MS Thesis, University of Cambridge, UK.
- D. S. Albin, S. H. R., 1987. Spray pyrolysis processing of optoelectronic materials. *Advanced Ceramic Materials; (USA)*, 2(3).
- Etacheri, V., Seery, M. K., Hinder, S. J. and Pillai, S. C., 2011. Oxygen Rich Titania: A Dopant Free, High Temperature Stable, and Visible-Light Active Anatase Photocatalyst. *Advanced Functional Materials*, 21(19), 3744–3752.
- Fiddes, A. J. C., 1993. Deposition of zinc oxide by spray pyrolysis. Doctoral Thesis, Durham University, UK.
- Filipovic, L, Selberherr, S, Mutinati, G. C and Brunet, E., Steinhauer, S., 2013. Modeling spray pyrolysis deposition, In *Proceedings of the World Congress on Engineering 2*, 987-992.
- Fuchs, T., Stange, R., Schmidmaier, G. and Raschke, M. J., 2011. The use of gentamicin-coated nails in the tibia: preliminary results of a prospective study. *Archives of Orthopaedic and Trauma Surgery*, 131(10), 1419–1425.
- Goerdts, A.-M., Assadian, O., Razavi, B., Igelbrink-Holter, D., Simon, A., Hübner, N.-O., *et al.*, 2013. Proposal for assessment of the antimicrobial efficacy of undiluted medical honey: Using a standardized phase 2/step 2 in vitro stainless steel disc carrier test model. *Wound Medicine*, 1, 20–24.
- Goodman, S. B., Yao, Z., Keeney, M. and Yang, F., 2013. The future of biologic coatings for orthopaedic implants. *Biomaterials*, 34(13), 3174–3183.
- Guild, C., Biswas, S., Meng, Y., Jafari, T., Gaffney, A. M. and Suib, S. L., 2014. Perspectives of spray pyrolysis for facile synthesis of catalysts and thin films: An introduction and summary of recent directions. *Catalysis Today*, 238, 87–94.
- Hanaor, D. A. H. and Sorrell, C. C., 2011. Review of the anatase to rutile phase transformation. *Journal of Materials Science*, 46(4), 855–874.
- Iida, Y. and Ozaki, S., 1961. Grain Growth and Phase Transformation of Titanium Oxide During Calcination. *Journal of the American Ceramic Society*, 44(3), 120–127.
- Jamuna-Thevi, K., Bakar, S. A., Ibrahim, S., Shahab, N. and Toff, M. R. M., 2011.

- Quantification of silver ion release, in vitro cytotoxicity and antibacterial properties of nanostructured Ag doped TiO<sub>2</sub> coatings on stainless steel deposited by RF magnetron sputtering. *Vacuum*, 86(3), 235–241.
- Kasemanankul, P., Witit-Anan, N., Chaiyakun, S., Limsuwan, P. and Boonamnuayvitaya, V., 2009. Low-temperature deposition of (1 1 0) and (1 0 1) rutile TiO<sub>2</sub> thin films using dual cathode DC unbalanced magnetron sputtering for inducing hydroxyapatite. *Materials Chemistry and Physics*, 117(1), 288–293.
- Kazemzadeh-Narbat, M., Kindrachuk, J., Duan, K., Jenssen, H., Hancock, R. E. W. and Wang, R., 2010. Antimicrobial peptides on calcium phosphate-coated titanium for the prevention of implant-associated infections. *Biomaterials*, 31(36), 9519–9526.
- Kazemzadeh-Narbat, M., Lai, B. F. L., Ding, C., Kizhakkedathu, J. N., Hancock, R. E. W. and Wang, R., 2013. Multilayered coating on titanium for controlled release of antimicrobial peptides for the prevention of implant-associated infections. *Biomaterials*, 34(24), 5969–5977.
- Kazemzadeh-Narbat, M., Noordin, S., Masri, B. A., Garbuz, D. S., Duncan, C. P., Hancock, R. E. W. and Wang, R., 2012. Drug release and bone growth studies of antimicrobial peptide-loaded calcium phosphate coating on titanium. *Journal of biomedical materials research. Part B, Applied biomaterials*, 100(5), 1344–1352.
- Kwakman, P. H. S., Van den Akker, J. P. C., Güçlü, A., Aslami, H., Binnekade, J. M., de Boer, L., *et al.*, 2008. Medical-grade honey kills antibiotic-resistant bacteria in vitro and eradicates skin colonization. *Clinical infectious diseases: an official publication of the Infectious Diseases Society of America*, 46(11), 1677–1682.
- Lai, H.-C., Tsai, H.-H., Hung, K.-Y. and Feng, H.-P., 2014. Fabrication of hydroxyapatite targets in radio frequency sputtering for surface modification of titanium dental implants. *Journal of Intelligent Material Systems and Structures*.
- Landi, E., Logroscino, G., Proietti, L., Tampieri, A., Sandri, M. and Sprio, S., 2008. Biomimetic Mg-substituted hydroxyapatite: from synthesis to in vivo behaviour. *Journal of Materials Science. Materials in Medicine*, 19(1), 239–247.
- Lee, S.-H., Kim, H.-E. and Kim, H.-W., 2007. Nano-Sized Hydroxyapatite Coatings on Ti Substrate with TiO<sub>2</sub> Buffer Layer by E-beam Deposition. *Journal of the American Ceramic Society*, 90(1), 50–56.
- Le, M., 2013. Some Comments on Orthopaedic Implant Infection: Biomaterials Issues. *Journal of Biotechnology & Biomaterials*, 03(03).
- Li, X., 2009. Electrohydrodynamic deposition and patterning of nano-hydroxyapatite for biomedical applications. Doctoral Thesis, University College London, UK.



- López, E. O., Mello, A., Sendão, H., Costa, L. T., Rossi, A. L., Ospina, R. O., Borghi, F. F., Silva Filho, J. G. and Rossi, A. M., 2013. Growth of Crystalline Hydroxyapatite Thin Films at Room Temperature by Tuning the Energy of the RF-Magnetron Sputtering Plasma. *ACS Applied Materials & Interfaces*, 5(19), 9435–9445.
- LU, S. D., 2005. *Introduction to Biomaterials*. Tsinghua University Press, 253p, Beijing, China.
- Lyndon, J. A., Boyd, B. J. and Birbilis, N., 2014. Metallic implant drug/device combinations for controlled drug release in orthopaedic applications. *Journal of controlled release*. *Journal of Controlled Release*, 179, 63-75.
- Maddocks, S. E. and Jenkins, R. E., 2013. Honey: a sweet solution to the growing problem of antimicrobial resistance?. *Future microbiology*, 8(11), 1419–1429.
- Mody, R. M., Zapor, M., Hartzell, J. D., Robben, P. M., Waterman, P., Wood-Morris, R., Trotta, R., Andersen, R. C. and Wortmann, G., 2009. Infectious complications of damage control orthopedics in war trauma. *The Journal of trauma*, 67(4), 758–761.
- Mooney, J. B. and Radding, S. B., 1982. Spray Pyrolysis Processing. *Annual Review of Materials Science*, 12(1), 81–101.
- Nakaruk, A., Ragazzon, D. and Sorrell, C. C., 2010. Anatase–rutile transformation through high-temperature annealing of titania films produced by ultrasonic spray pyrolysis. *Thin Solid Films*, 518(14), 3735–3742.
- Nakaruk, A. and Sorrell, C. C., 2010. Conceptual model for spray pyrolysis mechanism: fabrication and annealing of titania thin films. *Journal of Coatings Technology and Research*, 7(5), 665–676.
- Narayanan, R., Seshadri, S. K., Kwon, T. Y. and Kim, K. H., 2008. Calcium phosphate-based coatings on titanium and its alloys. *Journal of Biomedical Materials Research. Part B, Applied Biomaterials*, 85(1), 279–299.
- Oja, I., Mere, A., Krunks, M., Solterbeck, C.-H. and Es-Souni, M., 2004. Properties of TiO<sub>2</sub> Films Prepared by the Spray Pyrolysis Method. *Solid State Phenomena*, 99-100, 259–264.
- Perdnis D, 2003. thin film deposition by spray pyrolysis and the application in solid oxide fuel cells. *Doctoral Thesis*, ETH Zurich, Switzerland.
- Perednis, D. and Gauckler, L. J., 2005. Thin Film Deposition Using Spray Pyrolysis. *Journal of Electroceramics*, 14(2), 103–111.
- Rana, R., 2014. Health Ministry: Wounded Syrians may carry dangerous pathogens.
- Ratcliffe, N., Azambuja, P. and Mello, C. B., 2014. Recent Advances in Developing

- Insect Natural Products as Potential Modern Day Medicines. Evidence-Based Complementary and Alternative Medicine, 2014.
- Reidenbach, F., 1994. ASM Handbook: Volume 5: Surface Engineering. ASM International, 1056p, Materials Park, Ohio.
- Schneider, J. M., Rohde, S., Sproul, W. D. and Matthews, A., 2000. Recent developments in plasma assisted physical vapour deposition. Journal of Physics D: Applied Physics, 33(18), 173.
- Sears, W. M. and Gee, M. A., 1988. Mechanics of film formation during the spray pyrolysis of tin oxide. Thin Solid Films, 165(1), 265–277.
- Shinde, P. S., 2012. Photoelectrochemical Detoxification of water using spray deposited oxide semiconductor thin films. Doctoral Thesis, Shivaji University, India.
- Sitharaman, B., 2011. Nanobiomaterials Handbook. CRC press, 800p, London, England.
- Staiger, M. P., Pietak, A. M., Huadmai, J. and Dias, G., 2006. Magnesium and its alloys as orthopedic biomaterials: A review. Biomaterials, 27(9), 1728–1734.
- Stigter, M., Bezemer, J., de Groot, K. and Layrolle, P., 2004a. Incorporation of different antibiotics into carbonated hydroxyapatite coatings on titanium implants, release and antibiotic efficacy. Journal of controlled release: official journal of the Controlled Release Society, 99(1), 127–137.
- Stigter, M., Bezemer, J., de Groot, K. and Layrolle, P., 2004b. Incorporation of different antibiotics into carbonated hydroxyapatite coatings on titanium implants, release and antibiotic efficacy. Journal of controlled release: official journal of the Controlled Release Society, 99(1), 127–137.
- Surmeneva, M. A., Surmenev, R. A., Chaikina, M. V., Kachaev, A. A., Pichugin, V. F. and Epple, M., 2013. Phase and elemental composition of silicon-containing hydroxyapatite-based coatings fabricated by RF-magnetron sputtering for medical implants. Inorganic Materials: Applied Research, 4(3), 227–235.
- Surmeneva, M. A., Surmenev, R. A., Pichugin, V. F., Koval', N. N., Teresov, A. D., Ivanova, A. A., *et al.*, 2013. Adhesion properties of a silicon-containing calcium phosphate coating deposited by RF magnetron sputtering on a heated substrate. Journal of Surface Investigation. X-ray, Synchrotron and Neutron Techniques, 7(5), 944–951.
- Thian, E. S., Huang, J., Barber, Z. H., Best, S. M. and Bonfield, W., 2011. Surface modification of magnetron-sputtered hydroxyapatite thin films via silicon substitution for orthopaedic and dental applications. Surface and Coatings Technology, 205(11), 3472–3477.
- Tsuchiya, H., Macak, J. M., Müller, L., Kunze, J., Müller, F., Greil, P., Virtanen, S. and Schmuki, P., 2006. Hydroxyapatite growth on anodic TiO<sub>2</sub> nanotubes. Journal of

- Biomedical Materials Research Part A, 77A(3), 534–541.
- Uchida, M., Kim, H.-M., Kokubo, T., Fujibayashi, S. and Nakamura, T., 2003. Structural dependence of apatite formation on titania gels in a simulated body fluid. *Journal of Biomedical Materials Research. Part A*, 64(1), 164–170.
- Van Dijk, K., Schaeken, H. G., Wolke, J. C., Marée, C. H., Habraken, F. H., Verhoeven, J. and Jansen, J. A., 1995. Influence of discharge power level on the properties of hydroxyapatite films deposited on Ti6Al4V with RF magnetron sputtering. *Journal of Biomedical Materials Research*, 29(2), 269–276.
- Van Dijk, K., Verhoeven, J., Marée, C. H. M., Habraken, F. H. P. M. and Jansen, J. A., 1997. Study of the influence of oxygen on the composition of thin films obtained by r.f. sputtering from a Ca<sub>5</sub>(PO<sub>4</sub>)<sub>3</sub> OH target. *Thin Solid Films*, 304(1–2), 191–195.
- Wasa, K., Kitabatake, M. and Adachi, H., 2004. *Thin Films Material Technology: Sputtering of Compound Materials*. Norwich, NY; Heidelberg: Springer, 518p, Norwich.
- Weckbach, S., Losacco, J. T., Hahnhaussen, J., Gebhard, F. and Stahel, P. F., 2012. Challenging the dogma on inferiority of stainless steel implants for fracture fixation. An end of the controversy?. *Der Unfallchirurg*, 115(1), 75–79.
- Xia, W., Lindahl, C., Lausmaa, J. and Engqvist, H., 2011. Biomimetic Hydroxyapatite Deposition on Titanium Oxide Surfaces for Biomedical Application. in A. George (ed.), *Advances in Biomimetics*. 20, 429–452.
- Yajing, Y., Qiongqiong, D., Yong, H., Han, S. and Pang, X., 2014. Magnesium substituted hydroxyapatite coating on titanium with nanotubular TiO<sub>2</sub> intermediate layer via electrochemical deposition. *Applied Surface Science*, 305, 77–85.
- Yang, B., Uchida, M., Kim, H.-M., Zhang, X. and Kokubo, T., 2004. Preparation of bioactive titanium metal via anodic oxidation treatment. *Biomaterials*, 25(6), 1003–1010.
- Yang, Y., Kim, K.-H., Mauli Agrawal, C. and Ong, J. L., 2003. Effect of post-deposition heating temperature and the presence of water vapor during heat treatment on crystallinity of calcium phosphate coatings. *Biomaterials*, 24(28), 5131–5137.
- Ye, G. and Troczynski, T., 2008. Hydroxyapatite coatings by pulsed ultrasonic spray pyrolysis. *Ceramics International*, 34(3), 511–516.
- Yin, L.-Y., Manring, M. M. and Calhoun, J. H., 2013. A Rabbit Osteomyelitis Model to Simulate Multibacterial War Wound Infections. *Military Medicine*, 178(6), 696–700.
- Zhang, S., 2013. *Hydroxyapatite coatings for biomedical applications*, CRC press, 469p, UK.

**CURRICULUM VITAE (CV)**

Born in 1988 in Algeria. Studied Chemical Engineering in National Polytechnic School of Algiers from 2006 to 2011, then Elaboration and Physical-chemistry of Materials in Polytechnic Military School –Algeria during 2011-2012 academic year. Pursued the master studies in Nanomaterials, Nanoscience and Nanoengineering Department at Ataturk University - Graduate School of Natural and Applied Sciences in the period 2012-2015.